ISSN-print: 2073-0764

ISSN-online: 2959-4340

TuJnaS

Thamar University Journal of Natural & Applied Sciences

A Peer-Reviewed Scientific Journal

Volume 8

Issue (2)

December 2023

Thamar University Publications

Thamar University Journal of Natural and Applied Sciences (*TUJNAS*)

Thamar University Journal of Natural & Applied Sciences (TUJNAS) is a peer-reviewed journal. It is an open-access journal published twice a year by Thamar University, Dhamar, Yemen. The aim of the journal is to publish original and review articles in the fields of science, agriculture, engineering, medicine, environment, and computer science. The journal is published in English only.

The journal has the following international standard codes:

ISSN-print: 2073-0764

ISSN-online: 2959-4340

For more information on editorial policy, manuscript submission, ethics, etc., please visit the TUJNAS Journal website:

https://www.tu.edu.ye/journals/index.php/TUJNAS

Editorial Team

General Supervisor

Editor-in-chief

Editorial Director

✉ All correspondence should be sent to: ✉

Editorial Director,

Thamar University Journal of

Natural and Applied Sciences (TUJNAS)

Thamar University, P O Box: 87246 Dhamar, Republic of Yemen
E-Mail: tujnas@tu.edu.ye

Advisory Board

Assoc. Prof. Abdul Ghani Ali Mohammed

Position: Dean of Faculty of Agriculture & Veterinary Medicine, Thamar University, Dhamar, Yemen.

Address: Faculty of Agriculture & Veterinary Medicine, Thamar University, Dhamar, Yemen.

E-Mail: abdulghani.ali@tu.edu.ye

Assist. Prof. Fouad Mohammed Y. Al-Jarmouzi

Position: Dean of Faculty of Engineering, Thamar University, Dhamar, Yemen.

Address: Faculty of Engineering, Thamar University, Dhamar, Yemen.

E-Mail: aljarmouzi@tu.edu.ye

Assist. Prof. Nashwan Hamid Saleh Al-Tairi

Position: Dean of Faculty of Dentistry, Thamar University, Dhamar, Yemen.

Address: Faculty of Dentistry, Thamar University, Dhamar, Yemen.

E-Mail: nashwanh9@tu.edu.ye

Assoc. Prof. Adel Ali Ahmed Amran

Position: Dean of Faculty of Medical Science, Thamar University, Dhamar, Yemen.

Address: Faculty of Medical Science, Thamar University, Dhamar, Yemen.

E-Mail: adelamran@tu.edu.ye

Editorial Board

Prof. Dr. Levan Chkhartishvili (Georgia)

Research field: Semiconducting and Powder Composite Materials.

Position: Professor at the Department of Engineering Physics, Faculty of Informatics and Control Systems, Georgian Technical University, and researcher at F. Tavadze Metallurgy and Materials Science Institute, Semiconducting and Powder Composite Materials Laboratory.

Affiliation: Department of Engineering Physics, Faculty of Informatics and Control Systems, Georgian Technical University, 77 M. Kostava Ave., GTU Campus 4, Room 307, Tbilisi, 0160, Georgia.

E-Mail: levanchkhartishvili@gtu.ge , chkharti2003@yahoo.com

Prof. Dr. Saeed M. Al-Ghalibi (Yemen)

Research field: Bacteriology, Fungi, Medical microbiology, and Food Microbiology.

Position: Deputy Dean of Faculty of Science for Academic Affairs and Graduate Studies, Faculty of Science, Sana'a University, Sana'a, Yemen

Affiliation: Department of Biology, Faculty of Science, Sana'a University, Sana'a, Yemen.

E-Mail: s.alghalabi@su.edu.ye ,
Alghalibi@gmail.com

Prof. Dr. Abdulkarim A. Amad (Germany)

Research field: Animal nutrition and production feed and feeding.

Affiliation: Faculty of Agriculture, Thamar University, Dhamar, Yemen and Institute of Animal Nutrition, Department of Veterinary Medicine, Frei Universität Berlin, Berlin, Germany.

E-Mail: abdulkarim.Amad@tu.edu.ye ,
abeerobeid@yahoo.com

Prof. Dr. Nabil M. Al-Areeq (Yemen)

Research field: Petroleum Geology, Hydrology, Sedimentology, Integrated Water Resources Management, Data analysis and Resolving of Water Related Conflicts.

Position: Centre Director of Water Resources and Environment, Thamar University, Dhamar, Yemen.

Affiliation: Department of Geology and Environment, Faculty of Applied Science, Thamar University, Dhamar, Yemen.

E-Mail: alareeqnabil@tu.edu.ye ,
nabilalareeq@yahoo.com

Prof. Dr. Ibrahim Radman Al Shaibani (Yemen)

Research field: Veterinary Parasitology.

Position: Vice Dean for students' affair, Faculty of Veterinary Medicine, Thamar University, Dhamar, Yemen.

Affiliation: Faculty of Veterinary Medicine, Thamar University, Dhamar, Yemen.

E-Mail: ibrahim.alshaibani@tu.edu.ye , dr_ibra67@yahoo.com

Prof. Dr. Salah Mahdi Saleem Al-Bader (Iraq)

Research field: Fungal taxonomy, Fungal ecology, and Natural products as antifungal agents.

Affiliation: Department of Medical Laboratory Sciences, College of Science, Knowledge University, Erbil, Iraq.

E-Mail: salah.mahdi@knu.edu.iq

Prof. Dr. Abeer Omer A. Obeid (Yemen)

Research field: Organic chemistry, Polymers, Liquid Crystals, and synthesis of heterocyclic compounds, as well as Anti-cancer and Antibacterial applications.

Affiliation: Department of Chemistry, Faculty of Science, Sana'a University, Sana'a, Yemen.

E-Mail: ab.obaid@su.edu.ye , abeerobeid@yahoo.com

Prof. Dr. Abduh M. Abdulwahab (Yemen)

Research field: Single Crystal, Crystal Structure, Physical Characterization of Solid-State Materials and Solid-State Physics.

Affiliation: Department of Physics, Faculty of Applied Sciences, Thamar University, Dhamar, Yemen.

E-Mail: abduh.abdulwahab@tu.edu.ye , abduhabdulwahab@yahoo.com

Prof. Dr. Omar M. A. Al Shuja'a (Yemen)

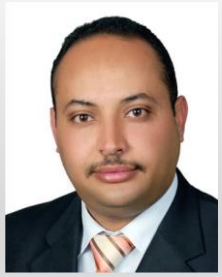

Research field: Materials Chemistry, Polymer Chemistry, and Physical Chemistry.

Position: Dean of the Center for Development and Quality Assurance, Al-Nasser University, Sana'a, Yemen.

Affiliation: Department of Chemistry, Faculty of Applied Sciences, Thamar University, Dhamar, Yemen.

E-Mail: omrshugaa@tu.edu.ye , abduhabdulwahab@yahoo.com

Assoc. Prof. AbdulSalam M. Al-Makdad (Yemen)

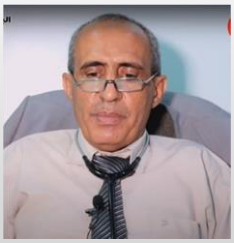

Research field: Diagnosis, management, and care of acute and chronic liver disease and GI diseases. Diagnostic and interventional GI endoscopy.

Position: President of the internal medicine department in AL-Wahda Teaching Hospital Maabar, Maabar City, Dhamar, Yemen.

Affiliation: Department of Internal Medicine, Faculty of Medicine, Thamar University, Dhamar, Yemen.

E-Mail: aalmakdad@tu.edu.ye

Assoc. Prof. Shaimaa A. A. Momen (Egypt)

Research field: Entomology.

Affiliation: Department of Entomology, Faculty of Science, Ain Shams University, Khalifa El-Maamon Street, 11566, Cairo, Egypt.

E-Mail: Shaimaa_momen@sci.asu.edu.eg ,
Shaimaa_momen@hotmail.com

Assoc. Prof. Essam A. Al-Moraissi (Yemen)

Research field: Oral and maxillofacial surgery, craniomaxillofacial trauma, temporomandibular joint disorders, orthognathic surgery, surgical pathology, cleft lip and palate, implant dentistry, lower third molar surgery, regenerative medicine, and adult mesenchymal stem cells.

Affiliation: Department of Oral and Maxillofacial Surgery, Faculty of Dentistry, Thamar University, Dhamar, Yemen.

E-Mail: dressamalmoraissi@tu.edu.ye

Assoc. Prof. Salah Abdul-Jabbar Jassim (Iraq)

Research field: Thin Films, Semiconductor Devices, and Solid-State Physics.

Affiliation: Department of Dentistry, AL Kunooze University College, Basrah, Iraq.

E-Mail: salah.abdul.jabbar@kunoozu.edu.iq ,
salahjassim200@yahoo.com ,
salah.jassim@alayen.edu.iq

Assoc. Prof. Amin Saif Ahmed (Yemen)

Research field: Energy and control systems engineering.

Affiliation: Department Mechatronics, Al-Saeed College of Engineering and Information Technology, Taiz University, Taiz, Yemen.

E-Mail: sameeralromima@yahoo.com , sameeralromima@gmail.com

Assoc. Prof. Dina Salah Eldin M. Abdelrhman (Egypt)

Research field: Gold Nanoparticles, Photochemistry, Nanotechnology, and Nanomedicine.

Affiliation: Biophysics, Physics Department, Faculty of Science, Ain Shams University, Khalifa El-Maamon Street, 11566, Cairo, Egypt.

E-Mail: dinasalah@sci.asu.edu.eg , dandy741@hotmail.com , dandy741@gmail.com

Assoc. Prof. Fawaz M. A. Al-Badaii (Yemen)

Research field: Microbiology, Antimicrobial resistance, Environmental Science, Heavy metals, and Adsorption Water quality.

Affiliation: Department of Biology, Faculty of Applied Sciences, Thamar University, Dhamar, Yemen.

E-Mail: fawaz.AlBadai@tu.edu.ye , abdualwhab1974@gmail.com

Assoc. Prof. Abdulwahab B. Alwany (Yemen)

Research field: Solid State Physics, Thein Films, Materials Science, and Nanoscience.

Affiliation: Department of Physics, Faculty of Science, Ibb University, Ibb, Yemen.

E-Mail: abdualwhab@yahoo.com , abdualwhab1974@gmail.com

Assoc. Prof. Ali Abdullah A. Al-Mehdar (Yemen)

Research field: Pharmacology & Therapeutics.

Affiliation: Department of Pharmacology and Toxicology, Faculty of Faculty of Medicine, Thamar University, Dhamar, Yemen.

E-Mail: ali.almehdar@tu.edu.ye , alialmehdar2006@yahoo.com

Assoc. Prof. Sameer A. M. Abdulrahman (Yemen)

Research field: Pharmaceutical Analytical Chemistry and Water Treatment.

Affiliation: Department of Chemistry, Faculty of Education and Sciences-Rada'a, Albaydha University, Albaydha 14517, Yemen.

E-Mail: sameeralromima@yahoo.com , sameeralromima@gmail.com

Assoc. Prof. Nada M. Al-Hamdani (Yemen)

Research field: Histology, and Physiology, specializing in Endocrinology.

Affiliation: Department of Biology, Faculty of Science, Sana'a University, Sana'a, Yemen.

E-Mail: n.alhamdni@su.edu.ye , hamdaninadam@gmail.com

Assoc. Prof. Abdulbari A. A. Saeed (UK)

Research field: Preparation and characterization of mesoporous from solid waste as catalysis for water purification, Separation technology using an adsorption process, Water and wastewater treatment, and Biofuel production from organic solid waste.

Affiliation: School of Engineering, Institute for Infrastructure and Environment (IIE), University of Edinburgh, Edinburgh EH9 3JL, UK.

E-Mail: alborani_75@yahoo.co.uk , Abdulbari.Saeed@ed.ac.uk

Assoc. Prof. Yahya Qaid Hasan Ali (Yemen)

Research field: Differential Equations, Numerical Analysis, and Adomian Decomposition Method.

Affiliation: Department of Mathematics, Faculty of Applied Sciences, Thamar University, Dhamar, Yemen.

E-Mail: qaid.Yahya@tu.edu.ye , yahya217@yahoo.com

Assoc. Prof. Abdullah Alwarafi (Yemen)

Research field: Social Pharmacy.

Position: Vice Dean for Student Affairs, Faculty of Dentistry, Ibb University, Ibb, Yemen

Affiliation: Pharmacy Department, Faculty of Dentistry, Ibb University, Ibb, Yemen.

E-Mail: abdullahalwarafi@gmail.com , dentistry@ibbuniv.edu.ye

Prof. Dr. Ahmed A. M. Alakwa (Yemen)

Research field: Agricultural Economics.

Position: Head of Scientific Research, Vice Presidency of the University for Postgraduate Studies and Scientific Research, Thamar University, P O Box 87246 Dhamar, Yemen

Affiliation: Faculty of Agriculture, Thamar University, Dhamar, Yemen.

E-Mail: Hawali.ahmed@tu.edu.ye , alakwaahmed55@gmail.com

Prof. Dr. Ahmed Ali Saleh Obayeha (Yemen)

Research field: Orthodontics, Pediatric Dentistry, and Preventive Medicine.

Position: Dean of the Faculty of Dentistry, Al-Razi University, Sana'a, Yemen

Affiliation: Faculty of Dentistry Sana'a University, Sana'a, Yemen.

E-Mail: a.Obaya@su.edu.ye , Ahmedobeyah@yahoo.com

Assoc. Prof. Fathi Ahmed ELShawish (Yemen)

Research field: Identification and characterization of genetic sources of indigenous and introduced fruits, propagation and breeding of fruit crops, and design and layout of gardens.

Position: Deputy Dean for Postgraduate Studies and Scientific Research, Faculty of Agriculture, Thamar University, Dhamar, Yemen

Affiliation: Faculty of Agriculture, Thamar University, Dhamar, Yemen.

E-Mail: Fathi.ELShawish@tu.edu.ye ,

Assoc. Prof. Khalid Al-Hussaini (Yemen)

Research field: Information & Communication Technology (ICT), Computer Communications (Networks), Communication Engineering, and Computer Engineering.

Position: University Rector's Advisor for Academic Development & Automation and Vice Dean for Student Affairs, Faculty of Computer Science & Information Systems, Thamar University, Dhamar, Yemen.

Affiliation: Department of Information Technology, Faculty of Computer Science & Information System, Thamar University, Dhamar, Yemen.

E-Mail: khalid.alhussaini@tu.edu.ye

Volume 8, Issue 2, December 2023

Articles

TUJNAS

Original Article

Thamar University Journal of Natural & Applied Sciences 8(2) (2023) 1 – 9

DOI: https://doi.org/10.59167/tujnas.v8i2.1710

Health Risk Assessment of Some Heavy Metals in Groundwater Samples in Rada'a City, Yemen

Abdo Mohd Meftah[1,*] Khairiah Qaid Al-Majdad[2,], and Noha Ahmed Elayah[1]**

[1]Department of Physics, Faculty of Applied Science, Thamar University, Dhamar 87246, Yemen

[2]Department of Physics, Faculty of Science and Education, Albaydha University, Yemen.

*Corresponding authors: at Department of Physics, Faculty of Applied Science, Thamar University, 87246, Dhamar, Yemen. E-mail: meftah2090@tu.edu.ye (A. M. Meftah) and at Department of Physics, Faculty of Science and Education, Albaydha University, Yemen. E-mail: almajdad22446688@gmail.com (K. Q. Al-Majdad)

Received: 5 August 2023. Revised (in revised form): 4 September 2023. Accepted 16 October 2023. Published 31 December 2023

Abstract

Groundwater is an important source of domestic drinking water supply, and groundwater quality assessment is necessary to reduce pollution to acceptable levels. Therefore, this study aims to determine the concentrations of heavy metals (HM) (Cr, Cd, Cu, Ni, Mn, Fe, and Zn) in the groundwater of Rada'a City and to evaluate the health risk. Groundwater samples were analyzed by inductively coupled plasma optical emission spectrometry (ICP-OES). The following average concentrations (mg/l) were determined in the groundwater 0.01035, 0.01702, 0.043718, and 0.03652 for Cu, Ni, Mn, and Zn were concentration values lower than the World Health Organization acceptable limit (WHO) 2, 0,07, 0.4, and 4 for Cu, Ni, Mn, and Zn, respectively. Still, at some locations in the study area, concentration values were found to be above the acceptable limit of 0.3 (mg/l) for Fe, the average concentrations were 0.42567 (mg/l). Based on the HM concentrations, the health risk was classified as non-carcinogenic. The health risk indices (HRI) were < 1 for all HMs in the groundwater samples, indicating no health risk. In addition, a high carcinogenic risk (Probability of Cancer Risk, PCR) of 4.42×10^{-4} on average was found from drinking water consumption, while the acceptable range for cancer risk is $\leq 1 \times 10^{-6}$ to 1×10^{-4}.

Keywords: Groundwater; Heavy Metals; Rada'a; Health Risk, ICP-OES

1. Introduction

Groundwater plays an important role in water supply for drinking, agriculture, industry, and households [1]. Groundwater may be contaminated with heavy metals (HM), either by anthropogenic (e.g., mining, wastewater, irrigation, industry, and agriculture) or natural resources (e.g., erosion of rock layers and volcanic eruptions) [2,3]. Therefore, groundwater has become a serious global problem [4]. HM enters our bodies through the water we drink, the air we breathe, and the food we eat, so its contamination of water, air, or food poses a potential threat to human health [5]. High molecular weight substances are elements with an atomic mass greater than 20, have metallic properties, and a density greater than 5 g/cm^3, so they are at least five times denser than water (1 g/cm^3), cannot be metabolized by the body, and are stable and bioaccumulative [6,7,8]. High molecular weight metals such as copper and zinc are essential elements for the normal growth and function of living organisms, while high concentrations of other metals such as cadmium, lead, chromium, arsenic, and manganese are highly toxic to humans and aquatic life [9,10]. These metals are not degradable and are stored in the human body, including fatty and nervous tissues. Their toxicity depends on the dose accumulated in cells [11].

Nowadays, pollution by HMS contaminants is one of the most important environmental problems due to their high toxicity and negative effects on human health. According to the report published by the World Health Organization. Drinking water with high concentrations of HMs has the potential to cause critical diseases such as cancer [12].

In the current study, the concentrations of heavy metals (Cr, Cd, Cu, Ni, Mn, Fe, and Zn) in the groundwater of Rada'a City were determined and the health risk was evaluated. Groundwater samples were analyzed using inductively coupled plasma optical emission spectrometry (ICP-OES).

2. Materials and Methods

2.1 Sampling Area

Rada'a City is the largest city in Al-Baida'a governorate and has a population of 56,383 according to the 2004 census. It is located at 14 º 24´ N 45 º 50 ´ E, southeast of the capital Sana'a, and has an average elevation of 2.25 km above sea level. Rada'a has a semi-arid climate with significant temperature variations between summer and winter. The sampling sites are listed in Table 1 and Figure 1. Physicochemical parameters and the concentration of HM were measured at 10 wells.

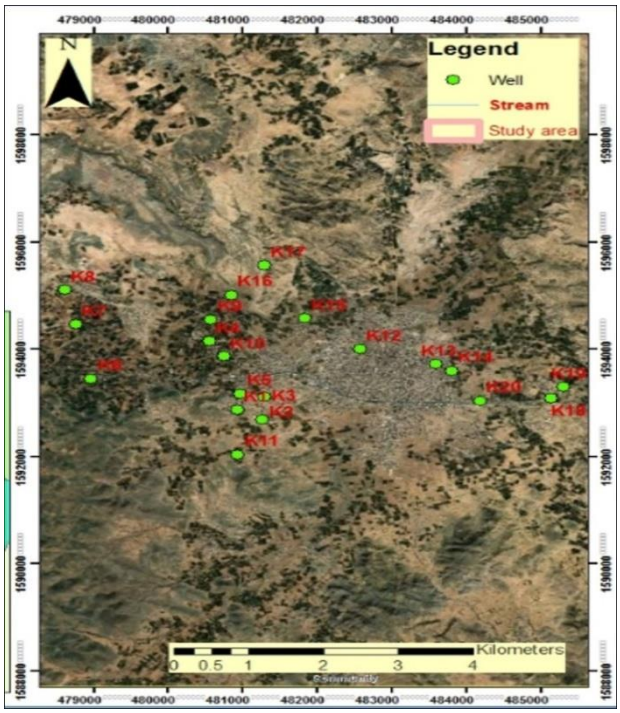

Figure 1: Map of well water sampling sites.

2.2 Sample Collection and Preparation

Samples were collected in December 2019 at various locations in separate polyethylene bottles for measurement of selected HMs (Cr, Cd, Cu, Ni, Mn, Fe, and Zn). Approximately 2 ml of 65% HNO_3 was added to prevent precipitation of the metals. The samples were then labeled, sealed, and transported to the laboratory, where they were stored in a cooler at a suitable temperature of 4 °C. The samples were then stored in a refrigerator at 4 °C until the analysis was completed [6,15,16].

Table 1: Locations of Sampling Sites.

Area	Code of sample	Latitude	Longitude
Alhugah	K1	14°24`29``	44°49`23``
Almuslaa	K3	14°24`37``	44°49`35``
Althybanaa	K4	14°25`11``	44°49`10``
Aljaf	K6	14°24`48``	44°48`17``
Waddi-Alkath	K8	14°25`42``	44°49`05``
Alashaa	K9	14°25`24``	44°49`11``
Alqusier	K12	14°25`06``	44°50`18``
Alsafaa	K15	14°25`25``	44°49`53``
Alkhathra	K17	14°25`57``	44°49`35``
Kaa Rada'a	K18	14°24`34``	44°51`11``

2.3 Measurement Technique

In this study, inductively coupled plasma optical emission spectrometry (ICP-OES) fabricated (VISTAMPX CCD simultaneous ICP - OES, VARIAN SPS model (EL 05063632) with argon (99.99%) as carrier gas was used to determine 7 elements in the groundwater samples. From the standard raw solution, the samples were treated with ICP-OES equipment at the maximum wavelength of each of the elements in which the standard treatment of the standard solution and form as testing the samples analyzed.

2.4 Measurement of water physicochemical parameters

Physicochemical parameters such as pH, electrical conductivity (EC) in micro-Siemens per cm (µS/cm), total dissolved solids (TDS) in (mg /l), and temperature (T) in ˚C of the samples were measured on-site using a portable pH meter. 0.5 L of the water sample was used to determine the physicochemical parameters, TDS, T, and EC [17]. The techniques used for using a portable multiparameter meter, model EC59, CE. The pH was measured using the pocket pH meter, model 107, CE. Measurements were taken three times and the average was recorded.

2.5 HMs Health Risk Assessment

In recent years, health risk assessment of the carcinogenic and non-carcinogenic effects of heavy metals in the human body has been conducted using methods adopted by the US Environmental Protection Agency (USEPA) in 2004. Health risk indices (HRI), hazard indices (HI) and probability of cancer risk (PCR) have been studied by many researchers [8,18].

2.5.1 Chronic daily intake (CDI) indices

Heavy metals enter the human body via several routes, including ingestion, skin contact, and inhalation, but compared to oral intake, all other routes are negligible. The CDI risks arising from the ingestion of a single trace element are calculated for the adult population as follows [19,20]:

$$CDI = \frac{A_w \times IRW \times EF \times ED}{BW \times AT} \quad (1)$$

where CDI is the chronic daily intake, also referred to as the exposure dose (mg/(kg. Day); Aw represents HM concentration in water (mg/l); IRW represents water intake rate (IRW equals 2l for adults); EF is used to denote exposure

frequency (EF equals 365 days per year); ED represents exposure duration (adults ED = 70 years); BW is body weight (equals 70 kg for adults); AT represents average exposure duration (equals 25,550 days).

2.5.2 Non-Carcinogenic Health Risk Assessment

The health risk indices (HRI) of a single element in each sample are evaluated [3,18,21,22]:

$$HRI = CDI/RfD \quad (2)$$

where RfD represents the reference dose of a particular element (mg/kg/day). The RfD equivalent for the heavy metals is 0.7 (Fe), 0.3 (Zn), 1.5 (Cr), 0.046 (Mn), 0.04 (Cu), 0.001 (Cd), and 0.02 (Ni) [20,23]. Whereas: HRI1 indicates no significant health risks; HRI ≥ 1 indicates significant health risks, which increase with increasing value of HRI [24]. The final value for the evaluation of noncarcinogenic risk is the hazard index (HI), which is the sum of the HRI values in each sample [25,26]:

$$HI = \sum HQ = HQ_{Cr} + HQ_{Cd} + HQ_{Cu} + HQ_{Mn} + HQ_{Ni} + HQ_{Fe} + HQ_{Zn} \quad (3)$$

HI is greater than one (HI ≥ 1), it means that the non-carcinogenic health risk of ingesting a particular element is above the permissible limits, while HI < 1 means that they are below the permissible limits [20].

2.5.3 Carcinogenic Health Risk Assessment.

The probability of cancer risk (PCR) for groundwater resources was estimated as an individual's incremental lifetime risk of developing cancer from exposure to a potential carcinogen. The PCR for each carcinogenic metal is calculated as follows [27,28]:

$$PCR = CDI \times CSF \quad (4)$$

where CDI was calculated using equation (1) and CSF is the cancer slope coefficient (mg/(kg. Day)) [29]. The acceptable health risk threshold is one in a million (1×10^{-6}), which means that one person in a million is likely to develop cancer if they drink well water contaminated with HMs [30]. However, it has been reported that a risk in the range of 1×10^{-6} to 1×10^{-4} is usually considered acceptable [31,32]. In this study, the CSF values used to calculate the PCR of heavy metals (carcinogens) are as follows: Cr (0.05), Cd (0.38), and Ni (0.91) [20].

3. Result and Discussion

3.1 Physicochemical parameter analysis

The results of the physicochemical parameters measured for the well water samples are shown in Table 2. The temperature varied from 25.3 to 36.3 °C with an average value of 30.17 °C from the 10 sites. T above the permissible limits of WHO. High water temperature promotes the growth of microorganisms and can exacerbate problems related to taste, odor, color, and corrosion. In addition, contaminants may become more toxic at higher temperatures, which could be due to the increase in their water solubility [33,34]. The pH ranged from 6.5 to 7.3 with an average value of 6.8 from the 10 sites. From this, it can be seen that all well water samples have pH values within the recommended WHO. High temperature and low pH can lead to increased toxicity of metals and radionuclides in the water. The chemical and biogeochemical processes that lead to a decrease in pH favor the dissolution of radionuclides and heavy metals into the water system at high concentrations [33]. The TDS content of the well water also varied from 422 to 895 mg/l, with the average value of the 10 sites being 578.9 mg/l. From the results, all well water samples had a TDS content that was within the minimum value of 600 mg/l recommended by WHO [35]. TDS concentrations in water vary considerably in different geological regions due to differences in mineral solubility [33]. Electrical conductivity (EC) is related to the concentrations of ions that can conduct electric current. Therefore, EC represents an estimate of TDS [34]. EC ranged from 839 to 1785 µs/cm with an average value of 1152 µS/cm for the 10 sites.

3.2 Heavy Metals Concentration analysis

Surmont of HM concentration, as shown in Table 3, while the concentration of cadmium (Cd) and Cr were below the detection limit (ICP - OE). The detection limit for Cd was 0.05 mg/l, which may be higher than the respective allowable limits (0.003 mg/l) in all samples. Cd causes skeletal disorders, liver damage, cardiovascular disease, dysfunction of the sex glands, and disturbs mineral balance in the body. Chronic Cd exposure can cause harmful effects such as lung cancer, proliferative lesions of the prostate, bone fractures, renal dysfunction, and hypertension [7]. In this study, the method detection limit for Cr in all samples was 0.07 mg/l, which may be lower than the respective permissible limits (0.05 mg/l). High concentrations of chromium (Cr) may be responsible for non-cancerous health risks such as neurological disorders, headache, and liver disease [7]. In general, the order of average concentration of selected metals in groundwater samples was Fe, Mn, Zn, Ni, and Cu in the vicinity of the study area.

Table 2: The physicochemical parameters.

No	Location of Sampling	T (°C)	pH	TDS (mg/l)	EC (µS/cm)
1	Alhugah	33.7	7.0	422	839
2	Almuslaa	35	6.7	507	1013
3	Althybanaa	28.5	6.5	700	1387
4	Aljaf	36.3	7.3	432	867
5	Waddi-Alkath	26	6.7	497	994
6	Alashaa	26.4	6.8	686	1344
7	Alqusier	25.3	6.8	492	987
8	Alsafaa	22. 7	6.8	895	1785
9	Alkhathra	25.0	6.8	766	1532
10	Kaa Rada'a	24.7	7.1	385	774
Min		**25.3**	**6.5**	**422**	**839**
Max		**36.3**	**7.3**	**895**	**1785**
SD		**4.681**	**0.237**	**165.5**	**325.9**
Average		**30.17**	**6.825**	**578.9**	**1152**
Permissible limits WHO		**25**	**6.5 – 8.5**	**600 – 1000**	**1000 – 1200**

The concentration of copper (Cu) in the drinking water samples ranged from 0.00767 to 0.01372 mg/l, with an average of 0.01035 ± 0.00221 mg/l, as shown in Figure 2. Cu in very high concentrations is toxic and can cause vomiting, diarrhea, loss of strength, and liver cirrhosis. The water turns blue-green when the corroded copper dissolves from inside the pipes and appears as a precipitate in the water [36]. The concentration of nickel (Ni) in drinking water samples ranges from 0.00694 to 0.05821 mg/l, with an average concentration of 0.01702 ± 0.01497 mg/l, as shown in Figure 3. (Ni) is a metal that is widely distributed on the earth's surface. This metal is present in food and drinking water as a result of natural and anthropogenic activities. Ni has a biological function but is toxic in larger amounts; nickel salts cause allergies and even cancer [11].

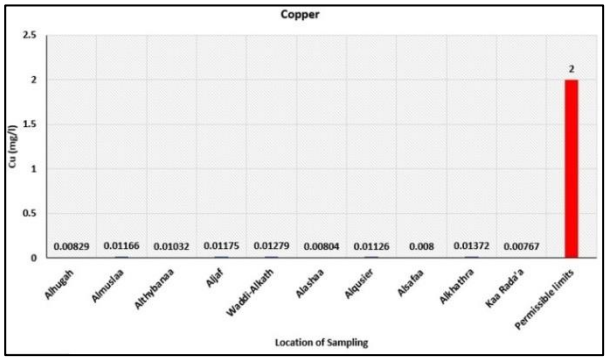

Figure 2: Copper concentrations in location of samples.

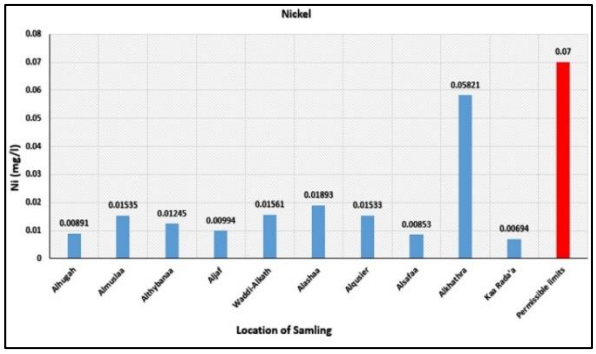

Figure 3: Nickel concentrations in location of samples.

Iron deficiency causes a disease called “anemia", and prolonged consumption of drinking water with high iron concentration can lead to a liver disease called hemosiderosis [37]. It can cause a metallic taste in drinking water, and exposure to high Fe concentrations has adverse effects on target organs such as the liver, cardiovascular system, and kidneys [36]. In the studied locations, the concentration of iron (Fe) in drinking water samples ranged from 0.00602 mg/l to 1.6778 mg/l, with an average value of 0.42567 ± 0.55929 mg/l. As can be seen in Figure 4, Fe concentration in Amuslan, Althybanaa, and Aljafand Alkhathra localities is above the respective permissible limits, which is probably due to the corrosion of steel and cast-iron pipes during water distribution [35].

Mn concentration in drinking water samples ranged from (below detection limit) BDL mg/l to 0.07692 mg/l, with an average of 0.0440 ± 0.0271 mg/l, as shown in Figure 5. The Mn concentration is below the respective permissible limits in all samples. The concentration of zinc (Zn) in the drinking water samples ranged from 0.00181 mg to 0.08524 mg/l, with an average concentration of 0.03652 ± 0.02579 mg/l. As can be seen in Figure 6, the Zn concentration in all samples is below the respective permissible limits. Zn is an important trace element that plays a crucial role in the physiological and metabolic processes of many organisms. Nevertheless, higher concentrations of zinc can be toxic to organisms [6].

3.3 Health Risk Assessment from Heavy Metals Concentration

3.3.1 Chronic daily intake (CDI) indices analysis

The heavy metals CDI were found in the order Fe > Mn > Zn > Ni > Cu by consuming well water. However, CDI levels for Fe, Mn, Zn, Ni, and Cu in all samples were below the respective RfD limit established by the USEPA.

The lowest observed Cu CDI mg/(kg. Day) was 0.000219, while the highest observed Cu CDI mg/(kg. Day) was 0.00039 with an average of 0.000293 ± 0.00006 mg/(kg. Day), The range of Ni for (CDI mg/(kg. Day)) was from 0.000198 to 0.00166, with an average of 0.000486 ± 0.000427 mg/(kg. Day) by drinking water consumption, as shown in Table 4. The lowest observed Mn CDI value was 0.00074 mg / (kg. Day), while the highest observed Mn CDI value was 0.0022 mg/(kg. Day) with an average of 0.00125 ± 0.00077 mg / (kg. Day) by consumption of drinking water. The range for Fe (CDI mg / (kg. Day)) was from 0.000302 to 0.0479, with an average of 0.01231 ± 0.015848 mg/(kg. Day) by consumption of drinking water. The lowest observed Zn-CDI mg/(kg. Day) was 0.00005, while the highest observed Zn-CDI was 0.00251 mg/(kg. Day) with an average of 0.00105 ± 0.000753 mg/(kg. Day) by consumption of drinking water.

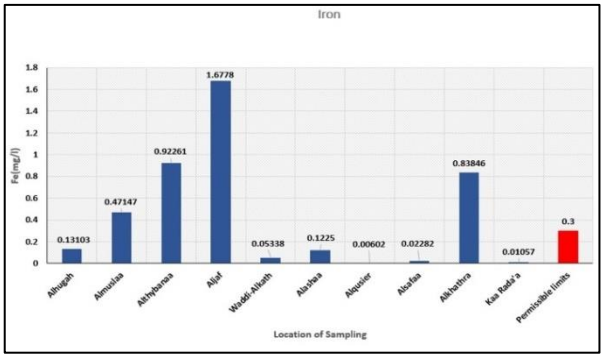

Figure 4: Iron concentrations in location of samples.

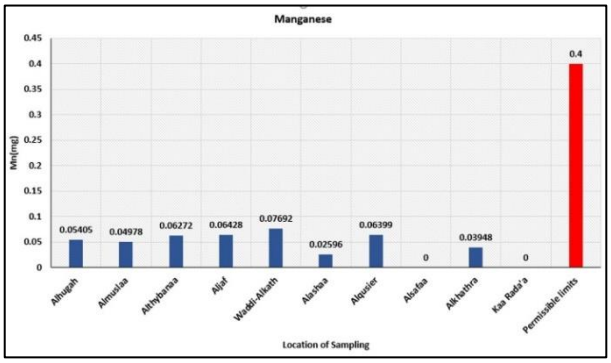

Figure 5: Manganese concentrations in location of samples.

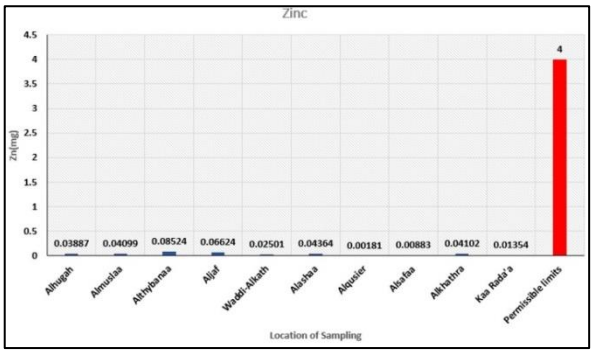

Figure 6: Zinc concentrations in location of samples.

3.3.2. Non-Carcinogenic Health Risk Assessment

As shown in Table 5, HRIs were found in the order of Mn, Ni, Fe, Cu, and Zn. The HRIs for all heavy metals indicate that there is no risk to the local population, indicating a low concentration of heavy metals. As can be seen in Table 5, the HRI for Mn, Fe, Cu, and Zn are less than 1 for all samples, indicating that there is no potential health risk from the concentration of heavy metals in drinking water. Compared with [36], the HRI of Fe, Ni, Cu, Mn, and Zn tended to be higher than the values reported for drinking water in this work and in [3,38]. To evaluate the total potential health risk posed by more than one heavy metal, the Hazard Index (HI) was used. (HI) is the sum of all health risk indices (HRI) calculated for individual heavy metals as shown in Figure 7. In Figure 7, all selected heavy metals were found in each sample, HI was lower than 1 which means that they are below their respective acceptable limits in all samples. There is no non-carcinogenic risk. There is no potential health risk from HM concentration due to the consumption of drinking water in the study area. As shown in Table 5, HRI were found in the order of Mn > Ni > Fe > Cu > Zn. The HRI for all heavy metals indicates that there is no risk to the local population, indicating low concentration of heavy metals. As can be seen in Table 5, the HRI for Mn, Fe, Cu and Zn in all samples are below < 1, indicating that there is no potential health risk from the concentration of heavy metals in drinking water. Compared to [36], the HRI of Fe, Ni, Cu, Mn and Zn tended to be higher than the values reported for drinking water in this work and in [3, 38].

Table 4: Chronic daily intakes (CDI) (mg/kg per day) of trace elements through drinking water.

No.	Location of Sampling	Cr	Cd	Cu	Ni	Mn	Fe	Zn
1	Alhugah	NC	NC	0.00023	0.000254	0.00154	0.00374	**0**.00111
2	Almuslaa	NC	NC	0.00033	0.000438	0.00142	0.0135	0.00117
3	Althybanaa	NC	NC	0.00029	0.000356	0.00179	0.0264	0.00251
4	Aljaf	NC	NC	0.00034	0.000284	0.00184	0.0479	0.00189
5	Waddi-Alkath	NC	NC	0.00036	0.000446	0.00220	0.00153	0.00071
6	Alashaa	NC	NC	0.00023	0.000541	0.00074	0.00350	0.00125
7	Alqusier	NC	NC	0.00032	0.000438	0.00183	0.00172	0.00005
8	Alsafaa	NC	NC	0.00023	0.000244	NC	0.000652	0.000252
9	Alkhathra	NC	NC	0.00039	0.00166	0.00113	0.0239	0.001172
10	Kaa Rada'a	NC	NC	0.00022	0.000198	NC	0.000302	0.000387
Min		**NC**	**NC**	**0.00022**	**0.000198**	**NC**	**0.000302**	**0.00005**
Max		**NC**	**NC**	**0.00039**	**0.00166**	**0.0022**	**0.0479**	**0.00251**
SD		**NC**	**NC**	**6.26E-05**	**0.000427**	**0.00077**	**0.01585**	**0.00075**
Average		**NC**	**NC**	**0.00029**	**0.000486**	**0.00125**	**0.01231**	**0.00105**
Permissible limits WHO		**1.5**	**0.001**	**0.04**	**0.02**	**0.046**	**0.7**	**0.3**

NC: Not Calculated, **SD:** Standard Deviation.

Table 5: Health risk indices (HRI) for different elements in the studied areas through drinking water.

No.	Location of Sampling	Cr	Ni	Mn	Fe	Zn
1	Alhugah	0.00575	0.0127	0.0335	0.00534	0.00370
2	Almuslaa	0.00825	0.0219	0.0039	0.0192	0.00390
3	Althybanaa	0.00725	0.0178	0.0389	0.0377	0.00837
4	Aljaf	0.00840	0.0142	0.0400	0.0684	0.00630
5	Waddi-Alkath	0.00900	0.0223	0.0478	0.00218	0.00273
6	Alashaa	0.00575	0.0270	0.0161	0.00500	0.00417
7	Alqusier	0.00800	0.0219	0.0398	0.00025	0.00017
8	Alsafaa	0.00575	0.0122	NC	0.00093	0.00084
9	Alkhathra	0.00975	0.0830	0.0246	0.0342	0.0039
10	Kaa Rada'a	0.00547	0.00990	NC	0.00043	0.00129
Min		**0.00547**	**0.0099**	**NC**	**0.00025**	**0.000173**
Max		**0.00975**	**0.083**	**0.0478**	**0.0684**	**0.00837**
SD		**0.00157**	**0.0213**	**0.0183**	**0.0228**	**0.0025**
Average		**0.007337**	**0.0243**	**0.0245**	**0.01736**	**0.0035**
Permissible limits WHO		**1**	**1**	**1**	**1**	**1**

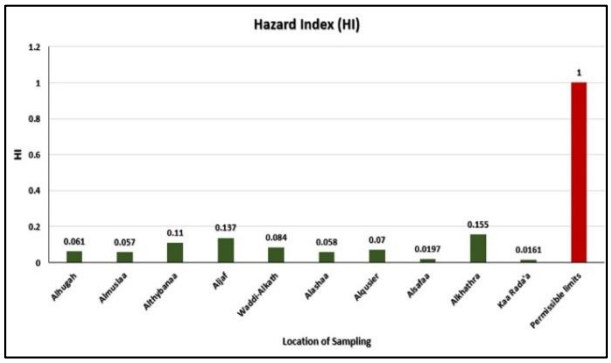

Figure 7: Hazard Index (HI) of HMs in location of samples.

3.3.3 Carcinogenic Health Risk Assessment

PCR calculated by drinking water and the results are shown in Figure (8). The probability of cancer risk of (Ni) for the adult population and based on the allowable range for cancer risk of ≤ 1 × 10^{-6} to 1 × 10^{-4} [31,32,39]. The lowest PCR was observed at 1.80× 10^{-4}, while the highest PCR was observed at 1.51× 10^{-3} with an average of 4.42 × 10^{-4} ± 4.42 × 10^{-4} from drinking water consumption. Other works in similar found in values lower than those of the study [30] in Iran the PCR for HMs carcinogenic in this study were determined Cd (5.1 ×10^{-9}), Cr (7.8 ×10^{-7}) and Ni (1.4 ×10^{-8}).

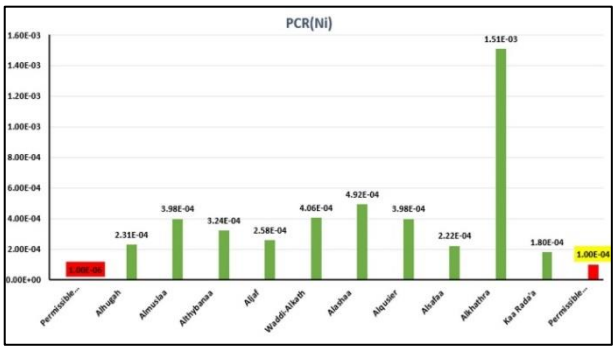

Figure 8: Hazard Index (PCR) of Ni in location of samples.

Table 6: Results of the Pearson correlation coefficient analysis between HMs (mg/l) and physicochemical parameters in the well water samples.

	T	PH	TDS	EC	Cu	Ni	Mn	Fe	Zn
T	1								
PH	0.3437	1							
TDS	-0.4851	**-0.6252**	1						
EC	-0.4881	**-0.6340**	**0.999**	1					
Cu	-0.1073	-0.1647	**0.579**	**0.5713**	1				
Ni	-0.1720	0.0401	**0.529**	**0.5097**	**0.6071**	1			
Mn	0.3819	-0.0069	0.127	0.1224	**0.6688**	0.0475	1		
Fe	0.0295	**-0.5639**	**0.795**	**0.7992**	0.4725	0.2181	0.3723	1	
Zn	**0.5931**	-0.3133	0.311	0.3121	0.2080	0.0808	0.4052	**0.7717**	**1**

The results obtained for HMs in water were compared with the studies of other researchers worldwide, as shown in Table 6. The lowest concentration of HMs was found in Egypt, Iran, and India (2017). Chin (2020) and Yemen (2016), the highest were found in Nigeria (2009 and 2017), India (2019), Iraq (2023), Libya (2022), and Saudi Arabia (2018), but the concentration of Zn was below the acceptable limit and in Yemen (Rada'a), the highest concentration of Fe was above the acceptable limit, but the concentration of Cu, Mn and Zn were below the acceptable limit.

3.4 Statistical Analysis

To evaluate the physical and chemical factors that may affect the source and mobility of HMs concentration in the well water of the study area, the relationship correlation was used to determine correlations between physicochemical parameters and HMs concentration [48]. Pearson correlation is used to determine linear correlations between different parameters and HMs as pairs in drinking water samples. Table 7 shows the Pearson correlation between heavy metals (Cu, Ni, Mn, Fe and Zn) and physicochemical parameters (temperature), PH, electrical conductivity (EC) and total dissolved solids (TDS) in groundwater. As showed a positive moderate correlation with T-Zn (0.5931). However, there was a weak correlation with the other elements. PH showed a negative moderate correlation with PH - TDS (0.6252), PH - EC (0.6340), and PH -Fe (0.5639). TDS showed positive strong correlation with TDS- EC (0.999) and moderate correlation with TDS — Cu (0.5792), TDS-Ni (0.5287) and strong correlation with TDS-Fe (0.79541).

Al loading in factor 1 showed positive correlation with Cu, Ni, Mn, Fe and Zn, indicating that these elements are directly derived from rock weathering [45]. EC showed positive moderate correlation with EC - Cu (0.5713), EC – Ni (0.5097) and strong correlation with EC — Fe (0.7992). Cu showed a positive moderate correlation with Cu -Ni (0.6071) and Cu — Mn (0.6687). Fe showed positive strong significant correlation with Fe — Zn (0.7717). These results can show that the elements measured in the present study have almost similar sources and the related sources can be associated with the geographical structure of the selected study area [30,45]. The pollution by HMs is significant due to weathering of rocks, fertilizers, and pesticides in the groundwater of the study area.

Table 6: Comparison of HMs concentration(mg/l) in groundwater with values taken from the open literature.

Country	Average concentration HMs in mg/ l							Reference
	Cr	Cd	Cu	Ni	Fe	Mn	Zn	
Nigeria	ND	ND	0.18	ND	0.71	ND	3.2	**[40]**
Yemen	ND	ND	ND	ND	0.01	0.005	ND	**[41]**
India	ND	ND	0.003	ND	0.051	0.227	0.342	**[42]**
Nigeria	ND	ND	0.17	ND	ND	0.43	ND	**[43]**
Iran	ND	ND	0.03	ND	ND	ND	0.04	**[15]**
Saudi Arabia	ND	ND	0.298	0.053	0.041	ND	ND	**[44]**
India	0.0369	0.0033	0.0527	0.0128	0.86426	0.1939	0.0877	**[45]**
Egypt	0.018	0.016	0.021	0.015	ND	ND	0,154	**[27]**
Iran	0.590	0.026	0.461	0.525	0.269	4.965	0.947	**[30]**
Iraq	0.055	0.0163	0.185	0.076	0.3	ND	0.45	**[46]**
China	0.68×10^{-3}	0.02×10^{-3}	0.57×10^{-3}	0.56×10^{-3}	0.63×10^{-3}	2.07×10^{-3}	0.79×10^{-3}	**[29]**
Libya	ND	ND	0.09	0.35	1.28	0.42	ND	**[47]**
Yemen	BDL	BDL	0.01035	0.01702	0.42567	0.00440	0.03682	**Present study**

ND: do not Detected, **BDL**: Below Detection Limits

4. Conclusion

Based on the results obtained in this study, the following were found:

1. The physicochemical parameters such as T were higher than the permissible limits of WHO, PH, TDS and EC were within the recommended WHO.
2. The average concentration of HMs in the water samples were Fe (0.426±0.559) Mn (0.044±0.026) Zn (0.036±0.026) Ni (0.017±0.0151) Cu (0.0103±0.002) mg/l, the concentrations of Cr, Cu, Mn, Ni and Zn were lower than the respective permissible limits in all the samples, but the concentration of Cd found was higher than the respective permissible limits.
3. In all samples, the concentration of Fe was higher than the respective permissible limits in four locations.
4. Non-carcinogenic health risk, while HRI and HI were lower than the permissible limits for the consumer (1), which means that there is no potential health risk from HM concentration in drinking water, but it can be concluded that the risks are not present, as possible exposure to HM through food and skin may also pose a risk.
5. Carcinogenic health risk, while the detected levels (PCR) in ten locations were higher than the safe levels, so there is a potential carcinogenic health risk from HM in drinking water. It is recommended to filter the water before using it as drinking water.
6. Correlation coefficient between HM concentrations and some physicochemical parameters as pairs in drinking water samples. Strong correlation with TDS — EC (0.999), TDS-Fe (0.79541), EC - Fe (0.79541), Fe — Zn (0.77174).
7. Therefore, this study recommends the government and other responsible agencies to:
   a) Implement appropriate drinking water treatment techniques that can reduce the current heavy metal levels,
   b) Educate the population to better storage of drinking water.
   c) Support the conduct of further studies on the health risks of the heavy metals Pb, As, Se, Co, and Hg to determine their contamination in air, rock, water, and soil samples.

Acknowledgments

The authors would like to thank the residents of the study area for their cooperation during the fieldwork, and we would like to thank all those who assisted us.

References

[1] Kamali Maskooni, E., Naseri-Rad, M., Berndtsson, R., Nakagawa, K. (2020) Use of heavy metal content and modified water quality index to assess groundwater quality in a semiarid area, *Water* **12**: 1115.

[2] Adewoyin, O., Kayode, O., Omeje, O., Odetunmibi, O. (2019) Risk assessment of heavy metal and trace elements contamination in groundwater in some parts of Ogun state, *Cogent Engineering* **6**: 1632555.

[3] Hussain, S., Habib-Ur-Rehman, M., Khanam, T., Sheer, A., Kebin, Z., Jianjun, Y. (2019) Health risk assessment of different heavy metals dissolved in drinking water, *International journal of environmental research and public health* **16**: 1737.

[4] Liu, Y., Ma, R. (2020) Human health risk assessment of heavy metals in groundwater in the luan river catchment within the north China Plain, *Geofluids* **2020**.

[5] Idode, L., Mahmoud, A., Hamza, Y. (2021) Determination of Heavy Metals in Hand Dug Well Water near Dumpsite in Fadaman Mada Bauchi*, Indiana Journal of Humanities and Social Sciences* **2**: 27-31.

[6] Cobbina, S.J., Duwiejuah, A.B., Quansah, R., Obiri, S., Bakobie, N. (2015) Comparative assessment of heavy metals in drinking water sources in two small-scale mining communities in northern Ghana, *International journal of environmental research and public health* **12**: 10620-10634.

[7] Hassan, M., Ngadda, Y.H., Adamu, A. (2020) Health Risk Assessment of some Heavy Metals in Drinking Water Due to Mining Activities in Gombe Area, Northeastern Nigeria, *Journal of Environmental Science, Toxicology and Food Technology* **14**: 37-42

[8] Yahaya, T.O., Oladele, E.O., Fatodu, I.A., Abdulazeez, A., Yeldu, Y.I. (2021) The concentration and health risk assessment of heavy metals and microorganisms in the groundwater of Lagos, Southwest Nigeria, *Journal of Advances in Environmental Health Research* **8**: 234-242.

[9] Kumar, A., Kaur, M., Mehra, R., Sharma, D.K., Mishra, R. (2017) Comparative study of radon concentration with two techniques and elemental analysis in drinking water samples of the Jammu district, Jammu and Kashmir, India, *Health Physics* **113**: 271-281.

[10] Mirzabeygi, M., Abbasnia, A., Yunesian, M., Nodehi, R.N., Yousefi, N., Hadi, M., Mahvi, A.H. (2017) Heavy metal contamination and health risk assessment in drinking water of Sistan and Baluchistan, Southeastern Iran, *Human and Ecological Risk Assessment: An International Journal* **23**: 1893-1905.

[11] Seleem, E.M., Mostafa, A., Mokhtar, M., Salman, S.A.

(2021) Risk assessment of heavy metals in drinking water on the human health, Assiut City, and its environs, Egypt, *Arabian Journal of Geosciences* **14**: 1-11.

[12] Virk, H.S. (2019) Heavy Metals Contamination of Groundwater in Patiala District of Punjab State, India, *Research & Reviews: A Journal of Toxicology* **9**: 34-42.

[13] Ahmad, N., Uddin, Z., Rehman, J.u., Bakhsh, M., Ullah, H. (2020) Evaluation of radon concentration and heavy metals in drinking water and their health implications to the population of Quetta, Balochistan, Pakistan, *International Journal of Environmental Analytical Chemistry* **100**: 32-41.

[14] Jidele, P., Dosunmu, O., Ajayi, K., Ademola, A. (2021) Measurement of radon and heavy metal concentrations in groundwater around Ota, Ogun State, Nigeria.: Radon and heavy metal in water, *EQA-International Journal of Environmental Quality* **42**: 42-49.

[15] Rezaei, A., Hassani, H., Jabbari, N. (2019) Evaluation of groundwater quality and assessment of pollution indices for heavy metals in North of Isfahan Province, Iran, *Sustainable Water Resources Management* **5**: 491-512.

[16] Al Sabahi, E., Al Nozaily, F.A., Abdullhafez, S. (2015) Evaluation of Groundwater Quality for Drinking Water by Using Physico-chemical Analysis in the City of Ibb, Yemen, *British Journal of Applied Science & Technology* **5**: 425-435.

[17] Srilatha, M., Rangaswamy, D., Sannappa, J. (2014) Studies on concentration of Radon and Physicochemical parameters in ground water around Ramanagara and Tumkur districts, Karnataka, India, *International Journal of Advanced Scientific and Technical Research* **2**: 641-660.

[18] Sheikhi Alman Abad, Z., Pirkharrati, H., Mojarrad, M. (2021) Health risk assessment of heavy metals in the soil of angouran mineral processing complex in iran, Pollution 7: 241-256.

[19] Ganesh, D., Kumar, G.S., Najam, L.A., Raja, V., Neelakantan, M., Ravisankar, R. (2020) Uranium quantification in groundwater and health risk from its ingestion in and around Tiruvannamalai, Tamil Nadu, India, *Radiation protection dosimetry* **189**: 137-148.

[20] Ukah, B., Egbueri, J., Unigwe, C., Ubido, O. (2019) Extent of heavy metals pollution and health risk assessment of groundwater in a densely populated industrial area, Lagos, Nigeria, *International Journal of Energy and Water Resources* **3**: 291-303.

[21] Ahmad, N., Jaafar, M., Nasir, T., Rafique, M. (2018) Determination of radon concentration and heavy metals (Ni, Pb, Cd, As, Cr) in drinking and irrigated water sampled from Kulim, Malaysia, *International Journal of Radiation Research* **16**: 341-349.

[22] Muhammad, S., Shah, M.T., Khan, S. (2011) Health risk assessment of heavy metals and their source apportionment in drinking water of Kohistan region, northern Pakistan, *Microchemical Journal* **98**: 334-343.

[23] Khokhar, L.A.K., Khuhawar, M.Y., Jahangir, T.M., Arain, G.M., Khokhar, F.M., Khaskheli, M.I., Khan, S., FarooqueLajwani, M., Abro, M.I., Zounr, Z.A. (2023) Prosperity risk assessment by heavy metal contamination on human health and multivariate statistical analysis of groundwater as a drinking source, *Arabian Journal of Geosciences* **16**: 136.

[24] El Wasif, A.E.S., El Dafrawy, S.M., Moalla, S., El Defrawy, M. (2019) Health risk assessment of dissolved heavy metals in some selected water samples: Dakahlia, Egypt, *International Journal of Applied Chemistry* **15**: 15-19.

[25] Ghaderpoori, M., Kamarehie, B., Jafari, A., Alinejad, A.A., Hashempour, Y., Saghi, M.H., Yousefi, M., Oliveri Conti, G., Mohammadi, A.A., Ghaderpoury, A. (2020) Health risk assessment of heavy metals in cosmetic products sold in Iran: the Monte Carlo simulation, *Environmental Science and Pollution Research* **27**: 7588-7595.

[26] Rahman, M.M., Bodrud-Doza, M., Muhib, M.I., Hossain, K.F.B., Sikder, M., Shammi, M., Akter, R., Uddin, M.K. (2020) Human health risk assessment of nitrate and trace metals via groundwater in Central Bangladesh, *Pollution* **6**: 253-266.

[27] Abdelhalim, A., Howard, G., Howden, N.J., Ahmed, M., Ismail, E. (2023) Carcinogenic and non-carcinogenic health risk assessment of heavy metals contamination in groundwater in the west of Minia area, Egypt, *Human and Ecological Risk Assessment: An International Journal* **29**: 571-596.

[28] Niknejad, H., Saeedi, R., Hosseini, S.A., Abedi Sarvestani, R., Abtahi, M., Hesami Arani, M., Babanezhad, E., Gholami-Borujeni, F. (2023) Health risk assessment of heavy metals in drinking water: a case study in western cities of Mazandaran province, Iran, *International Journal of Environmental Analytical Chemistry* **104**: 1-16.

[29] Qiao, J., Zhu, Y., Jia, X., Niu, X., Liu, J. (2020) Distributions of arsenic and other heavy metals, and health risk assessments for groundwater in the Guanzhong Plain region of China, *Environmental research* **181**: 108957.

[30] Lorestani, B., Merrikhpour, H., Cheraghi, M. (2020) Assessment of heavy metals concentration in groundwater and their associated health risks near an industrial area, *Environmental Health Engineering and Management Journal* **7**: 67-77.

[31] Mohammadi, A.A., Zarei, A., Majidi, S., Ghaderpoury, A., Hashempour, Y., Saghi, M.H., Alinejad, A., Yousefi, M., Hosseingholizadeh, N., Ghaderpoori, M. (2019) Carcinogenic and non-carcinogenic health risk assessment of heavy metals in drinking water of Khorramabad, Iran, *MethodsX* **6**: 1642-1651.

[32] USEPA (1999) A risk assessment–multi way exposure spread sheet calculation tool, United States Environmental Protection Agency Washington, DC.

[33] Ansah, E. (2015) Assessment of radionuclides activities and heavy metals contamination in sediments, water and fish in Lake Bosomtwi and Bui dam. Chemistry Master Thesis, Kwame Nkrumah University of Science and Technology, Kumasi, Ghana, pp. 120

[34] Al Aizari, H., Lebkiri, A., Fadli, M., Albaseer, S.S. (2017) Quality assessment of ground water in Dhamar City, Yemen, *International Journal of Environment* **6**: 56-71.

[35] WHO (2017) Guidelines for drinking-water quality, 4th ed., World Health Organization, Geneva, pp. 423

[36] Saleh, H.N., Panahande, M., Yousefi, M., Asghari, F.B., Oliveri Conti, G., Talaee, E., Mohammadi, A.A. (2019) Carcinogenic and non-carcinogenic risk assessment of heavy metals in groundwater wells in Neyshabur Plain, Iran, *Biological trace element research* **190**: 251-261.

[37] Mebrahtu, G., Zerabruk, S. (2011) Concentration and health implication of heavy metals in drinking water from urban areas of Tigray region, Northern Ethiopia, *Momona Ethiopian journal of science* **3**: 105-121.

[38] Kavcar, P., Sofuoglu, A., Sofuoglu, S.C. (2009) A health risk assessment for exposure to trace metals via drinking water ingestion pathway, *International journal of hygiene and environmental health* **212**: 216-227.

[39] Pan, Y., Peng, H., Hou, Q., Peng, K., Shi, H., Wang, S., Zhang, W., Zeng, M., Huang, C., Xu, L. (2023) Priority control factors for heavy metal groundwater contamination in peninsula regions based on source-oriented health risk assessment, *Science of The Total Environment* **894**: 165062.

[40] Adefemi, S., Awokunmi, E. (2010) Determination of physico-chemical parameters and heavy metals in water samples from Itaogbolu area of Ondo-State, Nigeria, *African Journal of Environmental Science and Technology* **4**: 145-148

[41] Alhababy, A.M. (2016) Groundwater Quality Assessment and Resources in Sana'a City, Yemen, *Aljouf University Science and Engineering Journal* **3**: 13-18.

[42] Kumar, V., Sharma, A., Kumar, R., Bhardwaj, R., Kumar Thukral, A., Rodrigo-Comino, J. (2020) Assessment of heavy-metal pollution in three different Indian water bodies by combination of multivariate analysis and water pollution indices, *Human and ecological risk assessment: an international journal* **26**: 1-16.

[43] Yusuf, A., Olasehinde, A., Mboringong, M., Tabale, R., Daniel, E. (2018) Evaluation of heavy metals concentration in groundwater around Kashere and its environs, upper Benue trough, Northeastern Nigeria, *Global Journal of Geological Sciences* **16**: 25-36.

[44] Alseroury, F., Almeelbi, T., Khan, A., Barakata, M., Al-Zahrani, J., Alali, W. (2018) Estimation of natural radioactive and heavy metals concentration in underground water, *Journal of radiation research and applied sciences* **11**: 373-378.

[45] Akhtar, N., Syakir, M., Rai, S., Saini, R., Pant, N., Anees, M., Qadir, A., Khan, U. (2020) Multivariate investigation of heavy metals in the groundwater for irrigation and drinking in Garautha Tehsil, Jhansi District, India, *Analytical Letters* **53**: 774-794.

[46] Aziz, F.F., Hussain, E.K. (2023) Spatiotemporal Variation of Heavy Metals and Pollution Indices in Groundwater Around Al-Diwaniyah Open Dump, *Journal of Ecological Engineering* **24**: 106–117

[47] Elmanfe, G.M., Tyeb, T.A., Abdelghani, K.A., Abdulathim, A.A., Asbeeh, J.A., Muftah, H.S., Ali, A.F. (2022) Assessment of Groundwater Wells Pollution by Some Heavy Metals in El-Beida City-Libya, *Journal of Pure & Applied Sciences* **21**: 270-275.

[48] Abdurabu, W.A., Ramli, A.T., Saleh, M.A., Heryansyah, A. (2016) The activity concentrations of 222Rn and corresponding health risk in groundwater samples from basement and sandstone aquifer; the correlation to physicochemical parameters, *Radiation Physics and Chemistry* **127**: 34-41

TuJNaS

Original Article

Thamar University Journal of Natural & Applied Sciences **8**(2) (2023) 11 – 13

DOI: https://doi.org/10.59167/tujnas.v8i2.1712

Allee Rate Effect in a Prey Model with a Holling Type II Functional Response

Omer Saad Ali[1]

[1] Al-Bahaa Primary School, Baghdad, Iraq

Corresponding authors: E-mail: pipe.math@gmail.com (O. S. Ali)

Received: 25 October 2023. Revised (in revised form): 27 November 2023. Accepted 3 December 2023. Published 31 December 2023

Abstract:

In this work, we have built a detailed model of a prey-predator system with mechanical Allee rate and Hollings type II functional response. The model's positive accumulation points' existence, uniqueness, boundaries, and stability analysis are taken into consideration. Numerical simulations are used to discuss Allee's impact on system dynamics.

Keywords: Prey Predator; Allee Effect; Halling Type II; Local Stability; Lyapunov Function

1. Introduction

Population dynamics is one of the most popular topics in biomathematics. A particular area of interest has always been the evolution of different societies, from aggregations of single species to more realistic representations of the coexistence and interaction of numerous species within the same ecosystem. One of the most important and well-researched models for the interaction of living organisms is the prey-predator paradigm. Vito Volterra and Alfred J. Lotka were the first to introduce this approach in 1926 and 1925 respectively [1]. Since Allee and other scientists have studied these models, it has been possible to use systems of ordinary or partial differential equations to represent most predator-prey interactions.

Allee discovered that a person's social desirability increases population growth, which increases density and consequently competition for resources [2]. This study was among the best studies that obtained benefits for population centers by concentrating resources in one place so that growth is conditional. The predator-prey paradigm of the avenue effect on prey growth has also attracted considerable interest. [3, 4, 5, 6, 7, 8, 9]. Longxing Qi and Lijuan Gan also investigated Allee's effects on prey with shelter [10].

In this research, we built a model consisting of a prey-predator, and it contains a response function of type II and Allee strong rate, and the study showed the effect of the Allee rate in the model.

The Halling type II functional response in predator development:

$$\frac{dx}{dt} = xh(x) - yB(x)$$
$$\frac{dy}{dt} = yB(x) - f(y)dy$$

where $h(x) = r\left(1-\frac{x}{k}\right)(x-b)$ and $B(x) = \frac{ax}{1+x}$ The beginning circumstances are x(0) and y(0) > 0. The prey population is represented by x, The predator population is represented by y, the predator mortality rate is represented by f(y), and the conversion efficiency of prey to predator is represented by c. K carrying capacity, h(x) per capita prey growth rate, r prey growth rate specific, b Allee effect threshold, B(x) prey-dependent functional response and a maximal attack rate are all represented. hence, we do:

$$\frac{dx}{dt} = rx\left(1-\frac{x}{k}\right)(x-b) - \frac{axy}{1+x} \quad ,$$
$$\frac{dy}{dt} = \frac{cxy}{1+x} - dy \quad ,$$

all parameters are positive, the average predator loss rate is d.

2. Existence of accumulation point

In this part, we will just look at the system's coexisting accumulation point (1). If the following set of equations has a positive solution, a positive accumulation point $E_1 = (x*, y*)$ exists and is unique within int. R_+^2 in xy space:

$$r\left(1-\frac{x}{k}\right)(x-b) - \frac{ay}{1+x} = 0 \quad , \qquad (1)$$
$$\frac{cx}{1+x} - d = 0 \quad , \qquad (2)$$

Here $*= \frac{d}{c-d}$, $y* = \frac{1+x*}{a}\left(r\left(1-\frac{x*}{k}\right)(x-b)\right)$, For a positive accumulation point, we have $b < x* < k$.

3. Boundedness of the model

Theorem (1): All of the system (1) solutions that start at R_+^2 are uniformly bounded.

Proof.

Assume that $(x(t), y(t))$ be any solution to the system (1) with the initial conditions (x(0), y(0)) being non-negative, describe the function:

$$M(t) = x(t) + \frac{a}{c}y(t) \, . \qquad (3)$$

Therefore, we are derivative equation (3),

$\frac{dM}{dt} = rx\left(1-\frac{x}{k}\right)(x-b) - \frac{axy}{1+x} + \frac{a}{c}\left(\frac{cxy}{1+x} - dy\right)$,
Now $0 \le x \le 1$, we have:

$\frac{dM}{dt} < r\left(1+\frac{b}{k}\right)x^2 - brx - \frac{ad}{c}y$,
$\frac{dM}{dt} < r\left(1+\frac{b}{k}\right) - brx - \frac{ad}{c}y$,
$\frac{dM}{dt} = H - n\,M$.

where $n = \min\left\{br, \frac{ad}{c}\right\}$, and $H = r\left(1+\frac{b}{k}\right)$

$$M(t) \le \frac{H}{n} + \left(M(0) - \frac{2}{n}\right)e^{-nt} \quad .$$

Thus $0 \le M(t) \le \frac{2}{n}$,as $t \to \infty$. As a result, the proof is successful since all solutions to system (1) are uniformly bounded.

4. Local Stability Analysis

In this section, we study the local stability of the model (1) around positive accumulation points, and it is fairly simple to construct the Jacobian matrix J(x,y) of the system (1) by computing the Jacobian matrix J(x,y) and the eigenvalues of system (1) at each of them.

$$J_1 = J(E) = \begin{pmatrix} f_1 f_2 \\ f_3 f_4 \end{pmatrix}$$

where:

$$f_1 = -2\frac{r}{k}x*^2 + rx*\left(1+\frac{b}{k}\right) + \frac{ax*y*}{(1+x*)^2} \quad , \quad f_2 = \frac{-ax*}{1+x*}$$
$$f_3 = \frac{cy*}{(1+x*)^2} \quad , \quad f_4 = 0$$

Then the distinctive equation of $J(E_1)$ is given by:

$\lambda^2 + U_1\lambda + U_2 = 0$, where $U_1 = -f_1, U_2 = -f_2 f_3$,

Thus, we have the following conclusions:

a) If $U_1 < 0$ (i.e. $2\frac{r}{k}x* > r\left(1+\frac{b}{k}\right) + \frac{ay*}{(1+x*)^2}$), then the positive accumulation is locally asymptotically stable.
b) If $U_1 > 0$ (i.e. $2\frac{r}{k}x* < r\left(1+\frac{b}{k}\right) + \frac{ay*}{(1+x*)^2}$), then the positive accumulation is unstable.

5. Global stability

Theorem: The following conditions apply: $s_1 < s_2$, $0 \le x \le 1$ and E is locally asymptotically stable. In this case E is globally asymptotically stable.

Thus,

$s_1 = r(x-x*)\left(\left(1-\frac{x}{k}\right)(x-b) - \left(1-\frac{x*}{k}\right)(x*-b)\right)$, $s_2 = ray*(x-x*)(1-x*)$,

Proof:
Consider the following function:

$$G(x,y) = \left(x - x* - x*\ ln\frac{x}{x*}\right) + \frac{ra}{c}\left(y - y* - y*\ ln\frac{y}{y*}\right).$$
$G(x,y) \epsilon\, C^1(R_+^2, R)$, $G(E) = 0$, and $G(x,y) > 0$;

$\forall (x,y) \neq E$. Now differentiate G from time t onwards and do some algebraic work taking this into account:

$$\frac{dG}{dt} = r(x-x*)\left(\left(1-\frac{x}{k}\right)(x-b) - \frac{ay}{1+x} - \left(1-\frac{x*}{k}\right)(x*-b) + \frac{ay*}{1+x*}\right) + ra(y-y*)\left(\frac{x}{1+x} - \frac{x*}{1+x*}\right)$$

$$\frac{dG}{dt} \le r(x-x*)\left(\left(1-\frac{x}{k}\right)(x-b) - \left(1-\frac{x*}{k}\right)(x*-b)\right) - ra(x-x*)\left(\frac{y}{1+x} + \frac{y*}{1+x*}\right) + ra(y-y*)\left(\frac{x}{1+x} - \frac{x*}{1+x*}\right),$$

$$\frac{dG}{dt} \le r(x-x*)\left(\left(1-\frac{x}{k}\right)(x-b) - \left(1-\frac{x*}{k}\right)(x*-b)\right) - ray*(x-x*)(1-x*).$$

$\frac{dG}{dt} = s_1 - s_2$.

6. Numerical simulation

We numerically simulate the aforementioned theoretical reasoning in this part. by MATLAB.

6.1 Strong Allee effect

The ODE model (1) has four parameters: r ,k , b, a , c, d. We choose the parameters:

Table 1: The parameters (r, k, b, a, c, and d) of the ODE model (1).

Index	Parameter					
	r	*k*	*b*	*A*	*C*	*d*
1	0.9	0.8	0.01	0.8	0.7	0.2
2	0.9	0.8	0. 1	0.8	0.7	0.2
3	0.9	0.8	0.01	0.8	0.5	0.2

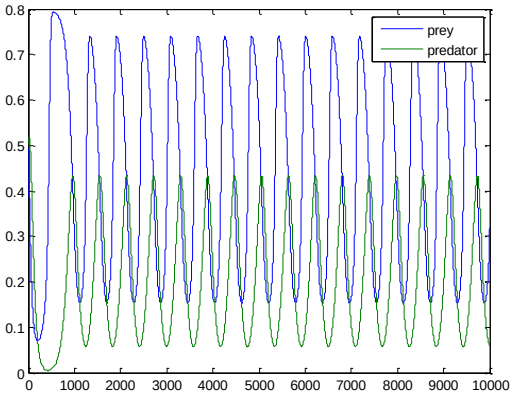

Figure 1: The periodic trajectories of the system.

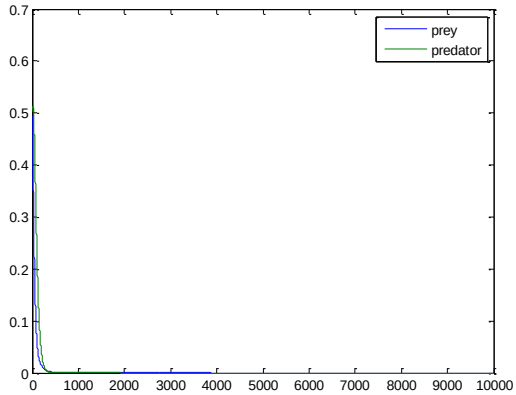

Figure 2: Trivial point of the system.

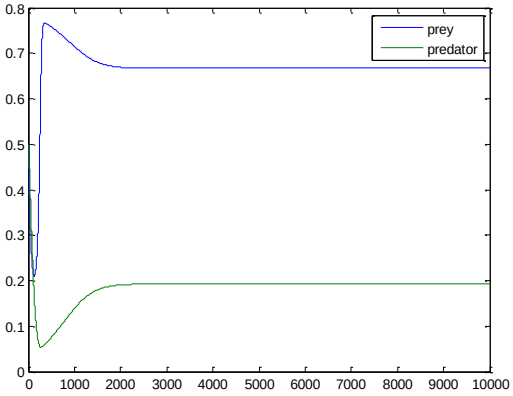

Figure 3: shows asymptotically stable of E = (x∗, y∗) = (0.666, 0.201).

According to Figure 1, we can find the system has periodic trajectories if we take set 1 in table and all conditions of local stale are hold. If we take set 2, then the system has trivial point as shown in Figure 2. If we take the set of parameters 3, then E = (x∗, y∗) = (0.666, 0.201) is asymptotically stable as shown in Figure 3.

7. Conclusions

In this article, a predator-prey paradigm is described with an Allee effect in prey growth, and a functional type II response to Holling in predator growth the system was studied in detail analytically for the positive equilibrium point. The existence of this point depends on the fulfillment of the following condition $b < x * < k$, and it is stable locally if the condition is fulfilled $U_1 < 0$, and when the conditions for existence and stability are met locally and the following condition $s_1 < s_2$, the positive point is globally stable. The study of the effect of the strong mechanism on the system made the parameter b possess characteristics that change the behavior of the system, so when we took the group (1) in the table, we observed that the system has a periodic cycle as shown in Figure 1, and we maintained that when the value of the parameter changed (b), Observing the behavior of the system changed suddenly, and we obtained the Figure 2, in both cases, all parameters were constant. While when the value of parameter (b) was constant and the value of the predation rate changed, the behavior of the system also changed, and we obtained a globally stable point. We can say, after studying the system, that the rate of change Allee plays a major role in the stability of the system.

References

[1] Lotka, A.J. (1925) Elements of Physical Biology, *Nature* **116**: 461-461.

[2] Cheng, L., Cao, H. (2016) Bifurcation analysis of a discrete-time ratio-dependent predator–prey model with Allee effect, *Communications in Nonlinear Science and Numerical Simulation* **38**: 288-302.

[3] Meng, X.-Y., Wang, J.-G. (2019) Analysis of a delayed diffusive model with Beddington–DeAngelis functional response, *International Journal of Biomathematics* **12**: 1950047.

[4] Banerjee, M., Takeuchi, Y. (2017) Maturation delay for the predators can enhance stable coexistence for a class of prey–predator models, *Journal of theoretical biology* **412**: 154-171.

[5] Hu, D., Cao, H. (2017) Stability and bifurcation analysis in a predator–prey system with Michaelis–Menten type predator harvesting, *Nonlinear Analysis: Real World Applications* **33**: 58-82.

[6] Aguirre, P., González-Olivares, E., Sáez, E. (2009) Three limit cycles in a Leslie–Gower predator-prey model with additive Allee effect, *SIAM Journal on Applied Mathematics* **69**: 1244-1262.

[7] Sen, M., Banerjee, M. (2015) Rich global dynamics in a prey–predator model with Allee effect and density dependent death rate of predator, *International Journal of Bifurcation and Chaos* **25**: 1530007.

[8] Nev, O., van den Berg, H. (2018) Holling Type I versus Holling Type II functional responses in Gram-negative bacteria, *Transactions of Mathematics and its Applications* **2**: tny001.

[9] Abdulghafour, A.S., Naji, R.K. (2018) A study of a diseased prey-predator model with refuge in prey and harvesting from predator, *Journal of Applied Mathematics* **2018**: 1-17.

[10] Qi, L., Gan, L., Xue, M., Sysavathdy, S. (2015) Predator-prey dynamics with Allee effect in prey refuge, *Advances in Difference Equations* **2015**: 1-12.

Thamar University Journal of Natural & Applied Sciences ***8****(2) (2023) 14 – 18*

DOI: https://doi.org/10.59167/tujnas.v8i2.1715

TUJNAS

Original Article

Phytochemical Analysis and Antibacterial Studies of Some Yemeni Medicinal Plants against Selected Common Human Pathogenic Bacteria

Nabil Ali Al-Mekhlafi[1,*], Fawaz Al-Badaii[2], Mona Saad Al-Ezzi[2], Ahmed Al-Yamani[1], Enass Almakse[1], Rogayah Alfaqeeh[1], Ghadeer Al-Hatar[1], Malkah Al-Twity[1], Musa Al-Masadi[1], Methak Abdullah[1] and Nasser Al-Qarhami[1]

[1] Department of Biochemical Technology, Faculty of Applied Science, Thamar University, Dhamar 87246, Yemen
[2] Department of Biology, Faculty of Applied Science, Thamar University, Dhamar 87246, Yemen

*Corresponding author: Nabil A. Al-Mekhlafi
Department of Biochemical Technology, Faculty of Applied Science, Thamar University, Dhamar 87246, Yemen
Cell Phone: +967772203999 and Email: nabilali7@tu.edu.ye

Received: 25 October 2023. Revised (in revised form): 2 December 2023. Accepted: 4 December 2023. Published 31 December 2023

Abstract

In traditional medicine, medicinal plants are often used to treat various infectious diseases in humans. **Objective**: This study aimed to identify the phytochemicals contained in thirteen parts of six Yemeni medicinal plants: *Artemisia Judaica*, *Ficus carica L.*, *Nerium oleander L.*, *Olea europaea*, *Santolina chamaecyparissus L.* and *Withania somnifera* and to investigate the antimicrobial activity of different concentrations of methanol extracts from the aerial part of the selected plants against *S. saprophyticus*, *Salmonella* and *E. coli* in vitro. **Methods**: Phytochemical screening was carried out using standard procedures and the antibacterial activity of different extracts of each plant was studied by agar well diffusion method. **Results**: Phytochemical analysis of the plant extracts revealed the presence of phenols, saponins, essential oils, flavonoids, steroids, tannins, cardiac glycosides and alkaloids. The occurrence of phytochemicals varied from plant to plant. Tannins and phenols were found in all samples, while all other test samples contained at least five of the phytochemicals tested. Almost all extracts were able to inhibit the growth of the bacterial strains, with the exception of the species *S. saprophyticus*, which was resistant to the methanolic extracts of *A. judaica* and *F. carica L*. However, the methanol extract (0.1 g/ml) of *S. chamaecyparissus L.* and O. europaea showed the largest zone of inhibition (35 mm and 20 mm, respectively) against *S. saprophyticus*. This is the first report on the antibacterial activity of *S. chamaecyparissus L.* species against *S. saprophyticus*. **Conclusions**: The present screening result shows that the methanol extract of the tested traditional Yemeni medicinal plants exhibits potent antibacterial activity, and the studied plants may represent a new source for the discovery of novel antibacterial compounds for the treatment of drug-resistant human pathogens.

Keywords: Phytochemical Analysis; Agar Well Diffusion Assay; Antibacterial Activity.

1. Introduction

Since ancient times, natural remedies have been an important part of the treatment and prevention of diseases in humans. In primary health care, especially in developing countries, natural products made from medicinal plants are becoming increasingly important [1]. Although the Yemeni population frequently uses herbal treatments, only a few species of the local flora have been studied experimentally [2].

Ficus carica L. is an important member of the genus Ficus. Phytochemical studies on *F. carica* have revealed the presence of numerous bioactive compounds such as flavonoids, vitamins, nicotinic acid, tyrosine, sapogenin, ficusin, bergaptene, psoralen, taraxasterol, rutin and furanocoumarin [3, 4]. On the other hand, previous studies on crude extracts of *F. carica* have discovered a broad spectrum of biological activities. The most interesting therapeutic effects include anticancer, hepatoprotective, hypoglycemic and hypolipidemic effects [5-7]. *Artemisia Judaica L.* is widely distributed in the Mediterranean region, including Egypt, Saudi Arabia, Jordan, and Yemen. Previous phytochemical studies on *A. Judaica L.* have identified several classes of natural products, such as hispidolin, cirsilineol, oxygenated monoterpenes and sesquiterpenes [8]. The biological studies of the essential oils of *A. judaica* have shown various effects, including helminthic, anti-inflammatory, analgesic, antioxidant, antimicrobial and antipyretic properties [9-11]. *Nerium oleander* is the only listed species of the genus Nerium and is used in traditional medicine to treat various diseases. Previous pharmacological studies have shown that *N. oleander* possesses antioxidant, anticancer, antiparasitic, analgesic, dermatologic, cardiovascular, anti-inflammatory, hypolipidemic, and central nervous system effects [12,13]. The most important phytoconstituents of this plant include cis- and trans-carenin, neriumoside, kanersoid, oleandrin, folinrin, adenerin, nerin, cardenolides, bufadienolides and digitoxigenin [14]. *Olea europaea L.* is a small tree belonging to the Oleaceae family. It is native to tropical and warm temperate regions of the world. Phytochemical studies on Olea europaea have led to the isolation of triterpenes, flavonoids, flavonoid glycosides,

iridoids, iridate glycosides, secoiridoid glycosides, biophenols, benzoic acid derivatives and other secondary metabolites [15, 16]. *Santolina chamaecyparissus L.,* also known as cotton lavender, is considered an aromatic plant. Several studies have described the essential oil composition of species growing in different Mediterranean regions and in India [17-19]. *Withania somnifera* is one of the most important species belonging to the genus Withania. Chemical investigation of various plant parts of *W. somnifera* has identified numerous compounds such as sitoindoside, anaferin, withanolides, withaferins and isopelletierin [20, 21]. The plant studied, family, part used, local name and traditional use are summarized in Table 1.

There are several reports on antibacterial activities from natural resources, focusing on antibacterial and/or antifungal activities associated with natural products against various diseases [22]. For the identification and development of potential new drugs against microbial diseases to reduce the development of resistance and adverse treatment effects, folk medicine offers a valuable and underutilized resource [23]. Scientific research therefore continues to prioritize the screening of plants for their therapeutic properties. It is well known that infectious diseases are the leading cause of death in the world, and the emergence of multidrug-resistant organisms threatens the clinical efficacy of many current drugs [24]. For this reason, ongoing efforts are being made to develop new antimicrobial agents, whether through their design and synthesis or through the discovery of natural sources of antimicrobial agents. Therefore, this study aimed to assess the phytochemical constituents and antimicrobial potential of methanolic extracts from the aerial parts of six Yemeni medicinal plants against three clinical pathogenic isolates.

2. Materials and Methods

2.1 Plant materials

Different parts of six Yemeni medicinal plants were collected in January 2021 from their natural habitat in Dhamar city, South Yemen for various areas (Table 1). They were identified by Mona Saleh Al-Sabari from the Faculty of Agriculture, Thamar University.

2.2 Preparation of Extracts for Antibacterial Activity

The collected plant material was first dried in the shade, ground and then 200 g of the dry powder of each aerial part of the plant material was soaked in methanol for 72 hrs at room temperature. The procedure was carried out three times. After the solvent was evaporated at 45 °C under reduced pressure in a vacuum rotary evaporator, the crude extracts were obtained. The resulting methanol extract of each plant was stored until use. The methanolic extracts were tested for their antibacterial activity.

2.3 Phytochemical Tests

Screening of the plant material for various phytochemical constituents was performed according to a standard procedure [37-39] as described in Table 2.

2.4 Antimicrobial activity assay:

2.4.1 Antibacterial activity of plants extract

The antimicrobial activity of the extracts was tested at various concentrations of 100-0.8 mg/ml. The methanol extracts of the tested plant samples were weighed and dissolved in DMSO to prepare a stock solution with a concentration of 100 mg/ml. The same stock solution was used to obtain the desired concentrations of 50, 25, 12.5, 6.3, 3.2, 1.6 and 0.8 mg/ml by the serial dilution method using the equation, $C_1V_1 = C_2V_2$, where C = concentrations and V = volume.

2.4.2 Microorganisms

Salmonella, *Escherichia coli*, and *Staphylococcus saprophyticus* were isolated from clinical samples of patients visiting the microbiology laboratory at Dr. Mohamed Khaled Hospital, in Dhamar City, Yemen. The organisms were isolated in nutrient agar medium and selectively cultured at 37 ˚C for 24 hrs. The bacterial strains were identified using standard biochemical tests.

2.4.3 Antibacterial activity Screening.

The antibacterial activity of the methanol extracts of the tested plant samples was determined using the agarwell diffusion method [40, 41]. The media used were Muller-Hinton agar. 0.1 ml of a freshly grown culture of the test organisms was spread evenly on the surface of the solidified agar using a sterile spatula. Wells with a diameter of 6 mm were made in the agar plate. Approximately 100 µl of different plant extracts were added to the wells and the plates were incubated at 37 °C for 24 hrs. Amoxicillin (30 µg/disk), doxycycline (30 µg/disk) and cefuroxime (30 µg/disk) were used as positive controls. The solvent control (DMSO) was included in each experiment as a negative control. Antibacterial activity was determined by measuring the diameter of the inhibition zones (mm).

Table 1: List of plants screened and their traditional uses.

Species	Family	Part used	Local name	Traditional uses	Reference
Artemisia Judaica L.	Asteraceae	Aerial part	Euthiran	Treatment of gastrointestinal disorders, enhanced eyesight, immune systems, capillary strength, arthritis, and cardiovascular health	[25-27]
Ficus carica L.	Moraceae	Leaves	Altiyn	Colic, indigestion, loss of appetite, diarrhea, sore throats, cough, bronchial problems, inflammatory, and cardiovascular disorders	[28, 29]
Nerium oleander L.	Apocynaceae	Leaves	Defla	Antidiabetic, abortifacient, itching, antigale, against hair loss, eczema and dental rages. used in snake and other venomous bites	[30-32]
Olea europaea L.	Oleaceae	Leaves and Stems	Zaytun	Antirheumatic, leishmaniasis, inflamed gums, diabetes, anti-gout, hypertension, and skin diseases of animals (camels)	[33, 34]
Santolina chamaecyparissus L.	Asteraceae	Aerial part	Qaisum	Analgesic, digestive, antispasmodic, fungicidal, bactericidal and antidiabetic	[18, 35]
Withania somnifera	Solanaceae	Leaves	U'beb	Ear pain, wound healing, and Burns	[36]

Table 2: Preliminary phytochemical tests for plant extracts.

Phytoconstituents	Test procedure	Observation
Alkaloids (Mayer's test)	2ml extract + 2 drops HCl + few drops of Mayer's reagent	White precipitate
Tannins (Braymer's Test)	2ml extract +2ml H_2O +2-3 drops $FeCl_3$ (3%)	Green precipitate
Saponins (Froth test)	5ml extract + 5ml H_2O + heat	Froth appears
Flavonoid (Shinoda test)	2ml extract + a piece of Mg ribbon + 3 drops conc. HCl	Reddish coloration
Phenols (Ferric chloride test)	2 ml extract + 4 drops $FeCl_3$ dilute	Blue-black coloration
Steroids (Liebermann-Burchard test)	2ml extract + 3 drops $(CH_3CO)_2O$ + few drops H_2SO_4	Brown ring at the junction
Cardiac glycosides (Killer Killiani test)	2ml extract + 1ml CH_3COOH +3 drops $FeCl_3$ + 2 drops H_2SO_4	Reddish brown at the junction
Volatile oils	2ml extract + 2ml HCl (1%)	White precipitate

3. Results and Discussion

3.1. Phytochemical profiling

Preliminary phytochemical analysis is the simplest method for the detection of secondary metabolites in plant extracts. Phytochemical constituents such as tannins, saponins, alkaloids, flavonoids, glycosides and several other aromatic compounds are secondary metabolites of plants that serve as a defense mechanism against attack by many microorganisms, insects and other herbivores. The result of phytochemical screening of the extracts showed the presence of different bioactive compounds in most of the selected plants (Table 3), which could be responsible for the observed antibacterial property. Tannins and phenols are present in all parts of the selected plants. Tannins are generally used as a remedy for inflammation, hemorrhoids, burns, gonorrhea and in tanning [42]. Saponins were found in 5 plant samples, with saponins mainly present in the leaves and fruits of *W. somnfera*. It was found that plants containing large amounts of saponins have an antibacterial effect [43]. Essential oils are present in all plants studied, except in the bark of the stems of *S. chamaecyparissus* and *W. somnfera* and in the fruits of *F. carica L*. Essential oils have been shown to be effective in the treatment and prevention of a variety of diseases, including antiseptic, carminative, antifungal, antiviral and asthmatic treatment [44]. Cardiac glycosides have been found at low levels in the fruits of *N. oleander* and the stem bark of *S. chamaecyparissus*. Cardiac glycosides are used to treat microbiological infections, constipation, edema and congestive heart failure [45]. Flavonoids are present in all tested plants except *O. europaea*. The flavonoids are responsible for their positive antioxidant properties. Alkaloids are found in four plant samples, with alkaloids occurring mainly in the flowers of *N. oleander*, the fruits of *W. somnfera* and the leaves of *O. europaea*. Alkaloids have been reported to have narcotic, antispasmodic, antibacterial, antimalarial and analgesic properties [46, 47].

3.2 Antibacterial activity

The antibacterial effect of methanolic extracts of six Yemeni medicinal plants has been studied against pathogenic bacteria, especially *Salmonella*, which causes diarrhea, fever and stomach pain. *E. coli* is the most common bacterium whose virulent strains can cause gastroenteritis, urinary tract infections and meningitis in newborns, and *S. saprophyticus*, which causes urinary tract infections. It is also responsible for complications such as acute pyelonephritis, epididymitis, prostatitis and urethritis. The results of testing the antibacterial methanolic extract on the test strains are shown in Table 4. Of the plant extracts tested, the methanolic extract of *S. chamaecyparissus* showed the highest activity of 35 mm (0.1 g/ml) and 30 mm (0.0125 g/ml) zone of inhibition against *S. saprophyticus*, followed by the methanol extract of *O. europaea* with 20 mm (0.1 g/ml) zone of inhibition against *S. saprophyticus.*

However, the results of this study show that the methanolic crude extract of *S. chamaecyparissus* contains components such as tannins and flavonoids with significant antibacterial properties, which enable the extract to overcome the cell barrier of Gram-negative bacteria [48]. This is the first report of antibacterial activity of this species against S. saprophyticus. Most of the studies revealed that the essential oil of *S. chamaecyparissus* showed the highest antibacterial activity against different bacterial strains [18, 49, 50]. On the other hand, S. saprophyticus was resistant to the different concentrations of methanol plant extracts of *A. judaica* and *F. carica L.*

Methanol extracts of *N. oleander L.* inhibited the growth of all bacteria tested, with the highest activity against *S. saprophyticus* with an inhibition zone of 18 mm observed at a concentration of 6.3 mg/ml. In a previous study [51], the petroleum ether extract from the leaves of *N. oleander* was tested against four bacteria (*E. coli, K. Pneumoniae, B. Subtilis* and *S. lutea*). The results showed that it was highly effective against the *E. coli* strain, with an inhibition zone of 1.9 cm at a concentration of 5.12 g/ml.

Table 3: Qualitative analysis phytochemicals in the selected medicinal plant

Medicinal Plants	*A. Judaica*	*F. carica*		*N. oleander*		*O. europaea*		*S. chamaecyparissus*			*W. somnfera*		
Part tested.	**Aerial parts**	**Fr.**	**L.**	**F.**	**L.**	**L.**	**S.**	**F.**	**L.**	**S.**	**Fr.**	**L.**	**S.**
Phenols	+++	+	++	+++	++	++	++	+	++	++	+	++	++
Saponins	+	-	+	-	-	+	+	+	-	-	+++	+++	-
Volatile oils	++	-	++	+++	++	++	+	+	++	_	+	++	-
Flavonoid	++	+	-	+++	-	-	-	+	++	+	+	-	-
Steroids	++	-	-	+	++	+	-	+++	++	+	-	+	-
Tannins	+	+	+	+	+	++	+	+	+	+	+	+	+
Cardiac glycosides	-	+	-	++	+	+	-	-	+	++	-	-	-
Alkaloids	-	-	++	+++	+	+++	+	-	-	-	+++	+	-

F = Flowers; L= Leaves; Fr = Fruits; S = Stem bark; + = present; − = absent; ++ = moderately present; +++ = highly present of phytochemical constituents.

Table 4: Antibacterial activity of different plant methanol extracts at various concentrations.

	***A. Judaica* (mg/ml)**								***F. carica L* (mg/ml)**							
Bacterial species	***100***	***50***	***25***	***12.5***	***6.3***	***3.2***	***1.6***	***0.8***	***100***	**50**	**25**	**12.5**	**6.3**	**3.2**	**1.6**	**0.8**
S. saprophyticus	R	R	R	R	R	R	R	R	R	R	R	R	R	R	R	R
Salmonella	R	R	11	R	12	11	10	13	R	R	R	R	9	12	10	10
E. coli	R	R	R	R	14	12	10	9	R	R	R	11	R	R	11	12
	***N. oleander L* (mg/ml)**								***O. europaea* (mg/ml)**							
Bacterial species	***100***	***50***	***25***	***12.5***	***6.3***	***3.2***	***1.6***	***0.8***	***100***	***50***	***25***	***12.5***	***6.3***	***3.2***	***1.6***	***0.8***
S. saprophyticus	12	11	12	12	18	16	15	15	20	14	15	10	15	18	17	19
Salmonella	7	14	13	15	11	8	7	R	13	12	8	12	11	12	13	12
E. coli	8	11	15	13	11	7	11	R	12	12	13	12	12	11	11	R
	***S. chamaecyparissus L.* (mg/ml)**								***W. somnifera* (mg/ml)**							
Bacterial species	***100***	***50***	***25***	***12.5***	***6.3***	***3.2***	***1.6***	***0.8***	***100***	***50***	***25***	***12.5***	***6.3***	***3.2***	***1.6***	***0.8***
S. saprophyticus	35	19	19	30	18	15	12	R	18	16	15	13	R	R	R	R
Salmonella	8	10	13	13	13	14	14	14	R	R	11	11	11	13	11	12
E. coli	11	10	R	R	R	R	11	R	R	R	11	11	12	15	13	11

	Amoxicillin	**Cefuroxime**	**Doxycycline**
Bacterial species	***30 µg***	***30 µg***	***30 µg***
S. saprophyticus	15	R	12
Salmonella	13	11	13
E. coli	R	R	9

R = no zone of inhibition.

The bacterium most sensitive to the methanol extracts of *W. somnifera* was *S. saprophyticus* with an inhibition zone of 18 mm (0.1 g/ml). In contrast, the same extract resisted *Salmonella* and *E. coli* at the same concentration of 0.1 g/ml. According to previous studies, *W. somnifera* methanol extracts had good efficacy against *E. coli* with an inhibition zone of 23 mm at 0.1 g/ml [52].

The study showed a non-monotonic correlation between the concentration of the plant extract and bacterial inhibition, with lower concentrations showing greater efficacy than higher concentrations. This phenomenon is attributed to several factors. First, at lower concentrations, the bioactive compounds effectively bind to the bacterial cell surface receptors, inhibiting important functions and preventing bacterial growth. However, as the concentrations increases, the effectiveness of the excess bioactive compounds decreases due to saturation of the receptors, resulting in a reduced inhibitory effect. Antagonistic interactions among bioactive compounds within plant extracts also contribute. These interactions are less pronounced at lower concentrations, which favors synergistic inhibition. Conversely, these interactions increase at higher concentrations, reducing the overall inhibitory effect. Another aspect is the chemical degradation of bioactive compounds, especially in the presence of oxygen or light. Higher concentrations can accelerate degradation and reduce the availability and effectiveness of the compounds against bacteria. In addition, certain plant extracts induce bacterial resistance at higher concentrations, which triggers a stress response that neutralizes or degrades the bioactive compounds and weakens the overall inhibitory effect. The factors contributing to this non-monotonic relationship depend on the particular plant extract, the bacterial species and the experimental conditions [53-58].

4. Conclusions

In summary, the phytochemical analysis of six Yemeni plants confirms that these plants were rich in tannins, phenols, essential oils, saponins, flavonoids, alkaloids and cardiac glycosides. These phytochemicals make the therapeutic properties of the plants studied more potent. The results also showed antimicrobial activities against *S. saprophyticus, Salmonella* and *E. coli* strains. Based on the results, it is evident that the methanol extract of the tested plants has strong antibacterial activity. The tested plants could serve as a new source for the discovery of new antibacterial chemicals for the treatment of drug-resistant human infections.

Acknowledgement

Authors are very thankful to the Department of Chemistry, Faculty of Applied Science, Thamar University, Yemen, and Microbiology laboratory of Dr. Mohamed Khaled Hospital, Dhamar City, Yemen for providing necessary laboratory facilities to carry out this work.

References

[1] Mutee, A., Salhimi, S., Yam, M., Lim, C., Abdullah, G., Ameer, O., Abdulkarim, M., Asmawi, M. (2010) In vivo anti-inflammatory and in vitro antioxidant activities of *Peperomia pellucida*, *International Journal of Pharmacology* **6**: 686-90.

[2] Mothana, R.A., Abdo, S.A., Hasson, S., Althawab, F., Alaghbari, S.A., Lindequist, U. (2010) Antimicrobial, antioxidant and cytotoxic activities and phytochemical screening of some yemeni medicinal plants, *Evidence-based Complementary and alternative medicine* **7**: 323-330.

[3] Singab, A.N.B., Ayoub, N.A., Ali, E.N., Mostafa, N.M. (2010) Antioxidant and hepatoprotective activities of Egyptian moraceous plants against carbon tetrachloride-induced oxidative stress and liver damage in rats, *Pharmaceutical Biology* **48**: 1255-1264.

[4] Joseph, B., Raj, S.J. (2011) Pharmacognostic and phytochemical properties of *Ficus carica* Linn–An overview, *International journal of pharmtech research* **3**: 8-12.

[5] Mawa, S., Husain, K., Jantan, I. (2013) *Ficus carica* L.(Moraceae): phytochemistry, traditional uses and biological activities, *Evidence-Based Complementary and Alternative Medicine* **2013**.

[6] Yancheva, S.D., Golubowicz, S., Yablowicz, Z., Perl, A., Flaishman, M.A. (2005) Efficient Agrobacterium-mediated transformation and recovery of transgenic fig (Ficus carica L.) plants, *Plant Science* **168**: 1433-1441.

[7] Rubnov, S., Kashman, Y., Rabinowitz, R., Schlesinger, M., Mechoulam, R. (2001) Suppressors of cancer cell proliferation from fig (*Ficus c arica*) resin: isolation and structure elucidation, *Journal of Natural products* **64**: 993-996.

[8] Al-Wahaibi, L.H.N., Mahmood, A., Khan, M., Alkhathlan, H.Z. (2020) Comparative study on the essential oils of *Artemisia judaica* and A. herba-alba from Saudi Arabia, *Arabian Journal of Chemistry* **13**: 2053-2065.

[9] Batanouny, K., Aboutabl, E., Shabana, M., Soliman, F. (1999) Wild medicinal plants in Egypt, ed., The Palm press, Cairo, pp. 22.

[10] El-Massry, K.F., El-Ghorab, A.H., Farouk, A. (2002) Antioxidant activity and volatile components of Egyptian *Artemisia judaica* L, *Food Chemistry* **79**: 331-336.

[11] Janacković, P., Novaković, J., Soković, M., Vujisić, L., Giweli, A.A., Dajić-Stevanović, Z., Marin, P.D. (2015) Composition and antimicrobial activity of essential oils of *Artemisia judaica*, A. herba-alba and A. arborescens from Libya, *Archives of biological sciences* **67**: 455-466.

[12] Ayouaz, S., Arab, R., Mouhoubi, K., Madani, K. (2023) *Nerium oleander* Lin: A Review of Chemical, Pharmacological and Traditional uses, *Journal ISSN* **2766**: 2276.

[13] Singhal, K.G., Gupta, G.D. (2012) Hepatoprotective and antioxidant activity of methanolic extract of flowers of *Nerium oleander* against CCl4–induced liver injury in rats, *Asian Pacific journal of tropical medicine* **5**: 677-685.

[14] Hase, G.J., Deshmukh, K.K., Murade, V.D., Pokharkar, R.D., Phatanagre, N.D., Hase, D.P., Dichayal, S., Gosavi, A.B. (2016) Phytopharmacology of *Nerium oleander* L. A review, *International Journal of Phytopharmacology* **7**: 0975-9328.

[15] Obied, H.K. (2013) Biography of biophenols: past, present and future, *Functional Foods in Health and Disease* **3**: 230-241.

[16] Jerman, T., Trebše, P., Vodopivec, B.M. (2010) Ultrasound-assisted solid liquid extraction (USLE) of olive fruit (*Olea europaea*) phenolic compounds, *Food Chemistry* **123**: 175-182.

[17] Derbesy, M., Touche, J., Zola, A. (1989) The essential oil of *Santolina chamaecyparissus* L, *Journal of Essential Oil Research* **1**: 269-275.

[18] Djeddi, S., Djebile, K., Hadjbourega, G., Achour, Z., Argyropoulou, C., Skaltsa, H. (2012) In vitro antimicrobial properties and chemical composition of *Santolina chamaecyparissus* essential oil from Algeria, *Natural Product Communications* **7**: 1934578X1200700735.

[19] El-Sahhar, K., Nassar, D.M., Farag, H.M. (2011) Morphological and anatomical studies of *Santolina chamaecyparissus* L.(Asteraceae) Ii. Anatomical characteristics and volatile oil, *Research Journal of Agriculture and Biological Sciences* **7**: 413-422.

[20] Jain, R., Kachhwaha, S., Kothari, S. (2012) Phytochemistry, pharmacology, and biotechnology of *Withania somnifera* and *Withania coagulans*: A review, *Journal of Medicinal Plants Research* **6**: 5388-5399.

[21] Sharifi-Rad, J., Quispe, C., Ayatollahi, S.A., Kobarfard, F., Staniak, M., Stępień, A., Czopek, K., Sen, S., Acharya, K., Matthews, K.R. (2021) Chemical Composition, Biological Activity, and Health-Promoting Effects of *Withania somnifera* for Pharma-Food Industry Applications, *Journal of Food Quality* **2021**: 1-14.

[22] Al-Haj, N., Mashan, N., Shamsudin, M., Habsah, M., Vairappan, C., Zamberi, S. (2010) Antibacterial activity of marine source extracts against multidrug resistance organisms, *American Journal of Pharmacology and Toxicology* **5**: 95-102.

[23] Nigussie, D., Davey, G., Legesse, B.A., Fekadu, A., Makonnen, E. (2021) Antibacterial activity of methanol extracts of the leaves of three medicinal plants against selected bacteria isolated from wounds of lymphoedema patients, *BMC Complementary Medicine and Therapies* **21**: 1-10.

[24] Pacios, O., Blasco, L., Bleriot, I., Fernandez-Garcia, L., González Bardanca, M., Ambroa, A., López, M., Bou, G., Tomás, M. (2020) Strategies to combat multidrug-resistant and persistent infectious diseases, *Antibiotics* **9**: 65.

[25] Khafagy, S., El-Din, A.S., Jakupovic, J., Zdero, C., Bohlmann, F. (1988) Glaucolide-like sesquiterpene lactones from *Artemisia judaica*, *Phytochemistry* **27**: 1125-1128.

[26] Abdalla, S., Zarga, M.A. (1987) Effects of cirsimaritin, a flavone isolated from A*rtemisia judaica*, on isolated guinea-pig ileum, *Planta medica* **53**: 322-324.

[27] El-Sayed, M.A., BaAbbad, R., Balash, A., Al-Hemdan, N.A., Softah, A. (2013) The potential anti Helicobacter pylori and antioxidant effects of *Artemisia judaica*, *Functional Foods in Health and Disease* **3**: 332-340.

[28] Guarrera, P.M. (2005) Traditional phytotherapy in Central Italy (marche, abruzzo, and latium), *Fitoterapia* **76**: 1-25.

[29] Mawa, S., Husain, K., Jantan, I. (2013) *Ficus carica* L.(Moraceae): phytochemistry, traditional uses and biological activities, *Evidence-Based Complementary and Alternative Medicine* **2013**: 1-8.

[30] Farooqui, S., Tyagi, T. (2018) *Nerium oleander*: It's application in basic and applied science: A Review, *International Journal of Pharmacy and Pharmaceutical Sciences* **10**: 1-4.

[31] Bnouham, M., Legssyer, A., Mekhfi, H., Ziyyat, A. (2002) Medicinal plants used in the treatment of diabetes in Morocco, *Dubai Diabetes and Endocrinology Journal* **10**: 33-50.

[32] Hammiche, V., Merad, R., Azzouz, M. (2013) Poisonous Plants for Medicinal Use from Around the Mediterranean, Paris: Springer.

[33] Flemmig, J., Kuchta, K., Arnhold, J., Rauwald, H. (2011) *Olea europaea* leaf (Ph. Eur.) extract as well as several of its isolated phenolics inhibit the gout-related enzyme xanthine oxidase, *Phytomedicine* **18**: 561-566.

[34] Ali, N.A.A., Al Sokari, S.S., Gushash, A., Anwar, S., Al-Karani, K., Al-Khulaidi, A. (2017) Ethnopharmacological survey of medicinal plants in Albaha Region, Saudi Arabia, *Pharmacognosy research* **9**: 401.

[35] Azevedo, T., Faustino-Rocha, A.I., Barros, L., Finimundy, T.C., Matos, M., Oliveira, P.A. (2023) Santolina chamaecyparissus L.: A Brief Overview of Its Medicinal Properties, *Medical Sciences Forum* **21**: 8.

[36] Ali, N.A., Jülich, W.-D., Kusnick, C., Lindequist, U. (2001) Screening of Yemeni medicinal plants for antibacterial and cytotoxic activities, *Journal of ethnopharmacology* **74**: 173-179.

[37] Salim, F., Low, A.L.M., Al-Mekhlafi, N.A. (2023) Phytochemicals Composition of Medicinal Plants from Kuala Keniam National Park, *Malaysian Journal of Chemistry* **25**: 43-51.

[38] Sofowora, A. (1993) Medicinal plants and traditional medicine in Africa. Spectrum Books Limited, ed., pp. 1-153.

[39] Trease, G., Evans, W. (1989) Pharmacognosy. 12th, ELBS/Bailliere Tindall, London, pp. 345-6.

[40] Özkan, G., Sagdiç, O., Göktürk Baydar, N., Kurumahmutoglu, Z. (2004) Antibacterial activities and total phenolic contents of grape pomace extracts, *Journal of the Science of Food and Agriculture* **84**: 1807-1811.

[41] Rojas, J.J., Ochoa, V.J., Ocampo, S.A., Muñoz, J.F. (2006) Screening for antimicrobial activity of ten medicinal plants used in Colombian folkloric medicine: A possible alternative in the treatment of non-nosocomial infections, *BMC Complementary and Alternative Medicine* **6**: 1-6.

[42] Boroushaki, M.T., Mollazadeh, H., Afshari, A.R. (2016) Pomegranate seed oil: A comprehensive review on its therapeutic effects, *International Journal of Pharmaceutical Sciences and Research* **7**: 430.

[43] Kawo, A., Kwa, A. (2011) Phytochemical screening and antibacterial activity of the aqueous extracts and fractions of ethanolic extracts of *Lawsonia inermis* leaf, *International Research Journal of Microbiology* **2**: 510-516.

[44] Raza, Q.S., Saleemi, M.K., Gul, S., Irshad, H., Fayyaz, A., Zaheer, I., Tahir, M.W., Fatima, Z., Chohan, T.Z., Imran, M. (2022) Role of essential oils/volatile oils in poultry production—A review on present, past and future contemplations, *Agrobiological Records* **7**: 40-56.

[45] Awe, F., Giwa-Ajeniya, A., Akinyemi, A., Ezeri, G. (2013) Phytochemical analysis of *Acalypha wilkesiana*, *Leucaena leucocephala*, *Pepperomia pellucida* and *Senna alata* leaves, *The International Journal of Engineering and Sciences (IJES)* **2**: 41-44.

[46] Rwai Waweru, W., Obado Osuwat, L., Karomo Wambugu, F. (2017) Phytochemical analysis of selected indigenous medicinal plants used in Rwanda, *Journal of Pharmacognosy and Phytochemistry* **6**: 322-324.

[47] Oomah, D. (2003) Isolation, characterization and assessment of secondary metabolites from plants for use in human health, *PBI Bull* **1**: 13-20.

[48] Scalbert, A. (1991) Antimicrobial properties of tannins, *Phytochemistry* **30**: 3875-3883.

[49] Ruiz-Navajas, Y., Viuda-Martos, M., Perez-Alvarez, J.A., Sendra, E., Fernández-López, J. (2012) Chemical Characterization and Antibacterial Activity of Two Aromatic Herbs (*Santolina chamaecyparissus* and *Sideritis angustifolia*) Widely Used in the Folk Medicine, *Journal of Food Safety* **32**: 426-434.

[50] Chirane, M.S., Benchabane, O., Bousbia, N., Zenia, S. (2019) Antioxydant and antimicrobial activities of essential oil and ethanol extract of *Santolina chamaecyparissus L*, *Revue Agrobiologia* **9**: 1660-1668.

[51] Jamal, M.A.H.M., Rahman, S., Islam, A., Karim, R., Alam, S., Rahman, Z. (2012) Minimum inhibitory concentration analysis of *Nerium oleander* against bacterial pathogens, *Asian Pacific Journal of Tropical Biomedicine* **2**: S1664-S1666.

[52] Gebeyehu, A.G., Walle, K.Z., Birhanu, M.Z., Gebeyehu, R. (2022) Structural Elucidation and Antibacterial Activity Studies of Leaf Extracts of *Withania somnifera*, *Indonesian Journal of Chemistry* **22**: 1586-1595.

[53] Cowan, M.M. (1999) Plant products as antimicrobial agents, *Clinical microbiology reviews* **12**: 564-582.

[54] Burt, S. (2004) Essential oils: their antibacterial properties and potential applications in foods—a review, *International journal of food microbiology* **94**: 223-253.

[55] Ullah, F., Ayaz, M., Sadiq, A., Ullah, F., Hussain, I., Shahid, M., Yessimbekov, Z., Adhikari-Devkota, A., Devkota, H.P. (2020) Potential role of plant extracts and phytochemicals against foodborne pathogens, *Applied Sciences* **10**: 4597.

[56] Górniak, I., Bartoszewski, R., Króliczewski, J. (2019) Comprehensive review of antimicrobial activities of plant flavonoids, *Phytochemistry reviews* **18**: 241-272.

[57] Askarinia, M., Ganji, A., Jadidi-Niaragh, F., Hasanzadeh, S., Mohammadi, B., Ghalamfarsa, F., Ghalamfarsa, G., Mahmoudi, H. (2019) A review on medicinal plant extracts and their active ingredients against methicillin-resistant and methicillin-sensitive Staphylococcus aureus, *Journal of Herbmed Pharmacology* **8**: 173-184.

[58] Compean, K., Ynalvez, R. (2014) Antimicrobial activity of plant secondary metabolites: A review, *Research Journal of Medicinal Plant* **8**: 204.

Thamar University Journal of Natural & Applied Sciences ***8****(2) (2023) 19 – 26*

DOI: https://doi.org/10.59167/tujnas.v8i2.1716

TUJNAS

Original Article

The Effect of Single Clove Garlic Extract (*Allium sativum)* Against Aspartame-Induced Hepatotoxicity in Diabetic Rats

Mohammed Ahmed Qasim[1], Fahmi S. Moqbel[1,*] and Nada M. H. Al Hamdani[2]

[1] Department of Biology, Faculty of Applied Science, Thamar University, Dhamar 87246, Yemen
[2] Department of Biology, Faculty of Sciences, Sana'a University, Sana'a, Yemen

*Corresponding author: Fahmi S. Moqbel
Department of Biology, Faculty of Applied Science, Thamar University, Dhamar 87246, Yemen
Email: fahmi.moqbel@tu.edu.ye

Received: 25 October 2023. Revised (in revised form): 18 November 2023. Accepted: 20 November 2023. Published: 31 December 2023

Abstract:

Background: Aspartame is a widely used synthetic sweetener used for dietary control and by diabetics. **Objectives**: This study aims to investigate the effect of a single garlic clove extract against aspartame-induced hepatotoxicity in diabetic rats. **Methods**: Forty-eight experimental male albino rats were randomly divided into eight groups (6 rats per group) as follows: Group (G)1: served as normal control and received distilled water orally, G2: rats treated with single clove garlic (SCG) extract (0.5 g/kg body weight), G3: rats were treated with SCG extract (0.5 g/kg body weight) and alkaline phosphatase (ALP) (200 mg/kg body weight), G4: rats treated with ASP (200 mg/kg body weight), G5: was the diabetic control group (induced by alloxan (ALX) 120 mg/kg body weight), G6: diabetic rats were treated with SCG extract (0.5 g/kg body weight), G7: diabetic rats were treated with SCG extract (0.5 g/kg body weight) and ASP (200 mg/kg body weight) and G8: diabetic rats were treated with ASP 200 mg/kg body weight. **Results**: The results obtained showed that treatment with ASP caused a significant increase in serum levels of serum alanine transaminase (ALT), aspartate transaminase (AST), and ASP in SCG extract-treated rats in G3 and G4 and diabetic rats in G7 and G8, while treatment with SCG extract caused a significant decrease in serum levels of ALT, AST and ALP in SCG treated rats in G2 and G6 and diabetic rats in G7 compared to the control group (G1). After treatment with ASP, histologic changes in the liver were observed in G4, which were more pronounced in G8, indicating liver damage compared to the control group, while treatment with SCG extract showed further changes in liver tissue in the diabetic rats of G7 and G8. **Conclusion**: The present study suggests that administering ASP in normal rats leads to liver dysfunction. Moreover, our results proved that the application of ASP in diabetic rats may cause additional damage compared to ASP in normal rats. This study demonstrated that treatment with SCG extract significantly attenuated the biochemical and histopathologic changes induced by ASP and alloxan. From the data obtained, it appears that treatment with SCG extract has a protective effect against the toxicity of ASF and alloxan on the liver of normal and diabetic rats.

Keywords: Alloxan; Single Clove Garlic; Hepatotoxicity; Aspartame.

1. Introduction

Alkaline phosphatase (ALP) (E951) is one of the most widely used artificial sweeteners in many products worldwide and in various countries [1]. It is widely used (62%) as a non-nutritive sweetener in foods, beverages, and pharmaceuticals [2]. ASP is an artificial sweetener that has almost 180-200 times the sweetening power of sucrose as it has a low caloric value of 4 Kcal/g [3,4]. It is increasingly used by diabetic patients, is widely used in weight loss, and deceives almost 200 million people worldwide [5,6].

During metabolism, ASP is broken down in the intestinal lumen into the three hydrolysis products phenylalanine (50%), aspartic acid (40%), and methanol (10%) [7,8,9,10]. The production of the essential amino acid phenylalanine is hazardous to the health of people born with a rare genetic disease called phenylketonuria (PKU). However, methanol production during ASP metabolism is not very high but still contributes to toxicity [11]. The effect Long-term consumption of ASP in rats leads to liver cell damage and changes in antioxidant status in the liver [12]. The long-term effect of aspartame (75 mg/kg) on the antioxidant status of the liver and brain with histopathologic changes in the liver and renal cortex in albino rats of the Wistar strain was investigated. Aspartame was reported to induce marked changes in the expression of key oncogenes. Harvey's sarcoma of rat viral homozygous h-Ras and viral homologous myeloma c-myc in rat livers [13]. Several clinical disorders, including hepatotoxicity, nephrotoxicity, neurotransmitter imbalance, and cognitive impairment [14]. Measurement of the activities of these marker enzymes in tissues and body fluids can be used to assess the degree of damage and toxicity of a chemical compound on organs/tissues [15,16].

Garlic (*Allium sativum* L): is a bulbous herb of the Alliaceae or Lilliaceae family. *Allium sativum*, commonly known as garlic, has more than 500 species in 30 genera and the average family is classified between Lilliaceae and Amaryllidaceae [17]. *Allium sativum* contains more than a hundred biologically useful secondary metabolites. Garlic also contains sulfur compounds such as aliin, allicin, allylpropyl, diallyl trisulfide, sallylcysteine, vinyldithiine, and S-allyl mercaptocysteine [18]. Other compounds such as enzymes, vitamins (A, B1, B2, B6, C, E), fibers (1.5%), water (65%), 17 amino acids (1.2%), carbohydrates, organic sulfur compounds (2.3%), proteins (mainly allinase; 2%), fatty acids, glycolipids, phospholipids, saponins, glycosides, and minerals such as calcium (Ca), iron (Fe), copper (Cu), magnesium (Mg), potassium (K), zinc (Zn), germanium (Ge) and selenium (Se) [19,20,21].

Garlic has many medicinal properties such as blood sugar-lowering, anti-inflammatory, anti-cancer, antioxidant, antiviral, antibacterial,

antifungal, cholesterol-lowering, and immunomodulating effects [22,23]. Due to cultivation practices and climatic conditions, the bulbs of garlic are sometimes not divided into cloves and produce a single clove of garlic known as single garlic clove, solo garlic, and pearl garlic. The amount of research on the bioactivity of single clove garlic is limited. Recently, a single clove of garlic was found to have a stronger hepatoprotective effect than regular garlic, known as multi-clove garlic, in the CCl4-poisoned rabbit model [24,25]. Garlic has been studied in various forms of extracts: aqueous, ethanol, and dried powder. Garlic extracts are effective in gentamicin-induced renal damage and oxidative stress in rats [26]. Adriamycin-induced toxicity was found for garlic powder [27].

Aspartame (ASP) is a dipeptide sweetener found as the main ingredient in most sugar-free products on the market today. The Food and Drug Administration (FDA) has approved the use of aspartame, but since then the safety of aspartame consumption has been questioned. In this study, the protective effect of a single clove of garlic on the biochemical and histologic changes against aspartame-induced nephrotoxicity in normal and diabetic rats was investigated.

2. Materials and Methods

2.1 Experimental animals

Forty-eight male albino rats with an average weight of 200 ± 50 g, obtained from the Biology Department, Faculty of Science, Sana'a University, participated in this study. The rats were housed in stainless steel cages and the entire experiment was conducted under ambient conditions at a room temperature of 25 ± 3 °C and humidity of 50 ± 3 % and under a 12-hour light and 12-hour dark schedule. The rats received food and water ad libitum 14 days prior to the experiment.

2.2 Chemicals

Alloxan (ALX) monohydrate: obtained from Dhafar Pharma Sana'a, Yemen (S.D Fine - Chem. Ltd., Mumbai, India). Aspartame (ASP): Aspartame obtained from Dhafar Pharma Sana'a, Yemen (Alexandria Company, Egypt). It is available in the form of tablets, each containing 20 mg of aspartame (aspartame 25 g/0.2 ml distilled water) to achieve a concentration of (200 mg/kg body weight) per rat [28].

2.3 Preparation of the extract from a single clove of garlic

Fresh garlic cloves were purchased from a local market in Sweida district near Dhamar city, Yemen, in October 2020. Dried and ground bulbs (approximately 100 g) were extracted with 300 ml ethanol (96%) in a Soxhlet apparatus for 72 hours. After extraction, the solvent was filtered and then evaporated with rotavapor. The alcoholic garlic extract obtained was stored at 4 °C until use.

2.4 Preparation of the diabetic rat

The animals were injected with alloxan (120 mg/kg body weight). Five days after injection, the rats with fasting blood glucose greater than 250 mg/dl were used for the experiments. Each animal was used only once in all experiments. Food and water were removed from the cages 12 hours before the experiment.

2.5 Experimental design

Forty-eight rats (24 diabetic, 24 normal rats) were used. The rats were divided into eight groups (six rats each) as follows:

Group 1: Normal control rats were administered 1 ml of distilled water.

Group 2: Normal rats were administered an extract of a single clove of garlic (SCG) (0.5 g/kg body weight).

Group 3: Normal rats were administered an extract of a single clove of garlic (SCG) 0.5 g/kg body weight and aspartame (ASP) 200 mg/kg body weight.

Group 4: Normal rats received aspartame (ASP) 200 mg/kg body weight dissolved in 25 g/0.2 ml distilled water.

Group 5: Diabetic control rats were administered 1 ml of normal saline.

Group 6: Diabetic rats were administered an extract of a single clove of garlic (SCG) (0.5 g/kg body weight).

Group 7: Diabetic rats were treated with an extract of a single clove of garlic (SCG), 0.5 g/kg body weight, and aspartame (ASP) 200 mg/kg body weight.

Group 8: Diabetic rats were treated with aspartame (ASP) 200 m /kg body weight.

All animals in the experimental groups were administered orally by gavage once daily for 30 days.

2.6 Body weight assessment

Rats in all experimental groups were weighed using electronic scales before the start of the experiment (day 0) and on day 3, day 10, day 20 and at the end of the experimental period (day 30). The changes in body weight were calculated using the following formula:

$$\textbf{Body weight gain (g)} = \frac{\textbf{Final body weight} - \textbf{Initial body weight}}{\textbf{Final body weight(g)}} \textbf{x 100} \qquad \textbf{(1)}$$

2.7 Relative liver weights

All rats were fasted overnight on day 29 of the experiment and live body weight (g) was determined on day 30 prior to euthanasia. At autopsy, the liver of each animal was removed, dried with tissue paper, and weighed on an electronic scale prior to fixation to determine and statistically analyze the change in organ weight relative to body weight. The relative liver weight of each animal was calculated using the following formula:

$$\textbf{Relative liver weight (g)} = \frac{\textbf{(Absolute liver weight (g)}}{\textbf{Body weight of rat on sacrifice day (g)}} \textbf{x 100} \qquad \textbf{(2)}$$

2.8 Collection of Blood Samples

On the 30th day of the experimental period, 5 ml of blood was collected from the ophthalmic vein (canthus) of each animal using capillary tubes in unsalted heparin tubes for biochemical analysis.

3. Biochemical analysis

3.1 Liver Function Tests

Serum aspartate transaminase (AST), alanine transaminase (ALT), and alkaline phosphatase (ALP) tests were measured. The blood samples were centrifuged at 3000 rpm for 10 minutes and then the blood serum was collected at 4 ºC for various physiological and biochemical assays. The blood samples were analyzed in the Automated Clinical Chemistry Analyzer, Dimension Type RXL Max (Dade Behring Delaware, DE 19714, U.S.A.) at Al-Asr Alhadith Specialized Medical Laboratory, Dhamar, Yemen.

3.2 Histologic Examination

At autopsy, the liver tissue of each group was washed in saline and fixed with 10% formalin, dehydrated in ethyl alcohol of various ascending grades, cleared in xylene and embedded in kerosene wax, cut into 4 µm thick sections, stained with hematoxylin and eosin (H & E) and examined under light microscope for histologic examination [29].

3.3 Statistical Analysis

All data were expressed as mean ± standard deviation (SD) and statistically analyzed using one-way ANOVA to examine the differences between the studied groups. Subsequently, Dunnett's test was performed and compared with the respective control group of animals. The test for multiple comparisons between the groups was performed using SPSS software (SPSS version 21 IBM Chicago, IL, USA). All tests were considered statistically significant at a P-value of < 0.05.

4. Result

4.1 Effect of single clove garlic (SCG) extract against aspartame-induced on body weight (g) in normal and diabetic rats

Table 1 shows that the final body weight of 193.80 ± 7.01 g in the normal control group increased significantly compared to the initial body weight of 152.60 ± 3.78 g. Rats administered ASP showed a lower body weight gain (-5 g) compared to the normal control rats (+41.2 g). The diabetic control rats showed a lower body weight gain (-7.4 g) compared to the body weight gain in the normal control rats (+41.2 g). While the body weight gain in diabetic rats administered ASP showed less body weight gain (-15 g) compared to the normal control rats (+41.2 g), induction of diabetes in diabetic control rats showed less body weight gain (-7.4 g) compared to the body weight gain in the normal control rats (+41.2 g).

As shown in Table 1, the SCG extract treated rats showed a significant increase in body weight (+59.87 g) compared to the body weight gain of the normal control group (+41.2 g), while the SCG extract +

ASP treated rats showed no significant changes in body weight (+40.8 g) compared to the normal control rats (+41.2 g).

Accordingly, the diabetic rats administered SCG extract showed no significant change in their body weight gain (+40 g) compared to that of the normal control rats (+41.2 g) but showed an increase in their body weight gain (+40 g) compared to that of the diabetic control rats (-7.4% g). Similarly, the diabetic rats administered SCG extract + ASP showed no change in their body weight gain (+40.4 g) compared to the body weight gain of the normal control rats (+41.2 g), moreover, a remarkable increase in their body weight gain (+40.4 g) was observed compared to that of the diabetic control rats (-7.4% g). As shown in Table 1.

4.2 Relative Liver Weight

The results in Table 2 show that the ASP treated rat group had a significant increase in relative liver weight of 4.47 ± 0.539 g compared to that of the normal control rats of 3.92 ± 0.247 g. In addition, a significant increase in relative liver weight of 4.66 ± 0.287 g was observed in the diabetic ASP treated rats compared to the normal control rats 3.92 ± 0.247 g. There was also an increase in relative liver weight of 4.03±0.296g in the diabetic control rats compared to the normal control rats 3.92 ± 0.247 g.

In Table 2, the rats administered SCG extract showed no remarkable increase in relative liver weight 3.59 ± 0.256 g compared to that of normal control rats 3.92 ± 0.247 g. In the rats administered the SCG extract with ASP, there was no significant increase in relative liver weight 3.60±0.258g compared to that of control rats 3.92±0.247g, while it decreased significantly compared to that of normal ASP rats 4.47±0.539g. Similarly, diabetic rats treated with SCG extract showed no significant increase in relative liver weight of 3.56 ± 0.043 g compared to control rats 3.92 ± 0.247 g and a significant decrease compared to diabetic control rats 4.03 ± 0.296 g.

The result presented in Table 2 shows that the rats treated with the ethanolic extract of SCG and ASP group showed no remarkable increase in relative liver weight (3.50 ± 0.273 g) compared to the normal control rats (3.92 ± 0.247 g) and a remarkable decrease in relative liver weight compared to the diabetic ASP rats (4.66 ± 0.287 g).

4.3 Serum Biochemical Markers

4.3.1 Liver Function Tests

A deeper scientific look at the results in Tables 3, 4 and 5 shows that the orally administered normal ASP-treated rats exhibited a remarkable increase in ALT, AST and ALP serum levels compared to the normal control group: 74.40 ± 11.92 U/L, 165.60 ± 21.41 U/L and 141.20 ± 14.34 U/L, respectively. In addition, diabetic ASP-treated rats showed a significant increase in ALT, AST and ALP serum levels 106.40 ± 2.96 U/L, 223.00 ± 6.00 U/ and 227.20 ± 2.58 U/L, respectively, compared to the control group 74.40 ± 11.92 U/L, 165.60 ± 21.41 U/L and 141.20±14.34 U/L, respectively.

Similarly, Table 3, 4 and 5 show that there was a significant increase in ALT, AST and ALP serum levels 116.40 ± 9.31 U/L, 227.80 ± 9.01 U/L and 229.60 ± 13.27 U/L in the diabetic control group as compared to the control group 74.40 ± 11.92 U/L, 165.60 ± 21.41 U/L and 141.20 ± 14.34 U/L respectively.

The results of the current study, as shown in Tables 3, 4 and 5, show that the SCG-treated rats showed no significant change in ALT, AST and ALP serum levels of 74.00 ± 11.72 U/L, 164.40 ± 7.12 U/L and 140.80 ± 14.54 U/L, respectively, compared to the control group 74.40 ± 11. 92 U/L, 165.60 ± 21.41 U/L and 141.20 ± 14.34 U/L, respectively. Consequently, the animals treated with SCG extract with ASP showed a significant decrease in ALT, AST and ALP serum levels 77.60 ± 27.18 U/L, 168.20 ± 13.06 U/L and 142.00 ± 24.80 U/L compared to normal ASP rats 110.60 ± 4.56 U/L, 218.60 ± 4.21 U/L and 232.00 ± 8.54 U/L, respectively. Diabetic SCG extract rats showed no significant change in ALT, AST and ALP serum levels 79.20 ± 8.10 U/L, 168.60 ± 14.63 U/L and 145.60 ± 37.18 U/L compared to normal control group 74.40 ± 11.92 U/L, 165.60 ± 21.41 U/L and 141.20 ± 14.34 U/L respectively. The results showed that there was a significant decrease in ALT, AST and ALP serum levels 79.20 ± 8.10 U/L, 168.60 ± 14.63 U/L and 145.60 ± 37.18 U/L, respectively, compared to the diabetic control group 116.40 ± 9.31 U/L, 227.80 ± 9.01 U/L and 229.60 ± 13.27 U/L, respectively.

Table 1: Effects of a single clove garlic extract (SCG) against aspartame-induced body weight changes in normal and diabetic rats.

	Mean ± SD Change in body weight (gm)		
Change of weight	**Initial weight body(g) 0th Day**	**Final weight body(g) 30th Day**	**Body weight gain(g)**
Normal control	152.60 ± 3.78	193.80 ± 7.01	+41.2
Normal SCG extract	220.53 ± 6.94	280.40 ± 9.47	+59.87
Normal SCG extract &aspartame	155.00 ± 4.24	195.80 ± 4.76	+40.8
Normal aspartame	168.80 ± 27.17	163.80 ± 26.12*	-5
Diabetic control	169.20 ± 7.25	161.80 ± 7.39*	-7.4
Diabetic SCG extract	246.60 ± 3.28	286.40 ± 9.86	+40
Diabetic SCG extract &aspartame	234.40 ± 17.41	274.80 ± 10.59	+40.4
Diabetic aspartame	234.20 ± 18.67	219.20 ± 20.82*	-15

Table 2: Effect of single clove garlic (SCG) extract against aspartame induced on relative liver weights (g) in normal and diabetic rats.

Relative weighs Group	**Relative liver weight (g) Mean ± SD**	**%Change**
Normal control	3.92±0.247	0.00
Normal SCG extract	3.59 ±0.256	-8.41
Normal SCG extract &aspartame	3.60 ±0.258	-8.16
Normal aspartame	4.47±0.539 a**b***	14.03
Diabetic control	4.03 ±0.296	2.80
Diabetic SCG extract	3.56 ±0.043	-9.18
Diabetic SCG extract &aspartame	3.50±0 .273 c**	-10.71
Diabetic aspartame	4.66 ±0.287 a**d**	18.87

Data were presented as mean ± standard deviation (SD) of 6 animals| group (n = 6) = Number of rats/groups. a: significant values compared to normal control. *p < 0.05; **p < 0.01; and *** p< 0.001.

In addition, the rats treated with diabetic SCG extract and ASP showed a significant decrease in ALT, AST and ALP serum levels 82.20 ± 12.93 U/L, 171.00 ± 5.47 U/L and 146.60 ± 2.40 U/L, respectively, compared to the diabetic ASP group 106.40 ± 2.96 U/L, 223.00 ± 6.00 U/L and 227.20 ± 2.58 U/L, respectively. The results also showed that there was a significant decrease in ALT, AST, and ALP serum levels 82.20 ± 12.93 U/L, 171.00 ± 5.47 U/L, and 146.60 ± 2.40 U/L compared to diabetic control rats 116.40 ± 9.31 U/L, 227.80 ± 9.01 U/L and 229.60 ± 13.27 U/L, respectively.

Table 3: Effects of single clove garlic (SCG) extract against aspartame-induced hepatotoxicity in normal and diabetic rats; levels of ALT.

Parameters Group	ALT (U/L)	% Change
Normal control	74.40 ± 11.92	**0.00**
Normal SCG extract	74.00±11.72	**-0.53**
Normal SCG extract &aspartame	77.60±27.18	**4.30**
Normal aspartame	110.60 ±4.56 ^{a***} ^{b***}	**48.65**
Diabetic control	116.40 ±9.31 ^{a***}	**56.45**
Diabetic SCG extract	79.20±8.10 ^{c***}	**6.45**
Diabetic SCG extract &aspartame	82.20±12.93	**10.48**
Diabetic aspartame	106.40 ±2.96 ^{a**} ^{d**}	**43.01**

G1: control group, G2: rats treated with SCG extract (0.5 g/kg body weight), G3: rats were treated with SCG extract (0.5 g /kg body weight), and aspartame (ASP) (200 mg/kg body weight) G4: rats treated with ASP (200 mg/kg body weight), G5: diabetic rats (Induced by alloxan (ALX) 120 mg/kg body weight), G6: diabetic rats treated with SCG extract (0.5 g /kg body weight), G7: diabetic rats treated with SCG extract (0.5 g /kg body weight), and ASP (200 mg /kg body weight) and G8: diabetic rats treated with ASP 200 mg /kg body weight.

Table. 4: Effect of single clove garlic (SCG) extract against aspartame-induced hepatotoxicity in normal and diabetic rats; levels of AST.

Parameters Group	AST (U/L)	% Change
Normal control	165.60 ±21.41	0.00
Normal SCG extract	164.40 ±7.12	-0.72
Normal SCG extract &aspartame	168.20±13.06	1.57
Normal aspartame	218.60±4.21^{a***}^{b***}	32.00
Diabetic control	227.80±9.01 ^{a***}	37.56
Diabetic SCG extract	168.60±14.63 ^{c***}	1.81
Diabetic SCG extract &aspartame	171.00±5.47	3.26
Diabetic aspartame	223.00±6.00 ^{a***} ^{d***}	34.66

G1: control group, G2: rats treated with SCG extract (0.5 g/kg body weight), G3: rats treated with SCG extract (0.5 g /kg body weight), and aspartame (ASP) (200 mg/kg body weight) G4: rats treated with ASP (200 mg/kg body weight), G5: diabetic rats (Induced by alloxan (ALX) 120 mg/kg body weight), G6: diabetic rats treated with SCG extract (0.5 g/kg body weight), G7: diabetic rats treated with SCG extract (0.5 g/kg body weight), and ASP (200 mg/kg body weight) and G8: diabetic rats treated with ASP 200 mg /kg body weight.

Table 5: Effect of single clove garlic (SCG) extract against aspartame-induced hepatotoxicity in normal and diabetic rats; levels of ALP.

Parameters Group	ALP (U/L)	% Change
Normal control	141.20 ± 14.34	0.00
Normal SCG extract	140.80±14.54	-0.28
Normal SCG extract &aspartame	142.00±24.80	0.56
Normal aspartame	232.00 ±8.54 ^{a***} ^{b***}	64.30
Diabetic control	229.60 ±13.27 ^{a***}	62.60
Diabetic SCG extract	145.60±37.18 ^{c***}	3.11
Diabetic SCG extract &aspartame	146.60±2.40	3.82
Diabetic aspartame	227.20 ±2.58 ^{a***} ^{d***}	60.90

G1: control group, G2: rats treated with SCG extract (0.5 g/kg body weight), G3: rats treated with SCG extract (0.5 g/kg body weight), and aspartame (ASP) (200 mg/ kg body weight) G4: rats treated with ASP (200 mg/kg body weight), G5: diabetic rats (Induced by alloxan (ALX) 120 mg/kg body weight), G6: diabetic rats treated with SCG extract (0.5 g/kg body weight), G7: diabetic rats treated with SCG extract (0.5 g/kg body weight), and ASP (200 mg/kg body weight) and G8: diabetic rats treated with ASP 200 mg /kg body weight.

4.4 Histopathological Examination

The liver cross-sections of the control group showed normal morphology, exhibiting normal hepatocytes with normal central vein and peripheral hepatic triads or tetrads embedded in connective tissue, as shown in Plate 1A, B & C. The liver cross sections of ASP (200 mg/kg body weight) treated rats showed congestion and some lesions such as hemorrhage compared to the control group as shown in panel 1D.

Plate 2A, B & C show the cross-sections of the liver of diabetic rats, which showed central vein (CV) and hepatocytes (HC), enlargement of many hepatocytes (arrows), congestion (C), and hydropic change. In the group treated with alloxan and SCG extract (0.5 g/kg body weight), the liver cross-sections showed slight congestion (C). The liver cross-sections of rats treated with ethanolic SCG extract, and ASP showed a slight hydropic change. The liver cross-sections of rats treated with alloxan, and ASP showed severe degeneration of many hepatocytes, as most cells had lost their cell borders (Plate 2d).

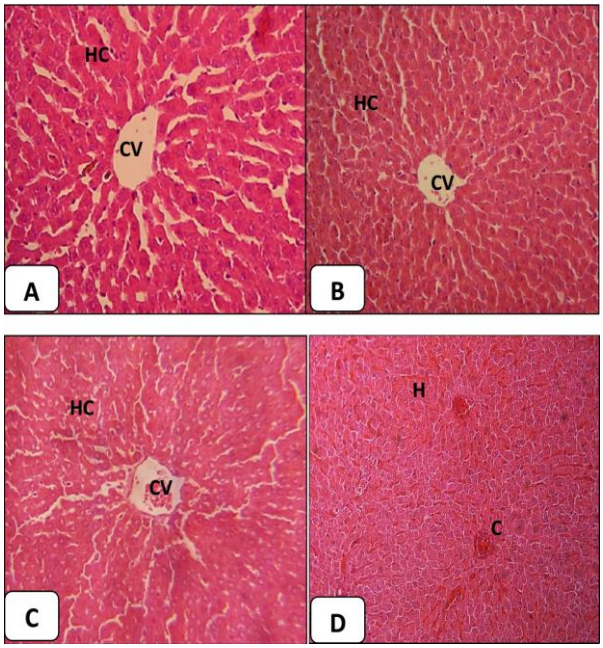

Plate 1: Photomicroscopic cross-sections of the liver of (A): G1 showing normal hepatocyte architecture (HC) and normal central vein (CV). (B): G2 showing normal central vein (CV) and hepatocyte (HC) architecture. (C): G3 showing normal central vein (CV) and hepatocyte (HC) structure. (D): G4 with congestion (C) and hemorrhage (H) of the central vein (CV) and hepatocytes (HC); H& E (X100) and H& E (X400).
G1: control group, G2: rats treated with SCG extract (0.5 g/kg body weight), G3: rats treated with SCG extract (0.5 g/kg body weight) and aspartame (ASP) (200 mg/kg body weight), G4: rats treated with ASP (200 mg/kg body weight).

5. Discussion

5.1 The Change in Body Weight

The results of the present study showed that body weight gain decreased significantly in the ASP-treated group compared to the normal control group. We also reported that administration of ASP in diabetic rats showed a significant decrease in body weight gain compared to that of the normal control group. Our findings are in agreement with the study of [30 ,31], Abd-Elfatah *et al*., (2012) who reported that albino rats receiving ASP showed a significant decrease in body weight. The observed decrease in body weight of treated animals could be a result of protein depletion due to the unavailability of carbohydrates as an energy source [32,33].

The result of the present study is in agreement with the study of Anton *et al.* (2010) and Abd-Elwahab *et al.* (2017) [34,35] who used data to find that sweeteners ASP can affect both fat and carbohydrate metabolism in addition to increasing energy expenditure. Consequently, the results showed a significant decrease in body weight in the diabetes control group compared to the body weight of the normal control group.

In contrast, the rats orally administered the normal SCG extract with ASP showed no change in body weight compared to the normal control rats. However, the rats given the normal SCG extract orally showed a significant increase in body weight compared to the normal control rats. The diabetic group treated with SCG extract and the group treated with SCG extract and ASP also showed a significant increase in body weight compared to the body weight of the diabetic control group.

The results of the current study are in agreement with the studies of [36,37] who treated rats with garlic extract before alloxan treatment and showed a significant increase in body weight of the diabetic rats, which is because the active ingredients of garlic such as S-allylcysteine and organic sulfur can lead to weight gain in alloxan-induced diabetic rats. These results confirm a study by [38]. The treatment of rats with aqueous garlic extract compensates for the reduction in body weight and causes a significant increase in body weight of alloxan-treated rats. These results show that the extract from a single clove of garlic has a protective effect on the changes in body weight caused by the administration of aspartame and alloxan.

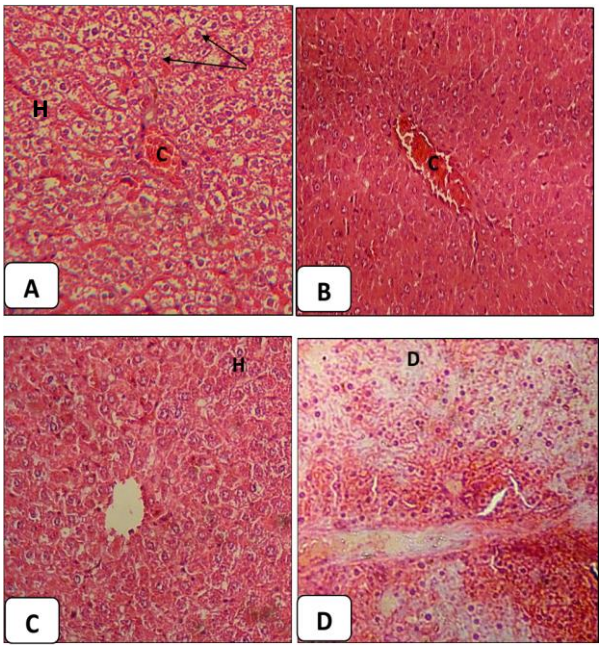

Plate 2: Photographic cross-sections of the liver of diabetic rats (A): G5 showing hydropic change, enlargement of many hepatocytes (arrows) and congestion (C), central vein (CV) and hepatocytes (HC). (B): G6 with mild congestion (C), central vein (CV) and hepatocytes (HC). (C): G7 with mild hydropic changes (H) of the central vein (CV) and hepatocytes (HC). (D): G8 shows severe degeneration of many cells and most cells have lost their cell borders (D) of the central vein (CV) and hepatocytes, H & E (X 100) and H & E (X 400).
G5: diabetic rats (induced by alloxan (ALX) 120mg/kg body weight), G6: diabetic rats treated with SCG extract (0.5 g/kg body weight), G7: diabetic rats treated with SCG extract (0.5 g/kg body weight) and ASP (200 mg/kg body weight) and G8: diabetic rats treated with ASP 200 mg/kg body weight.

5.2 The Relative Liver Weight

The results of the groupsreated group showed a significant increase in relative liver weight compared to the relative liver weight of the normal control group. In addition, the diabetes group treated with ASP showed a significant increase in relative liver weight compared to the normal control group. These results are consistent with the study of [39], in which diabetic rats with CCL_2 were evaluated for hepatotoxicity, as evidenced by increased liver weight relative to body weight and elevated liver enzymes. In the study [40], gentamicin was administered at a dose of 80 mg/kg, which also caused a significant increase in liver weight. The increase in liver weight in the ASP group was most likely due to inflammatory cells, enlargement, congestion, and hemorrhage in the liver, which were evident in the overall appearance of the liver. These symptoms were similar to the results of our study.

The current results are not consistent with the study by [41], who reported a significant decrease in some organ weight of the liver of the aspartame group (40mg/kg body weight). This may be attributed to the difference in dose, treatment duration, and sex or size of the rats. The results of the current study showed that there were no changes in relative liver weights. On the contrary, there was no significant difference between the relative liver weight in the SCG extract treated group and the SCG extract with ASP compared to the normal control group.

However, there was a significant decrease in relative liver weight in the diabetic group treated with SCG extract alone and in the group treated with SCG extract and ASP compared to the diabetic control group and the normal control group. In a study [42], the effects of garlic at a dose of (500 mg/kg body weight) administered to experimental animals for 4 weeks and the general morphological effects on the liver were observed. A low concentration of allicin has a limited role in lowering cholesterol levels by inhibiting the metabolic pathways of cholesterol biosynthesis. In a previous study [43], it was reported that administration of black garlic (200 mg/kg body weight) resulted in a significant decrease in liver weight. These results demonstrate the protective effect of SCG extracts on the changes in relative liver weight induced by aspartame and alloxan in normal and diabetic rats.

5.3 The liver enzymes (ALT, AST, and ALP) levels

The results of the current study have shown that oral administration of ASP affects liver function tests by increasing the levels of liver enzymes (ALT, AST and ALP) compared to the normal control group. These results are in line with [44,45,46] who found that ASP causes a significant increase in the liver function markers AST, ALT and ALP, leading to the formation of free radicals that cause cell damage and release the marker enzymes into the bloodstream. Estimating the activities of the marker enzymes in serum allows an assessment of liver function. Excessive alcohol consumption has been reported to be associated with altered liver metabolism and liver injury with leakage of cytoplasmic liver enzymes into the bloodstream [47,48,49,50].

In the current study, the results showed that liver enzymes were significantly elevated in ALT, AST and ALP in the diabetes control group compared to the normal control group. Thus, these results are consistent with [51], who found that high blood glucose causes a significant increase in ALT, AST and ALP levels in the blood. Thus, as previously reported, our results can be explained by the oxidative stress caused by hyperglycemia, which plays an important role in the development of diabetes and its complications. The increase in ALT, AST and ALP activities after hypoglycemia is stimulated by the production of reactive oxygen species (ROS) and impaired antioxidant enzymes, leading to oxidative stress and organ dysfunction [52].

Our results have shown that there was a significant increase in ALT, AST, and ALP levels after administration of ASP to the diabetic group compared to the normal control group. These results are consistent with those of [53], whose results, as previously reported, can be explained by the oxidative stress caused by high blood glucose, which plays an important role in the development of diabetes and its complications. The results have also shown that after the administration of SCG extract alone and SCG extract and induction of ASP, there was a significant decrease in ALT, AST, and ALP blood levels compared to the group treated with ASP. This decrease was due to the efficacy of ALT, AST, and ALP after the administration of SCG extract, which is attributed to the protective effect of garlic-derived S-allylcysteine on liver damage and oxidative stress [54]. Moreover, the results of the SCG extract-treated group after induction of diabetes by ALX inhibited the higher increase of ALT, AST, and ALP compared to the diabetic control group. Certainly, these results are consistent with the study of [55], which indicates that diabetes can lead to liver dysfunction. Thus, the effect of garlic was reported in both alloxan- and streptozotocin-induced diabetic rats.

The study [56] suggests that the presence of polyphenols and flavonoids in garlic extract may be responsible for the antioxidant activity and the increase in serum levels of ALT, AST and ALP. From the present data, treatment with SCG extract significantly improves the impaired liver functions of ALX-induced diabetic rats. However, the results of the same study show that ALT, AST and ALP levels decreased significantly in the diabetic group treated with SCG extract compared to the diabetic control group. The researchers found that garlic extracts contain certain compounds such as germanium and selenium, which play an important role in normalizing oxygen utilization in the cells [57].

5.4 Histopathological

Histologic analysis provided reliable support for the data obtained by biochemical analysis in rats receiving ASP that exhibited severe histologic changes in the form of congestion and hemorrhage. In this study, male albino rats treated with ASF showed histopathological changes in their livers, namely disintegration of hepatocytes, depletion of cytoplasm and disorganization of cellular organelles. In addition, glycogen granules decreased while the amount of collagen fibers in the portal area increased. In this respect, the histopathological changes in the liver of male albino rats were similar to those of female albino rats in the study [30].

The results state that aspartame was rapidly metabolized with minimal toxicity and liver damage at the border, while other studies showed visceral vacuoles in the hepatocytes after administration of ASP. These toxic agents caused an imbalance in the arrangement of cytoskeletal components, leading to cytoplasmic discharges. The production of methanol and aspartic acid, which led to the release of free radicals, was due to the ingestion of ASP [58,59,60]. The researcher also found that the liver of the diabetic rats with ASP had other severe histologic changes compared to the control group, in which many cells degenerated and most cells lost their cell borders (D), as shown in (Plate 2d). Thus, the results are in agreement with [28], who found that the liver of diabetic-treated rats showed degeneration of many cells and most cells lost their cell borders. The results are also in agreement with [46], who found that consumption of ASP by diabetics could further aggravate the health condition of these individuals. These results can be explained by the fact that oxidative stress triggered by hyperglycemia plays a key role in the development of diabetes and its complications. This opinion is consistent with our study in which a significant increase in lipid peroxidase was observed in liver tissue of rats after 28 days of treatment with ASP. A similar result was reported [60]. Thus, the results are in correlation with our results which showed changes in liver functions and an increase in hepatotoxicity markers after administration of ASP to normal and diabetic rats [28,61].

In addition, the results of our study showed that the liver sections of diabetic rats exhibited hydropic changes, enlargement of many hepatocytes and congestion, as shown in (Plate 2a). These results are consistent with those of [28]. The diabetic-treated liver showed enlargement of many hepatocytes and necrosis in some areas of hepatocytes. It was also shown that administration of ALX to experimental rats selectively caused pancreatic β-cell membrane destruction and cytotoxicity after its intracellular accumulation [62]. In addition, the depletion of glycogen in diabetic rats would increase hyperglycemia and cause damage to the liver and the whole body [63].

In the comparison to the control group, histopathological abnormalities were detected in the liver of both the SCG extract and the SCG extract with ASP (see Table 1a, b and c). In contrast, mild hepatic congestion was observed in the central vein and hepatocytes of the diabetic rats with SCG extract (see panel 2b). Thus, the results of this study show that garlic has a high level of antioxidant activity. Recent in vitro studies by [64,65] have confirmed the vasoactive properties of garlic's sulfur compounds. The aged garlic extract contains the active and stable component S-allylcysteine, which allows standardization of S-allylcysteine. Table 2c shows that the liver of diabetic rats with SCG extract and ASP exhibited mild hydropic changes in the central vein and hepatocytes compared to that of the diabetic ASP group. Thus, the results are in agreement with the study [66], which reported that garlic such as allicin, alliin, and two major organosulfur compounds S-allylcysteine are potent free radical scavengers. In the present study, we reported that these compounds may be responsible for protecting tissues from damage and various diseases, as garlic extract has high antioxidant content and health-promoting potential. Furthermore, a study by [67] has shown that S-allylcysteine and organic sulfur compounds found in garlic scavenge hydroxyl radicals and radicals from oxidative and nitro stress in the laboratory.

6. Conclusion

The current study has shown that the administration of aspartame causes liver dysfunction in normal rats. At the same time, it was confirmed that treatment with a single clove of garlic (SCG) leads to a protective effect against the toxicity of aspartame on the liver. Aspartame caused further damage in diabetic rats compared to the effect of aspartame treatment in normal rats. The data obtained indicates that treatment with an extract of a single clove of garlic (SCG) could significantly improve impaired liver functions in diabetic rats. Our results suggest that single clove garlic extract (SCG) has a protective effect on aspartame and alloxan-induced changes in body weight and relative liver weight in both normal and diabetic rats.

References

[1] Mangnuson, B.A., Burdock, G.A., Doll, J., Kroes, R.M., Marsh, G.M., Pariza, M.W., Spencer, P.S., Waddell, W.J., Walker, R. and Williams, G.M. (2007) Aspartame: a safety evaluation based on current use levels, regulations, and toxicological and epidemiological studies, *Critical Reviews in Toxicology* **37**: 629-727.

[2] Rencuzogullari, E., Tuylu, B.A., Topaktas, M., Ila, H.B., Kayraldiz, A., Arslan, M., Diler, S.B. (2004) Genotoxicity of aspartame. *Drug Chemical Toxicology* **27**:257–268.

[3] Ishiwata, H., Simon, R.A., Adverse Reactions to Food Additives, in: D'Mello, J.P.F., (Ed.), Book (2003) Adverse Reactions to Food Additives, CABI, Oxon, UK, pp. 235-240**.**

[4] Henkel, J. (2007) Sugar substitutes: Americans opt for sweetness and lite, *Food and Drug Administration ,Consumer* **33:** 12-16.

[5] Garriga, M.M ., Metcalfe, D.D (1988) Aspartame intolerance, *Annals of allergy* **61**:63-69.

[6] Portela, G.S., Azoubel, R., Batigalia, F. (2007) Effects of Aspartame on Maternal-Fetal and Placental Weights, Length of Umbilical Cord and Fetal Liver: A Kariometric Experimental Study, *International Journal Morphology* **25**: 549- 554.

[7] Trocho, C., Pardo, R., Rafecas, I., Virgili, J. X., Remesar, X., Fernandez-Lopez, J.A. and Alemany, M. (1998). Formaldehyde derived from dietary aspartame binds to tissue components in vivo, *Life Science*s. **63:** 337-349.

[8] Humphries, P., Pretorius, E., Naude, H. (2008) Direct and indirect cellular effects of aspartame on the brain, *European Journal of Clinical Nutrition* **62:** 451-462.

[9] George, V., Arora, S., Wadhwa, B.K., Singh, A.K. (2010) Analysis of multiple sweeteners and their degradation products in lassi by HPLC and HPTLC plates, *Journal of Food Science and Technology* **47:** 408-413.

[10] Zafar, T., Naik, Q.A.B., Shrivastava, V.K. (2017) Aspartame: Effects and Awareness, *MOJ Toxicology* **3**:23-26.

[11] Heber, D. (2004) Vegetables, fruits and phytoestrogens in the prevention of diseases, *Journal of Postgraduate Medicine* **50**: 145-149.

[12] Abhilash, M., Paul, M.V.S., Arghese, M.V.V., Nair, R.H. (2011) Effect of long term intake of aspartame on antioxidant defense status in liver, *Food and Chemical and Toxicology* **49**: 1203–1207.

[13] Gombos, K., Varjas, T., Orsós, Z., Polyak, E., Peredi, J., Varga, Z., Ember, I. (2007) The effect of aspartame administration on oncogene and suppressor gene expressions, *In Vivo* **21**: 89–92.

[14] Morales, F.M., Cervantes, E.M., Espinoza, M.A.I., Martinez, O.H.A. (2015) Nutritional and biochemical effects of Aspartame intake in rats under experimental diet, *Journal of Experimental Biology and Agricultural Sciences* **3:** 298-306.

[15] Malomo, S.O. (2000) Toxicological implication of ceftriaxone administration in rats, *Nigerian Journal of Biochemical Molecular Biology* **15:** 33-38

[16] Yakubu, M.T., Bilbis, L.S., Lawal, M., Akanji, M.A. (2003) Effect of repeated administration of sildenafil citrate on selected enzyme activities of liver and kidney of male albino rats, *Nigerian Journal Pure Applied Science.* **18**: 1395-400.

[17] Mirunalini, S., Arulmozhi, V., Arulmozhi, T. (2010) Curative Effect of Garlic on Alcoholic Liver Disease Patients, *Jordan Journal of Biological Sciences* **3**: 147-152.

[18] Shah, C.S., Qadry, J.S. (1971) A Textbook of Pharmacognosy, ed., Messrs B.S. Shah, India, pp. 351.

[19] Blumenthal, M., Goldberg, A., Brinkmann, J. (2000) Herbal medicine-Expanded commission Emono graphs, *International Archive Medical* **6:** 35-41.

[20] Abd El-Halim, S.S., Mohamed, M.M. (2012) Garlic powder attenuates acrylamide-induced oxidative damage in multiple organs in rat, *Journal of Applied Science. Research* **8**:168–173.

[21] Shitaw, K. (2015) Studies on the levels of fluoride in selected spices cultivated and consumed in Ethiopia. *Department of Chemistry, College of Natural and Computational Sciences,* Master of Science in Analytical Chemistry Thesis, Addis Ababa University, Addis Ababa.

[22] Cruz, C., Pedraza-Chaverri, J. (2008) Garlic powder ameliorates Cisplatin-induced Nephrotoxicity and oxidative stress, *Journal of Medical and Food* **11:**582–586.

[23] Rafieian-Kopaei, M., Asgary, S., Adelnia, A., Setorki, M., Khazemi, S., Shamsi, F. (2011) The effects of Cornelian cherry on atherosclerosis and atherogenic factors in hypercholesterolemic rabbits, *Journal of Medical Plants Research* **5**: 2670-2676.

[24] Alsoudi, A.A.S. (2017) Effect of garlic extract for the Mitigation of CCL4 on Rabbit Tissues. *Biology Department, College of Science,* Master Thesis Thesis, Sana'a University.

[25] Naji, K.M., Al-Shaibani, E.S., Alhadi, F.A., Al-Soudi, S.a.A., D'souza, M.R. (2017) Hepatoprotective and antioxidant effects of single clove garlic against CCl4-induced hepatic damage in rabbits, *BMC Complementary and Alternative Medicine* **17**: 1-12.

[26] Maldonado, P.D., Barrera, D., Medina-Campos, O.N., Hernandez-Pando, R., Ibarra-Rubio, M.E., Pedraza-Chaverr, J**.** (2003) Aged garlic extract attenuates gentamicin induced renal damage and oxidative stress in rats, *Life Science*s **73**: 2543–2556.

[27] Thabrew, M., Samarawickrema, N., Chandrasena, L., Jayasekera, S. (2000) Protection by garlic against adriamycin induced alterations in the oxido-reductive status of mouse red blood cells, *Phytotherapy Research* **14**: 215-217.

[28] Khidr, B.M., El-Sokkary, G.H., Saleh, S. (2017) Study on morphological changes induced by aspartame on liver of normal and diabetic male albino rats, *Journal of Histology and Histopathology* **4**: 10.7243

[29] Velmurugan, B., Selvanayagam, M., Cengiz, E.I., Unlu, E. (2007) Histopathology of lambda-cyhalothrin on tissues (gill, kidney, liver and intestine) of Cirrhinus Mrigala, *Environment Toxicology and. Pharmacology* **24**: 286–91.

[30] Abd-Elfatah, A.A., Ghaly, I.S., Hanafy, S.M. (2012) Cytotoxic effect of ASP (diet sweet) on the histological and genetic structures of female albino rats and their offspring, *Pakistan Journal of Biology Science* **15**: 904–918.

[31] Azeez, O., Alkass, S. (2018) Effect of long-term consumption of aspartame on body weight, *International Journal of Current Advanced Research* **7**: 14464-14474.

[34] Anton, S.D., Martin, C.K., Han, H., Coulon, S., Cefalu, W.T., Geiselman, P., Williamson, D.A. (2010) Effects of stevia, aspartame, and sucrose on food intake, satiety, and postprandial glucose and insulin levels, *Appetite* **55**: 37-43.

[35] AbdElwahab, A.H., Yousuf, A.F., Ramadan, B.K., Elimam, H. (2017) Comparative Effects of Stevia rebaudiana and Aspartame on hepato-renal function of diabetic rats: Biochemical and Histological Approaches, *Journal of Applied Pharmaceutical Science* **7**: 034-042.

[36] Grover, J., Yadav, S., Vats, V. (2002) Medicinal plants of India with anti-diabetic potential, *Journal of Ethnopharmacology* **81**: 81-100.

[37] Ojo, R.J., Memudu, A.E., Akintayo, C.O., Akpan, I.S. (2012) Effects of pre-induction administration of Allium sativum on some biochemical parameters in alloxan induced diabetic rats, *Research Journal of Applied Sciences, Engineering and Technology* **4**: 5129-5135.

[38] Baluchnejadmojarad, T., Homayounfar, M.H., Hosseini, M. (2003) Beneficial effect of aquaeous garlic extract on the vascular reactivity of streptozotocin diabetic rats, *Journal of Ethnopharmacol*ogy. **185**: 139-144.

[39] Kalender, S., Ogutcu, A., Uzunhisarcikli, M., Ac¸ikgoz, F., Durak, D., Ulusoy, Y., Kalender, Y. (2005) Diazinon-induced hepatotoxicity and protective effect of vitamin E on some biochemical indices and ultrastructural changes, *Toxicology.* **211:** 197-206.

[40] Noorani, A. A., Gupta, K., BhadAda, K. and Kale, M. K. (2011). Protective Effect of Methanolic Leaf Extract of Caesalpinia Bonduc (L.) on Gentamicin-Induced Hepatotoxicity and Nephrotoxicity in Rats, *Iranian Journal of Pharmacology Therapeutics* **10**: 21-25.

[41] Ab Qayoom, N., Shrivastava, V.K. (2019) Effects of Short-term Consumption of Aspartame on Some Biochemical and Hematological Parameters in Female Swiss Albino Mice, *International Journal of Zoology Research* **15**: 21-27.

[42] Farnaz, S. and Zahid, M., (2011) Effects of feeding garlic *(allium sativum*) on body weight and serum cholesterol levels in rats, *Pakistan. Journal of Physiology* **1**:7-11.

[43] Shin, J.H., Lee, C. W., Oh, S. J., Yun, J., Kang, M.R., Han, S.B., Kang, J.S., (2014) Hepatoprotective effect of aged black garlic extract in rodents, *Toxicology Research*, vol. **30:** no. 1, pp. 49–54.

[44] Choudhary, A.K., Selvaraj, S., Sheela Devi, R. (2014) Aspartame induce modification in membrane bound and antioxidant enzymes in liver and kidney of Wistar albino rats, *Current Nutrition & Food Science* **10**: 275-287.

[45] Choudhary, A.K., Devi, R.S. (2014) Serum biochemical responses under oxidative stress of aspartame in wistar albino rats, *Asian Pacific Journal of Tropical Disease* **4**: S403-S410.

[46] Adaramoye, O.A., Akanni, O.O. (2016) Effects of long-term administration of aspartame on biochemical indices, lipid profile and redox status of cellular system of male rats, *Journal of basic and clinical physiology and pharmacology* **27**: 29-37.

[47] Srinvasan, S., Pragasam, V., Jenitha, X., Kalaiselvi, P., Muthu, V., Varalakshmi, P. (2004) Oxidative stress in urogenital tuberculosis patients: A predisposing factor for renal stone formation-amelioration by vitamin E susplementation, *Clinical Chemical Acta* **350**: 57-63.

[48] Das, D., Mukherjee, M.M., Das, A.S., Mitra, C. (2005) Aqueous extract of black tea (*Camellia sinensis*) prevents chronic ethanol toxicity, *Current Science* **88**: 952–61.

[49] Giannini, E.G., Testa, R., Savarino, V. (2005) Liver enzyme alteration: a guide for clinicians, *Cmaj* **172**: 367-379.

[50] Ashok, I., Wankhar, D., Sheeladevi, R., Wankhar, W. (2014) Long-term effect of aspartame on the liver antioxidant status and histopathology in Wistar albino rats, *Biomedicine & Preventive Nutrition* **4**: 299-305.

[51] Swaminathan, R. (2004) Handbook of Clinical Biochemistry, 1st ed., Oxford University Press, UK, pp. 32.

[52] Manna, P., Das, J., Ghosh, J., Sil, P.C. (2010) Contribution of type 1 diabetes to rat liver dysfunction and cellular damage via activation of NOS, PARP, IκBα/NF-κB, MAPKs, and mitochondria-dependent pathways: Prophylactic role of arjunolic acid, *Free Radical Biology and Medicine* **48**: 1465-1484.

[53] Agamy, N.F., Ismail H., Youssef, M. I., Fawzi, M. (2008) Comparative study on the effects of steviosides and ASP on glucose, urea and creatinine levels of normal and type 2 diabetic rats, *Journal of High Institute of Public Health* **38**: 102-112.

[54] Pedraza-Chaverri, J., Yam-Canul, P., Chirino, Y.I., Sanchez-Gonzalez, D.J., Macias-Macias, C.M., Cruz, C., Medina-Campos, O.N. (2008) Protective effects of garlic powder against potassium dichromate-induced oxidative stress and nephrotoxicity, *Food and Chemical Toxicology*. **46**: 619-27.

[55] Thomson, M., Al-Amin, Z.M., Al-Qattan, K.K., Shaban, L.H., Ali, M. (2007) Anti-diabetic and hypolipidaemic properties of garlic *(Allium sativum)* in streptozotocin-induced diabetic rats*, Dubai Diabetes and Endocrinology Journal* **15**:108-115.

[56] Ajith, T.A., Nivitha, V., Usha S. (2007) Zingiber officinale Roscoe alone and in combination with alpha-tocopherol protect the kidney against cisplatin-induced acute renal failure, *Food and Chemical Toxicology* **45**: 921-927.

[57] El-Khayat, Z., Rasheed, W., Ramzy, T., Hussein, J., Agaiby, M., Morsy, S., Morsy, F., Shaffie, N. (2010) Protective Effect of Garlic Oil against Liver Injury in Experimental Animals, *Journal of Medicinal Plants Research* **4:** 2359-2369.

[58] Tanemura, K., Kurohmaru, M., Kuramoto, K., Matsumoto, M., Hayashi, Y. (1994) Age-related changes in cytoskeletal components of the BDF1 mouse Sertoli cell. *Tissue and Cell* **26**: 447-55.

[59] Butchko, H.H., Stargel, W.W., Comer, C.P., Mayhew, D.A., Benninger, C., Blackburn, G.L., de Sonneville, L.M., Geha, R.S., Hertelendy, Z., Koestner, A. (2002) Aspartame: review of safety, *Regulatory Toxicology and Pharmacology* **35**: S1-S93.

[60] Iman, M.M. (2011) Effect of aspartame on some oxidative stress parameters in liver and kidney of rats, *African Journal of Pharmacy and Pharmacology* **5**: 678-682.

[61] El-Sokkary, G.H., Khidr, B.M., Saleh, S. (2016) Aspartame-induced oxidative stress on liver and kidney in normal and diabetic adult male rats, *Indian Journal of Applied Research* **6**: 511-3.

[62] Mathew, P.T., Augusti, K.T. (1975) Hypoglycaemic effects of onion, Allium cepa linn on diabetes mellitus-a preliminary report, *Indian Journal Physiology and Pharmacology* **19**: 213-217.

[63] Remedio, R.N., Barbosa, R.A., Castellar, A., Gomes, R.J. (2011) Histochemical and ultra-structural analysis of hepatic glycogen and collagen fibers in alloxan-induced diabetic rats submitted to long-term physical training, *Tissue and Cell* **43**: 207-215.

[64] Lawson L.D., Gardner, C.D. (2005) Composition, stability, and bioavailability of garlic products used in a clinical trial, *Journal of Agricultural and Food Chemistry* **53**: 6254-6261.

[65] Benavides, G.A., Squadrito, G.L., Mills, R.W., Patel, H.D., Isbell, T.S., Patel, R.P., DarleyUsmar, V.M., Doeller, J.E., Kraus, D.W. (2007) Hydrogen sulfide mediates the vasoactivity of garlic, *Proceedings of the National Academy of Sciences* **104**: 17977-17982.

[66] Asdaq, S.M., Inamdar, M.N. (2010) Potential of Garlic and Its Active Constituent, S-allyl Cysteine, as Antihypertensive and Cardioprotective in Presence of Captopril, *Phytomedicine* **17**:1016-1026.

[67] Pedraza-Chaverrí, J., Barrera, D., Maldonado, P.D., Chirino, Y.I., Macías-Ruvalcaba, N.A., Medina-Campos, O.N., Castro, L., Salcedo, M.I., Hernández-Pando, R. (2004) S-allylmercaptocysteine scavenges hydroxyl radical and singlet oxygen in vitro and attenuates gentamicin-induced oxidative and nitrosative stress and renal damage in vivo, *BMC Clinical Pharmacology* **4**: 1-13.

Thamar University Journal of Natural & Applied Sciences ***8****(2) (2023) 27 – 38*

DOI: https://doi.org/10.59167/tujnas.v8i2.1717

TUJNAS

Original Article

Assessment of Groundwater Resources in the Hard Basement Rocks of Yemen, Al Bayda City Case Study

Ahmed Abdul Aziz* and Abdulaleem Al Kadhy

Geology Department, Faculty of Applied Science, Taiz University, Taiz, Yemen

*Corresponding author: Ahmed. Abdul Aziz
Email: drahaziz2@gmail.com

Received: 31 October 2023. Revised (in revised form): 23 December 2023. Accepted: 24 December 2023. Published: 31 December 2023

Abstract:

The present study was carried out with the aim of assessing the availability of groundwater in a typical hard basement complex area in Yemen, the catchment area of Al-Bayda City catchment in the mountainous region of the country. The main objective of this study is to evaluate and quantify the groundwater resources available in this area. The available regional data on climate, topography, and geology as well as ASTER and Landsat imaginary data were collected, reviewed, and analyzed together with local hydrogeological studies and well inventories and then used to identify the general geohydrology of the catchment, characterize the local aquifer system, assess the groundwater situation and quantify the available groundwater in the study area. The results of this study show that the aquifer system accounts for only about 5 % of the entire catchment area and has a total thickness of 10 - 30 m. This aquifer has a small lateral extent and is interrupted by faults, dykes, and plutonic intrusions. Limited amounts of groundwater occur in isolated bodies along the main wadis at the base of the aquifer system. The groundwater level in these bodies has dropped by 19 m since 1983, on average by 0.5 m per year. Groundwater recharge for the current state is estimated at 1.95 million m^3/year, which is only 3% of the total annual precipitation. The total amount of groundwater withdrawn is estimated at 2.2 million m^3/year, which is 80% below the current (2023) total annual demand of around 11 million m^3. The study underlines the need to implement an urgent action plan to improve groundwater recharge through water extraction techniques. The research results can be used for the improvement and development of water resources in this area in particular and in the Yemen region in general.

Keywords: Assessment Groundwater Resources; Water Availability; Hard Basement Aquifers; Al Bayda City; Yemen

1. Introduction

Yemen, a country located in the southwest of the Arabian Peninsula with 555,000 Km^2 area and 30 million population, is an arid to semiarid climate with limited surface water and hence relies extensively on groundwater. Yemen has experienced an extreme water crisis, characterized by severe water shortages, very limited access of the population to safe drinking water, and rapid depletion of groundwater aquifers. The scarcity of water resources has become increasingly precious, resulting in serious environmental problems with socio-economic consequences. Yemen can be divided into two physical parts, the mountainous part in the west and the plateau in the east. The mountainous part of Yemen is composed mostly of volcanic rocks on the western slope and metamorphic or hard basement on the eastern slope [1]. In hard basement rocks, groundwater availability is limited to the weathered and fractured aquifers. The extent and potential of such aquifers are low, and their stored volume is small, which may lead to seasonal depletion or exhaustion of groundwater.

Al Bayda Governorate is an example of an area located on the hard basement complex rocks of Yemen. It is located in the central part of Yemen, lies within the arid zone, and is covered by the hard basement rocks for over 95 % of it is land area. Groundwater is available through dug wells but the yields of the wells are small and possibly only sufficient for drinking water supply. Being the capital of Al Bayda Governorate and representing an important city in the eastern highlands of Yemen, Al Bayda city has witnessed massive population growth and urban development. The water demand has increased with time but the availability of water decreased. Despite its significance in enhancing the availability of water resources in Al Bayda, there is no rare information about the hydrology of the region. In Al Bayda and the eastern mountains in general. Since the early 1970s, only three groundwater resource studies have been conducted in the region. The first was a comprehensive hydrogeological study, conducted by SGHORIAH in 1977/78 [2], but covered the lower part of Wadi Bayhan. The second was performed by ILACO [3], which covered some areas within Al Bayda Province including Al Bayda city. The third one was performed by GSHEC in 2008/9 [4] which aimed at evaluating the availability of groundwater in Wadi Bayhan to be used for supporting Al Bayda city water supply. The lack of information about water resources prevents proper planning and development. Therefore, there exists an urgent need for fast accurate data showing past and present water resource conditions (status) to help manage and utilize these valuable natural assets sustainably.

This research, therefore, has attempted to assess the change in the groundwater situation of the Al Bayda city catchment area. This study aims to review and update the hydrogeological information about the area with the main topic of groundwater quantity available in the area. The

geological and hydrogeological situation of the area has been identified. The aquifer system underlying the study area has been characterized and then the obtained data have been used for evaluating the change that occurred in the groundwater system of the area. Hopefully, the results of this study will help the decision makers to provide solid and proper management for existing water resources and even find other alternative resources for water resources.

2. Description of the Study Area

2.1. Background to the Study Area

The basement rocks of Yemen are exposed basically in the west of the country, covering about 20 percent of its surface. The most prominent exposure of these rocks occurs in the eastern part of the mountainous region where it appears as a triangular belt covering about 40,000 sq. km area [5]. The basement region is bordered by the mountains zone to the west, the southern coastal plains to the south, the Empty Quarter, and the Ramlat Al Sbaatayn desert to the north and east (Figure 1). It is landscape is undulated (subdued) relief, with some local, bare hills, often there is no soil material at all rock outcrops. Plant cover is sparse in the hills and consists of shrubs and small trees in the valleys. The region observes arid climatic conditions characterized by warm, low rainfall, and high evaporation. The mean temperature range is 4° C to 29 ° C in January and 26° C to 41 ° C in July, and the relative humidity ranges from below 22 % to 80% [6]. The average rainfall in this region is generally below 200 mm and the average annual evaporation ranges from 1600-3000 mm [1]. Such a climate is crude to the sustainability of natural water bodies and also infiltration and percolation of the rainwater into the ground as much is lost into space.

Al Bayda, Governorate is located in the central part of Yemen and has an area of 11000 km^2 and a population of 0.8 million in 2023 [7]. It is situated at the top of the eastern mountain slope (~2000 m a.s.l). Five Wadi systems originated within the boundaries of Al Bayda and convey surface water to topographically lower zones, to the Ramlat al Sabaatain basin, and the Gulf of Aden basin. Groundwater resources in Al Bayda are very limited; it occurs only as a shallow local aquifer system that can be found in weathered, fractured, and faulted zones or the narrow alluvial fills of the wadi beds. Depth to groundwater is usually less than 15 m in these zones and lowest yields [3]. The people living in Al Bayda depend on the collector/dug wells that yield a small and possibly only sufficient drinking water supply. Al Bayda City, the capital of Al Bayda Governorate, has been selected as the target area in this study because of its importance and history of water shortage.

2.2. Location and population of the area

Al Bayda catchment, which is the study area, lies at the southern edge of the eastern mountainous region just to the north of the main water divide. The catchment has a drainage area of 330 km^2 and forms the upstream part of Wadi Bayhan and extends between latitudes 13° 55' and 14° 06' north and longitudes 45°25' and 45° 40' east (Figure 1). The area includes Al Bayda capital city and 10 groups of villages with a total population of 100000, i.e. a total population density of around 330/km^2 compared to 100 /Km^2 in the basement region. The population of the area has increased by 6 times during the last 40 years. The catchment area of Al Bayda has special social and economic importance not only because it includes the highest population density and agricultural activity in the region but also because it encompasses the well field that supplies water to 42,000 inhabitants of Al Bayda capital city [4]. The drinking water requirement of the city and rural areas is met through dug/collector wells that dry up during dry seasons. The water supply of Al Bayda City is derived from the fractured basement through hand-dug wells. More than 400 dug wells are found drilled in the watershed, but their production has declined [4]. The people in the city are striving very hard to collect water for drinking and household use. There is therefore a need for proper assessment of groundwater resources in the area to mitigate water scarcity. Assessment of groundwater resources availability in the region is a pre-requisite and an important step towards solving water sacristy in the area where groundwater is the only source of water supply.

3. Material and Methods

In this study, an attempt was made to gather maximum information about the hydrogeology of the area using different techniques viz., ASTER data, satellite images, hydrogeological reconnaissance, etc. The methodology adopted in this work included the collection, reviewing, processing, analysis, and comparison of available data concerning the groundwater resources of the area. The collected data included meteorological records, geologic and topographic maps, wells inventories and hydrogeological data, remote sensing, and field measurements. The meteorological records were available from Radaa station, 100 km west of Al Bayda city. The topographic map of Al Bayda (Yemen Survey Authority, 1981 at a scale of 1: 50,000) [8], and geological maps of Al Bayda region (Kruck, and Schäffer, 1991 [9] and Robertson Group Plc, 1992) [10]. The well inventories of ILACO (9/1983) [3] and that conducted by GSHEC (9/2008) [4], in addition to the drilling and pumping tests performed by SGHORIAH [2] and the field measurements conducted by the authors in 2013. The satellite image (Landsat 7ETM+ image acquired on January 14, 2005) and SRTM data were downloaded from the archive of the Global Land Cover Facility (GLCF) [11]. The fieldwork of 2013 included well point inventory, water sample collection, cross-section measurements, and well discharge measurements at various locations.

The collected data were subjected to various processing steps. including, scanning, mosaicking, referencing, correction, verification, and analyzing until producing the final outputs (maps). The initial step was to prepare topographic and geologic maps that would serve as a base map on which the boundaries of the catchment area, drainage pattern, lithological units, and lineaments could be overlain; The next step was to locate and describe the aquifer system in terms of its occurrence and characteristics, the final step was to quantify the groundwater availability and usability in the area. The data processing steps were done by using ERDAS-Imagine 8.4, Arc Map 9.4, Surpher11, 3dem, etc.

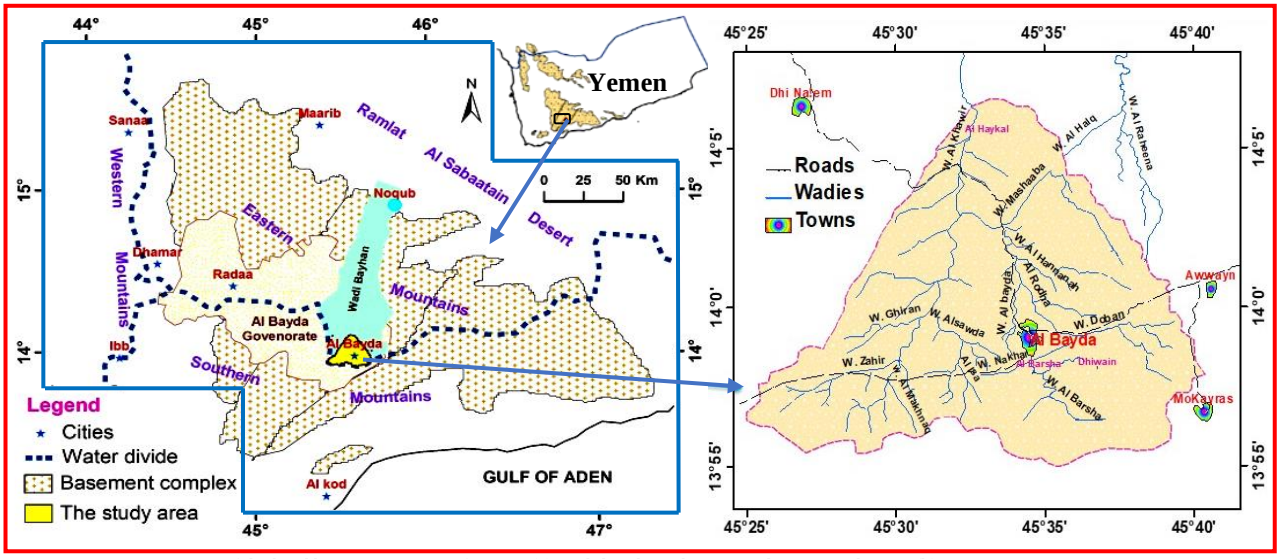

Figure 1: Location map of the hard basement region of Yemen (a), and the Al Bayda City catchment, study area (b).

The processed Landsat (ETM+) and ASTER data were used for addressing the topographical and geological variations, tracing the drainage lines, and mapping the alluvial cover of the study area. The well inventory data including locations, altitudes, depths lithology, etc., were used for the preparation of the hydrogeological cross sections which were used for characterizing the geometries of the aquifer system of the area. Areas of thick alluvial deposits were demarcated with the help of these imageries as well as ASTER data. For the first time, various maps, such as topographic, drainage, geologic, and hydrogeological maps have been prepared in this study, which were utilized for delineating the main surface hydrological features and then for preparation of hydrogeological cross sections for the aquifers in the area.

Assessment of groundwater resources in the study area has been done through the identification of its occurrence, depths, use, and quantification of its recharge and discharge areas. The water depth maps for the study area were plotted using ArcGIS and Surfer programs. A careful analysis of the water table contours provided an understanding of the groundwater flow pattern, which in turn, helped to delineate groundwater saturation zones. A comparative analysis has been made between the results of previous studies to evaluate the groundwater situation and its change during the last 30 years (1983-2013). Empirical equations were used to calculate the quantity of water available in the aquifer system of the area. As a result, estimates of ground-water use, demand, and deficit were calculated. Finally, the obtained information about the study area has been discussed in the following sections.

4. Results and Discussions

4.1. Topography and Climate

The study area is located at the edge of the eastern highlands, just to the north of the main water divide between the eastern and southern mountains slops (Figure 1). The digital elevation model (DEM), generated around Al Bayda catchment shows that the elevation of the catchment varies from 1900 to 2300 m above sea level (Figure 2a). The catchment area is a pen plain sloping slightly at north and surrounded in the south, west and east by mountainous ranges. The drainage system of the area is dendritic with a large number of short tributaries that have been dissected by hills and geologic structures. Small hills, short ridges, bare rock plateau. narrow wadis and shallow depressions are the main morphological features in the area (Figure 2b). The hills and ridges have gently sloping surfaces and rise to elevations of 50 to 200 m from the wadi floors. The wadis which are covered by alluvial deposits are mostly narrow (70-150 m width), and in some places, they become wider (200-500m) or disconnected by hills to form small basins. The ground surface dominated the area is shallow rocks and bar rocks outcrops (see pictures in Figure 2). Often there is no soil material at all in rock outcrops. The soils are found in the wadis. Only the deeper soils are suitable for cultivation. Whether they are cultivable or not depends on the availability of water.

The climate of the basement region is arid to semi-arid with low and erratic rainfall and high evaporation rates. According to AREA (2005), the region has moderate weather with an average temperature of 24 °C. The maximum and minimum temperatures are about 32 °C in July and 4 °C in January. The relative humidity ranges between a maximum of 70 % in winter and a minimum of 45% in summer [6]. Rainfall occurs in two seasons of the year but varies from year to year. The average annual rainfall is about 200 mm, but varies from year to year, fluctuating between 100 and 400 mm/year [12]. As there is no rain gauge station in the study area, the available daily rainfall records of the nearest rainfall station at Radaa for 15 years (1978-1992) were collected and averaged on an annual and monthly basis as presented in Figure 3. In Radaa, the average annual rainfall is 220 mm/year, fluctuating between 100 and 370 mm/year (Figure 3a). Most of the rainfall occurs in March and April as well as in July and August with maximum quantities of 53, 37, 22, and 38 mm, respectively (Figure 3b). Potential evaporation estimated by the Penman method was about 2400 mm in summer and 2000 mm in winter months with an annual average of 2280 mm [3]. As the potential evaporation is high during rainy seasons much of the surface rainwater (about 90%) evaporates to the atmosphere. Only 10% of the total rainfall forms the runoff part and may infiltrate into groundwater recharge [12].

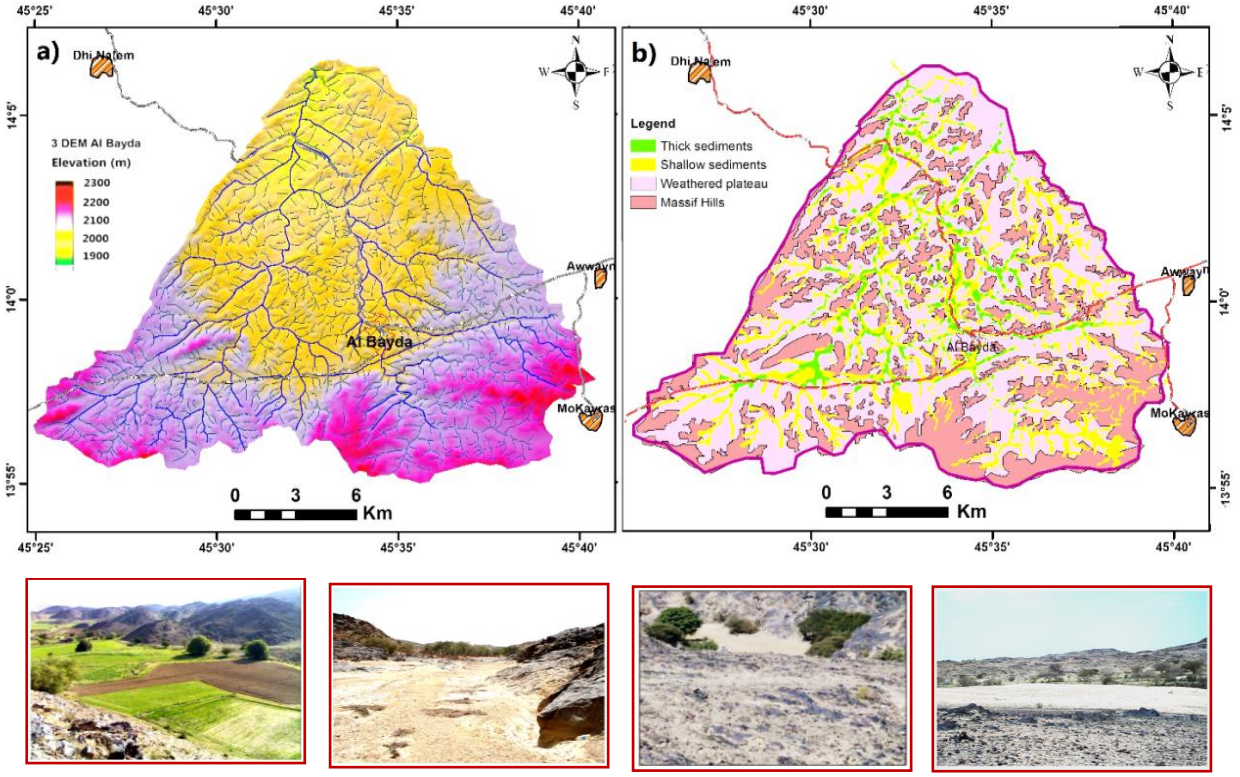

Figure 2: Topography (DEM) and drainage map generated from SRTM of the study area (a); Morphological features of Albayda City catchment area (b), and field photos showing examples of morphological features in the area.

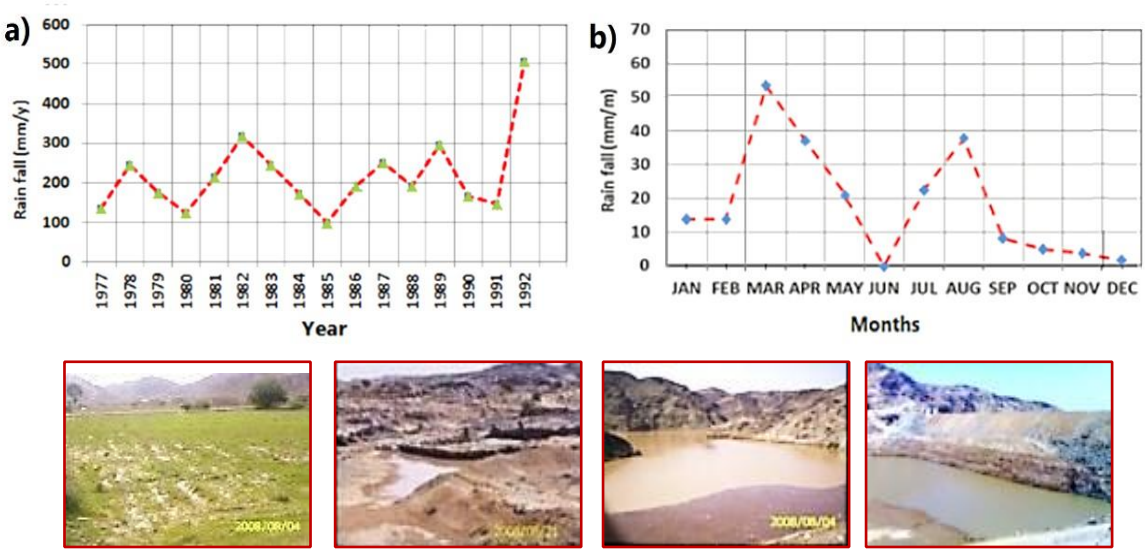

Figure 3: Mean annual values of rainfall at Radaa station from 1977 to 1992 (a) and mean monthly values Al Khabar rainfall station (b); Field photos showing examples of surface water features found in Albayda catchment.

4.2. Geology and Structure

The geology of Al Bayda is dominated by the Precambrian Basement Complex composed mainly low grade metamorphic rocks over 2700 million years of age [13]. A geological overview map of the study area is generated by tracing and lithologic units from the satellite image (Figure 4a) and geologic maps of Robertson 1992 and El Selwi, 2005. As can be seen in Figure 4b, the surface geology of the study area is made up only of two lithologic groups: The old core basement includes Archaean high-grade migmatized gneisses; the Layered basement is predominantly of the Neoproterozoic age and includes: schist, ophiolitic mélange and arc metavolcanics, and Intrusive rocks comprise of granodiorite, gabbro and granite, occur as zoned plutons traversing the older units [14-16]. Intrusive dikes and sometimes dike swarms, often associated with faulting, cut the Precambrian rocks in many places [5]. Overlaying the basement rocks, but in the wadi channels and shallow depressions, are the recent alluvial deposits that consist of silts, clays, and fine sands with some intercalation of gravels. The thickness of alluvial deposits ranges between 2 m and 5 m in the southern part of the area and increases to 15 m in the central parts of wadis and at the conjunctions of the main faults [3]. Based on the geological and morphological maps (Figs. 2b and 4b), the thematic layer of each formation has been calculated. The results indicated that the alluvial deposits cover about 60 km^2 (15%) and the remaining area (270 km^2 or 85%) is covered by hard basement rocks.

The region in general has been affected by at least three tectonic phases that were caused by folding, faulting, and fracturing. Folding is indicated by the presence of ridges that bound the catchment from the west and east and the presence of lowlands in the central part of the area. Faulting is represented by a large number of faults of different directions, ages, and origins, varying from high-angle thrusts to almost vertical strike-slip faults [5]. In this study, the faults of the area were traced from the geologic map of Eselwi (2005) and completed using satellite image interpretation. The predominant trends of fault systems are NE, NW, N-S, and E-W. The NE faults are the oldest and have been traversed by the NW and by the NW faults consequently. Two faults are of highly effective influence on the surface hydrogeological features of the area. These are the NE-SW fault that traverses the area from the southwest into the northeast and the E-W fault that delineates the southern part of the catchment to south of Al Bayda city. The two faults are cross-cut by the other local faults creating a large number of sub-basins. Comparison of the drainage pattern of the area and lineament directions shows that the drainage pattern is controlled by the main structural elements. The present wadi system usually follows the faults. The alluvium in most of the wadi beds and the weathered rock zone underlying the wadis form the groundwater reservoir storing the infiltrating rainwater and runoff waters from the surrounding hills. However, many faults and fractures in the area have been intruded by dykes that may interrupt the groundwater flow.

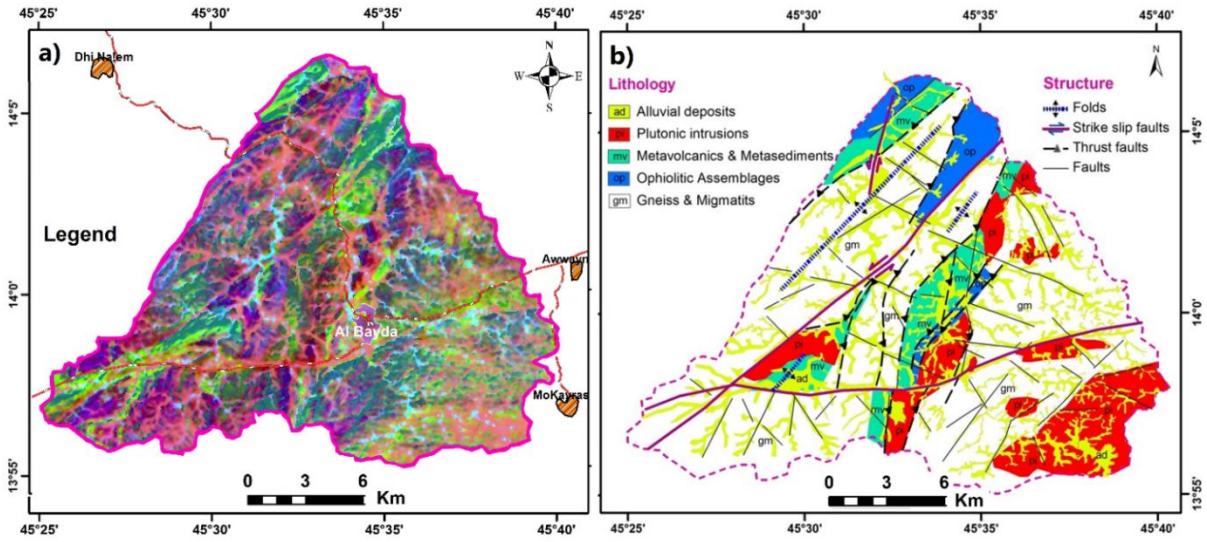

Figure 4: Satellite image (a) and interpreted geology map (b) of Al Bayda catchment area.

4.3. Hydrogeological Sitting

The hydrogeological setting of the Al Bayda area was affected by many factors including geological, structural, and climatic conditions that have been discussed above. Based on the topographic, drainage, and geologic maps (Figs. 2 and 4) as well as the rainfall data, the hydrogeology of the study area can be described here through the identification of surface and subsurface hydrological features, including rainfall-runoff, aquifer characteristics, and groundwater situation, as in the following section.

4.3.1. Surface Water System

Rainfall and runoff are the only ways to input water into the hydrologic system of Al Bayda catchment. The principal features of rainfall in the area are seasonal, poor distribution, and variable from year to year. Daily rainfall amount is usually the result of only one rainstorm of low intensity (> 10 mm), which does not generate any form of surface water feature. Since the catchment is a rough surface area and mostly covered with bare rocks, flash floods do not occur, and the surface runoff occurs only after heavy rainstorms. During and after heavy rainstorms (> 10 mm), water runs off over the ground, first collecting in shallow depressions, and then overflowing into the tributaries and somewhere into the main wadis where it may generate other surface water features such as springs streams, bonds, and marshes, which in turn either evaporated or infiltrated to the aquifer.

As previously mentioned, the 330 km^2 area of the catchment consists of the 270 km^2 area that is bar rocks from which runoff occurs, and the 60 km^2 area of the wadis into which runoff flows. The mean annual rainfall is considered to be 200 mm and the runoff coefficient in the study area is estimated to be 8.4 % of total annual rainfall [17]. Therefore, the total annual rainfall over the entire catchment area is (0.200 m x 330 x 10^6 m^2) 66 Mm^3. The total runoff is (0.200 m x 330 x 10^6 m^2 x 0.084) 5.5 Mm^3. Most of this amount is evaporated or used for irrigation. There are three small dams (Al Barsha, Al Haykal, and Dhiwain) and some manmade structures (see pictures Figure 3). The total surface water stored behind such dams is estimated to be 0.9 Mm^3. This amount represents about 16% of the total surface water resources that have been already utilized. Therefore, there is at least 80 % of surface water available for further development inside the area. This water can be exploited by the construction of small boulder surface or subsurface dams.

4.3.2. Aquifer System

In arid and semi-arid areas of the hard basement, where rocks are generally impervious, groundwater occurs mainly in the weathered overburden (regolith) and structural traps (fractures, fissures, and intrusive bodies) in the hard rocks [18]. Recent research studies showed that aquifers located in hard rock formations (granite, gneiss, schist) were considered a highly heterogeneous media that is made of two main superimposed hydrogeological layers, each layer characterized by quite homogeneous specific hydrodynamic properties [19-21]. The occurrence and depth of groundwater in the basement aquifer system are controlled by the pervasiveness of secondary structural entities. The depth of the water table in hard areas varies from place to place and from season to season [22,23]. In general, the groundwater potential and yielding capacity of the basement aquifers differ much from place to place due to variability in their thickness, hydraulic properties, and recharge mechanisms [21].

In this study, an attempt is made to characterize the aquifer system of the area. It was based on the data presented in this study and the well inventories and drilling and testing that were carried out in the region. The good inventory data for 168 wells (location, elevation, depth, lithology, water level, yield, salinity, etc.) obtained from ILACO [3] were used to construct several hydrogeological cross-sections. Examples of these cross-sections are shown in Figure. 5. The hydraulic properties of the aquifer system of the area were taken from SOGREAH (1978) [2] and other studies that were conducted in hard basement regions in other countries [e.g. 22, 23, 24].

The representative SW-NE and SE-NW cross sections AA, and BB (Figure 5) reveal that the aquifer system in Al Bayda formed of (1) topsoil and sandy/alluvium; (2) weathered zone or regolith, and (3) fractured bedrock. The alluvium zone varies in thickness from 3 to 10 m and could reach 15 m in some locations. The weathered zone behaves similarly to the alluvium in terms of thickness vis a viz the wad orientation and varies also from 2 m to 15 m. Isolated fractured zones extend for a few tens of meters into the fresh basement. The compound aquifer thickness from the topographic surface to the fresh basement varies from less than 10 m to 30 m. The aquifer systems show a wide variation in geometry from place to place, which is the result of variations in basement topography. As can be seen in Figure 5, the aquifer system in the study area occurs as isolated bodies as it is disconnected by faults, dykes, and plutonic intrusions. The water table is locally very irregular following the bedrock topography. It occurs at shallow depths upstream of Wadis and becomes deeper towards the central parts of the numerous water bodies.

Based on similarity in hydrogeological properties, the basement aquifers in the study area can be subdivided into two potential aquifer types, viz. the weathered (regolith) and the fractured (deep) aquifer systems. The first is thin (< 10 m thick), consisting of one or two zones (alluvium and weathered), and found across all the wadis and most of the tributaries. The second is comparatively thicker (10-30 m), consisting of three layers (alluvium, weathered and fractured), and usually found as isolated bodies distributed along the main wadi channels, closer to the hills, and at the intersections of the major faults. The general characteristics of the two types are summarized in Table 1. The shallow aquifer system covers 33 km^2 or 10% of the total surface area, while the deep aquifers constitute only about 16.5 km^2 or 5 % of the catchment area. The surface distributions of the shallow and deep aquifers were illustrated in the constructed hydrogeological map (Figure 6).

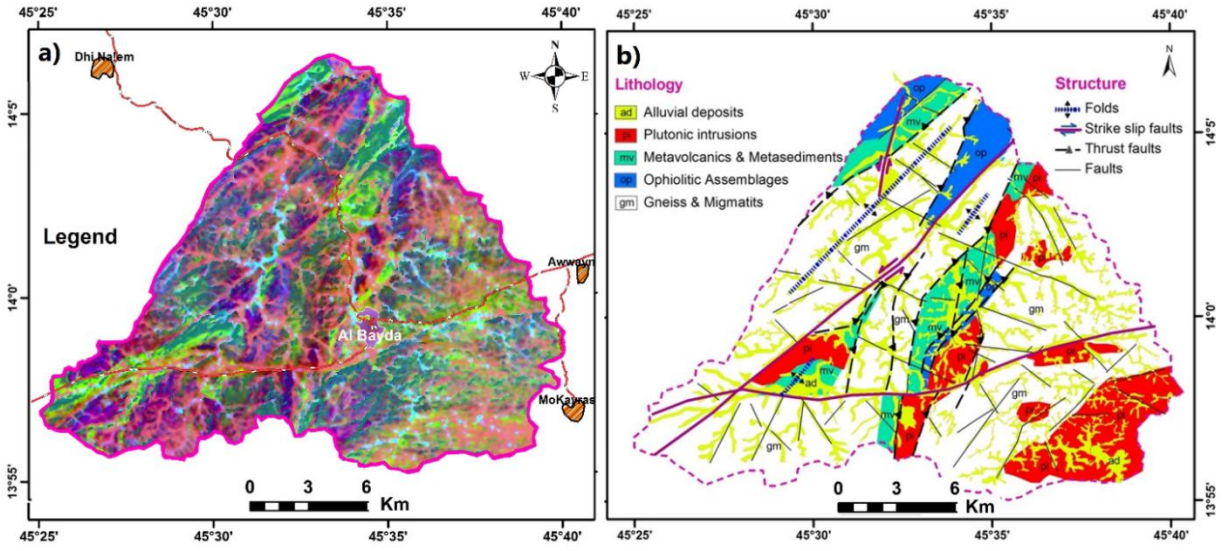

Figure 4: Satellite image (a) and interpreted geology map (b) of Al Bayda catchment area

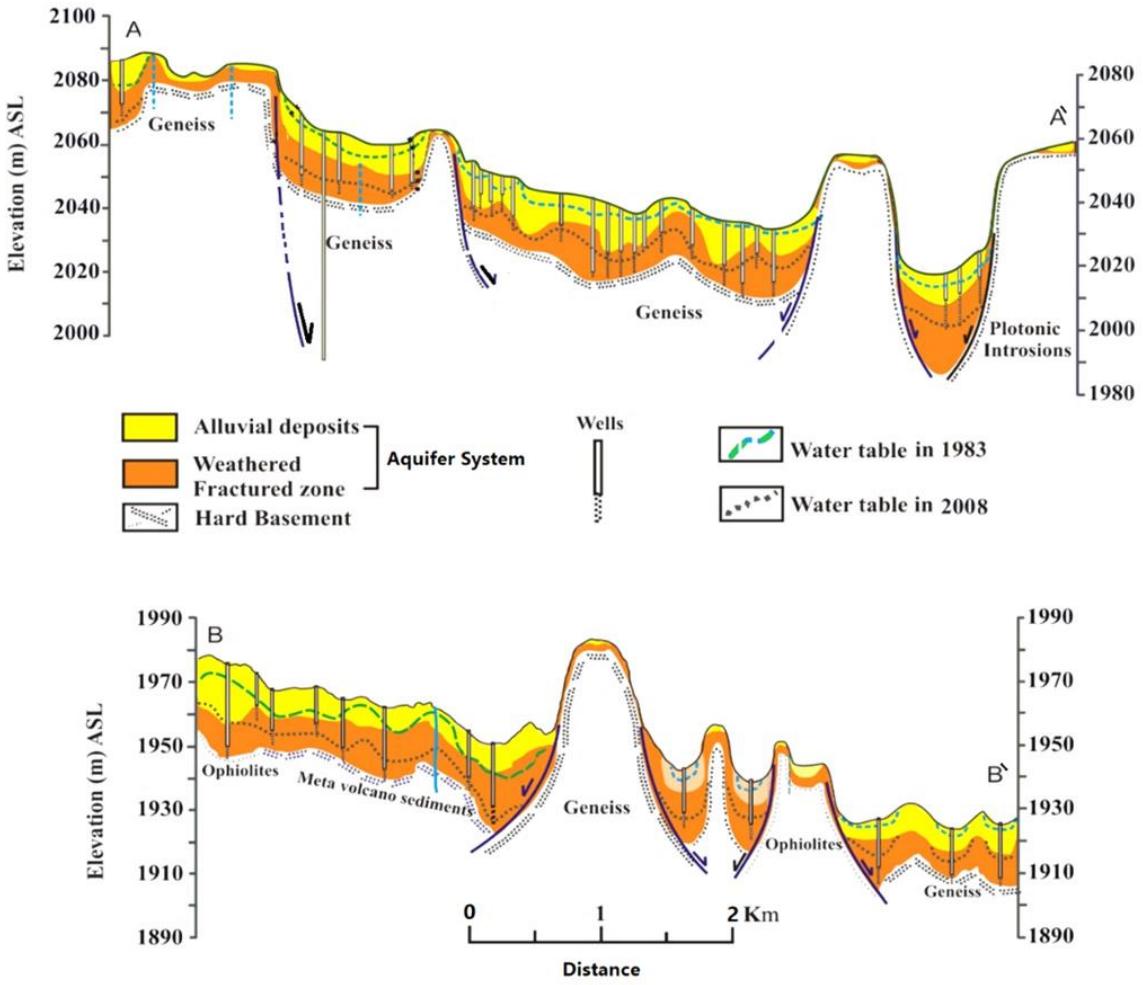

Figure 5: Hydrogeological cross-section AA' (W. Zahir) and BB' (W. Hananna), showing the aquifer zones and variability groundwater levels with bedrock topography. Locations of the cross-section profiles are shown in Figure 6.

Pumping tests carried out by SOGREAH (1977) in the lower part of Wadi Bayhan show that the weathered zones aquifers have hydraulic conductivities of < 0.8 m/d, transmissivity values of < 40 m^2/d, specific yield of < $1x10^{-3}$, and well yield of < 86 m^3/d. The fractured aquifers have hydraulic conductivities of < 8 m/d, transmissivity values of < 80 m^2/d, specific storage of < $1x10^{-3}$, and yield of < 86 m^3/d [2]. Despite its wide distribution, the shallow aquifer should not be considered an aquifer. It has a small thickness, and the water is usually found below the boundary of its zone. The deep aquifer can be considered the main storage compartment in the area but its yield is low depending on its saturation thickness.

Table 1: Characteristics of the aquifer system in the hard basement rocks of Al Bayda.

Aquifers Type	Shallow Aquifer (Alluvium & Weathered)	Deep Aquifer (Fractured)
Area km^2	33	16.5
Thickness (m)	4 -10	11- 30
Depth of water table (m)	4-10	11-25
Saturated thickness (m)	0-5 seasonal	0 -10
Depth of wells (m)	< 10 m	10-30
Well yields (L/s)	<1	2 - 2.5, 0.5 – 1.7
Hydraulic Conductivity (m/d)	0.003 - 36	0.02 – 0.39
Transmissivity (m^2/s)	0.01 - 0.87	0.2 – 87
Storage Coefficient (%)	1 - 0.01	< 0.01

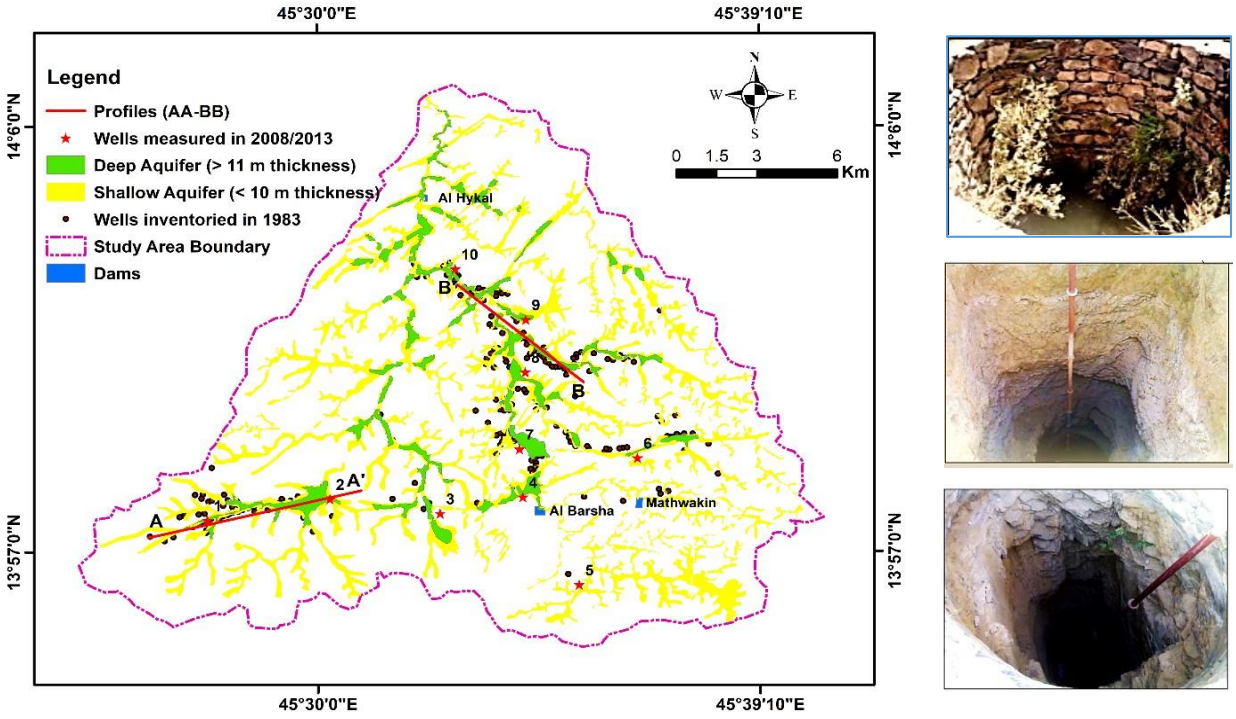

Figure 6: Map shows surface distribution of aquifer systems, locations of wells and measuring points for the hydrological years 1983, 2008 and 2013, and field photographs showing types of wells in the study area.

4.4. Groundwater Situation

The groundwater situation in the study area is discussed by defining its occurrence, depth, use, and quality; the past and the recent water situation were also compared. The groundwater resources situation in the Al Bayda catchment has been presented on the hydrogeological cross sections and map (Figs 5 and 6). It can be noted that the main factors controlling the occurrence and depth of groundwater are, the quantity of rainfall, the thickness of the aquifer (the thicker the aquifer the lower the water level), and also the quantity of abstraction or use of groundwater. In shallow aquifer systems, groundwater does not exist throughout the year and dries out soon after the rains end. In the deep aquifer, groundwater usually occurs at the base of the weathered zone but varies in depth from place to place following basement topography. A considerable rise in the water table (3-6 m) is observed in the area during the rainy seasons.

4.4.1. Groundwater Use

Groundwater is used exclusively to satisfy the water needs of the different uses. In the past, groundwater was used mostly for irrigation. At present, most of the groundwater is used for domestic purposes with limited amounts being used for small-scale irrigation during the rainy season. For obtaining groundwater, dug wells and collector wells are commonly used. There were about 300 wells in 1983 which increased to 400 wells in 2008, of which 8 wells for the city. The distribution of the wells is shown in Figure 6. The wells in the area have depths of 10-30 m, diameters of 2-3 m, and water levels of 5-25 m below land surface. Most wells are not lined, and some wells are lined with stones or concrete. Water lifting devices include manual rope-bucket and diesel-powered pumps. Typical examples are shown in Figure 6. Quality analyses of groundwater samples from the wells of Al Bayda catchment reported by ILACO and GSHEC indicate that salinity may not be a problem for this aquifer as low electrical conductivities (ranging from < 300 mg/L to 1500 mg/L) were found in the groundwater.

4.4.2. Change in Groundwater Situation

The change in the groundwater situation that occurred during the periods between 1983 and 2008 is presented in water depth contour maps (Figs. 7a and b). These maps were prepared by using the depths of groundwater for 168 wells inventoried by ILACO in the summer of 1983 and for 30 wells measured by GSHIC in September 2008. Figure 7a shows that water depths were generally 0 to 3 m below the surface in most parts of the catchment; near-surface water levels of 3 to 10 m were found in the northern parts of the catchment. Three prominent depletion cones (10, 12 m, 14 m b.g.s) were observed in waterlogged areas near Al Bayda, city (W. Al Barsha, W. Zaher, and Al Isa) in the city well fields. Figure 7b shows that the depth of groundwater has increased all over the area. It is generally 10 to 25 m below the surface in most parts of the catchment. Several depletion cones were generated in the area including the three depletion cones that formed in 1984 at the city well fields. As shown by arrows representing groundwater flow directions, the groundwater is limited to the cone of depressions, flowing from all sides towards extensive pumping areas.

A comparative analysis has been made also for ten wells measured in the three periods (1983, 2008, and 2013. The results are summarized in Table 2 and presented in Figures (8a and b). As can be seen in Figure 8a, the depth to water level was very shallow in 1983 and ranged between 0 and 10 m with an average depth of 4.5 m. In 2013, the depth of water in the ten wells increased to a range between 10 and 25. The deepest groundwater levels were observed in wells 3, 6, and 8 which are located in the intensive pumping areas (Al Bayda city well fields). However, the salinity variation in the ten selected wells shown in Figure 8b indicated that there was no significant variation over the years. The water salinity in 1983 was near the average of 2013. The lowest salinity values were observed in wells no.4. 5, and 6 which are located in the intensive pumping areas. Salinity is low in the southern part of the study area and increases gradually with groundwater flow toward the north. Generally, the groundwater lying at deeper depths is of good quality as compared to shallow groundwater.

Based on the statement discussed above, the changes in groundwater conditions over the 30 years, between 1983 and 2013 can be summarized as follows: **1)** In 1983, the water levels were encountered in the alluvial zone at depths varying from 0 to 10 m; the thickness of the saturated zone was more than 20 m. The yield of wells was ranging between 0.2 and 4.7 l/s with an average of 0.5 l/s or 47 m^3 per day. **2)** In 2013, the depth of the water increased to range between 12 and 25 m, and the saturated thickness decreased to 6 m. In total, there was a net fall in water level over the 30 years by about 19 meters, with a rate of 0.5 m per

year. The yield of wells has decreased to range between 0 and 2.4 l/s with an average of 0.2 l/s or 18 m^3 per day. Generally, there is no significant change in water salinity over the years. Quality analyses of groundwater samples from the wells of Al Bayda catchment reported by ILACO and GSHEC indicate that salinity may not be a problem for this aquifer as low electrical conductivities (ranging from < 300 mg/L to 1500 mg/L) were found in the groundwater. The quality of groundwater in the area is generally good for multi-purpose use.

4.5. Groundwater Availability

Groundwater availability in aquafer is determined and influenced largely by the recharge and discharge rates. The principal controls on groundwater recharge are the topography, soil properties, vegetation, and meteorological variables such as precipitation, temperature, wind, etc [24,25]. Discharge from the aquifer is influenced by the rate of recharge and its controlling factors. In the case of the study area, groundwater recharge occurs either directly by infiltration from rainfall or indirectly by infiltration from runoff, whereas discharge occurs only by well abstraction. To quantify the water available in the aquifer system underlain the study area, the water balance analysis method has been used, which was based on the two main comports (i.e. Recharge through the infiltration from direct rainfall and Discharge through the abstraction from wells). The recharge, discharge, and potential in storage were estimated using a combination of available previous data, rainfall-run-off data, and computation of the water balance for the Wadi Bayhan by (SOGREAH (1978), and by ILACO (1984), and GSHEC (2009). The available water production records of Al Bayda Local Water Authority were taken into consideration. It is worth mentioning that both recharge and discharge occur from wadi fill deposits. Table 3 contains all data and information that were used for water balance components to arrive at an estimate of the groundwater recharge and discharge from the aquifer systems of Al Bayda catchment area.

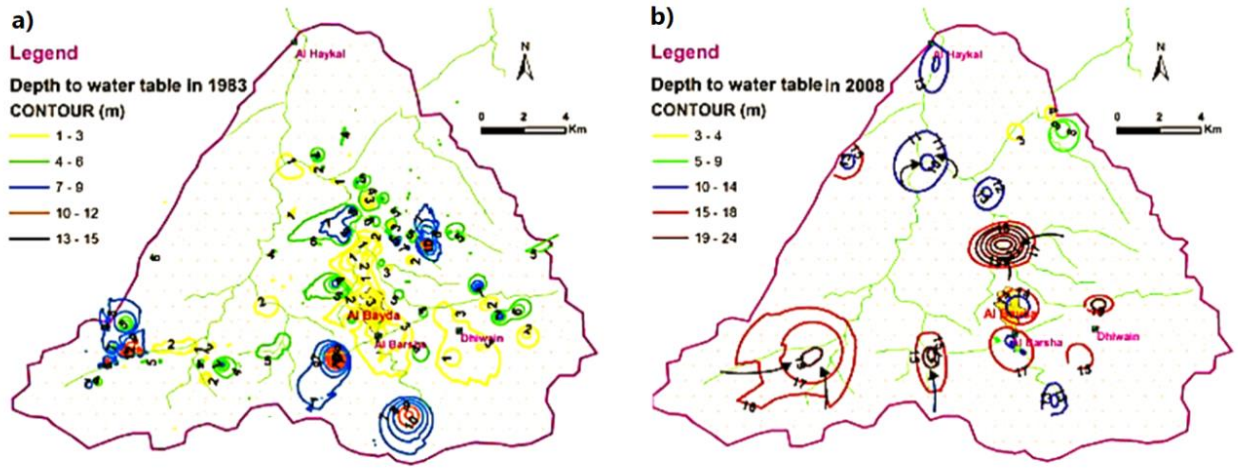

Figure 7: Groundwater depth contour maps showing patterns and flow directions in Al Bayda area for 1983 (a) and 2008 (b).

Table 2: Groundwater measurements in ten selected wells for the years 1983 and 2013.

No.	Location		Well depth (m)		Water Depth (m)		Yield (m3l/d)		Salinity EC (µS/cm)	
	Lat. N	Long. E	1983	2013	1983	2013	1983	2008	1983	2013
1	551702	1543737	18	20	2.6	19	2.4	<2	810	940
2	553512	1544700	8	16	8.3	15	5	<2	2000	1000
3	558370	1543823	16	27	6.5	24	7	<2	680	800
4	561471	1544530	8	16	2.2	12	2.3	4	700	1000
5	564848	1542229	14	17	11.2	16	5	<2	460	400
6	566191	1546365	18	22	3.7	19	12.8	<1	1400	900
7	562413	1546103	25	16	3	13	5	<2	1400	600
8	561064	1550059	14	27	1.2	25	6	<1	2000	1500
9	561420	1551383	12	17	0.7	15	5	2	1500	1200
10	558396	1556774	18	15	3.4	13	7	<2	2200	2000
	Average		**15**	**19**	**4.4**	**19**	**5.7**	**1.2**	**1315**	**1034**

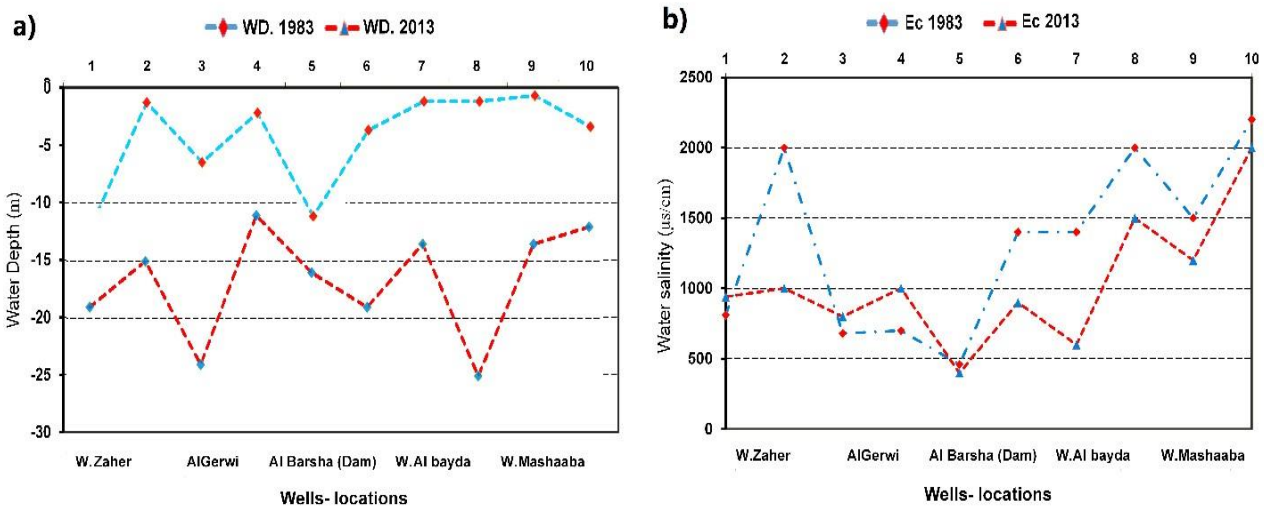

Figure 8: Long-term variation in water depth (a) and salinity EC (b) in ten selected wells for 1983 and 2013.

4.5.1. Recharge Estimation

Estimation of spatial and temporal variation of groundwater recharge is a prerequisite for resourceful management of aquifers, particularly where these estimates form the basis for assigning groundwater withdrawal rates [23,25]. Recharge has been estimated in (semi-) arid regions using a variety of techniques, including physical, chemical, isotopic, and modeling techniques. These techniques have been described in previous studies and reviews [26 and 27]. Studies on hard basement areas reported that the natural recharge rates in such areas are ranging between 3% and 15% [26,28]. In the present study, the quantity of recharge is estimated by using the infiltration factor method through the equation: $R = 0.001 \times P \times A \times Ci$; where R is the total amount of infiltration; P is the mean annual rainfall (200 mm); A is the infiltrated area (60 km^2), and Ci is the infiltration coefficient of alluvial deposits. TSHWC (1992), estimated that the infiltration coefficient from direct rainfall is 5% and that from direct runoff in the wadis is 30%. [29]. It is worth to mansion that flashflood does not occur in the study area. Runoff occurs only 2 to 4 times a year but most of intercepted water in the wadis is immediately evaporated or used by farmers. The infiltration from direct rainfall over the study is estimated to be (0.200 m × 60 × 10^6 m^2 × 0.05) 0.6 Mm^3 per year, and the infiltration from direct runoff is (4.5 × 0.3) 1.35 Mm^3 (Table 3). Hence, the total recharge is 0.6 + 1.35 = 1.95 Mm^3 which represents only 3% of the total annual rainfall. This value is on the limit of the range given previously by SOGOREAH (9 - 11 Mm^3/year) for the upper Wadi Bayhan (1500 km^2.). Also, it is well within the range obtained by TS - HWC (1992) on a national basis (0.5 - 3.0 Mm^3/year/l00 Km^2). A comparison of this amount (i.e., 1.95 Mm^3) with that estimated by ILACO and GSHEC, indicated that there was a continuous decrease in groundwater recharge over time. This is due to the continuous depletion of groundwater levels. Continuous decrease of saturation thickness reduces the rate of infiltration into the aquifer. Therefore, it is necessary to increase the rate of infiltration to the aquifers through the construction of surface and subsurface dams.

4.5.2. Discharge Estimation

Discharge from the aquifer system of the area occurs mainly by abstraction through the wells, natural evaporation and groundwater outflow are neglected. Given the lack of data on the amount of water pumped from Al Bayda wells, the abstraction volumes obtained from previous studies in addition to the abstraction records of Al Bayda city wells (NWSA) were extrapolated to estimate the current condition. The extrapolation takes into account the number of years that have passed, the trends observed in the past, and the present conditions in the area.in 1983, 300 wells were producing about 5.2 Mm^3 [3], with an average yield of 47 m^3/day. However, in 2008, there were about 400 wells in the area but the total abstraction volume is estimated to be 2.6 Mm^3, and the average yield of wells was 18 m^3/d [4]. This means that the total abstraction volume has decreased by about 50 % during 25 years between 1983 and 2008, and the average yield of the wells has decreased by 60 %, and hence the rate of decrease of wells yield is 20% per 10 years. Accordingly, the total abstraction volume for 2014 can be estimated by multiplying the number of wells (400) and the average daily pumping rate (14.6 m^3/day). Hence, total discharge is (400 × 14.6 × 365) 2.2 Mm^3. Comparison of this amount with the calculated amount of recharge (1.95 - 2.2 Mm^3), gives an imbalance in groundwater storage by 0.25 Mm^3 (Table 3).

4.6. Evolution of Water Supply in Al Bayda City

Data regarding water sources of Albayda area were collected and analyzed to evaluate the supply of groundwater within the catchment area. Over time different kinds of water sources have been developed in the area. Before 1970, the water supply of Al Bayda was limited to traditional wells and springs that were present in the vicinity of the city until the 1970s. After that, a large number of wells were drilled in the area and used for irrigation. The result has been a decline in aquifer water tables, causing the springs and traditional wells to dry up. By the 1980s, significant urban and rural groundwater supply systems have been developed within the area. During the 1990s, more wells were drilled in Al Barsha and Al-Isa well fields. By 2004, the Local Water and Sanitation Authority (NWSA) Al Bayda built a small dam in Wadi Al Barsha to the south of the city. The existing water supplies for Al-Bayda city come from 8 wells distributed in three well fields (Wadi Al Barshah south of the city and Al Isa and W. Zahir to the east of the city. The water production capacity of Al Barsha wells was about 400,000 m^3 in 2004 but decreased in 2008 to 200,000 m^3/year. Water is transported to various distribution networks and small tanks via two pumping lines. Currently, only around 40% of the city's population is connected to the public water network. The people connected to the water network, have access to 10-20 l/c/d. The remainder population relies on private water sources, purchasing their water from water tankers.

The development of population and the growth of municipal demands versus renewable water resources and shortage in the Al Bayda area between 1984 and 2024 are shown in Figure 9 and listed in Table 4. The total population of the area has increased from 24600 in 1984 to 80,000 in 2014 and will be 110,000 by 2024. The total water demand of the study area is estimated to be 4.8 Mm^3 in 1984, 7.8 Mm^3 in 2004, and is estimated to be 11 Mm^3 by 2024 (Table 4). On the other hand, the renewable water resource has decreased from about 5.2 Mm^3 in 1983, to about 2.6 Mm^3 in 2008, and is estimated as 1.95 Mm^3 in 2014 and expected to be 1.4 Mm^3 by 2024. Thus, the water deficit in Al Bayda has increased from minus 4.25 Mm^3 in 1984 to be minus 7.3 Mm^3 in 2014 and expected to be 9.3 by 2024. Concerning Al Bayda city, the total annual demand for the city is estimated to be 2.2 Mm^3 in 2014 and is expected to be 3 Mm^3 in 2024. The annual per capita share of water in Al Bayda has decreased from 216 Mm^3 in 1983 to 24 m^3 in 2014 and is expected to be less than 12.7 m^3 by 2024. The current water shortage is estimated to be 400 % of renewable water resources. The availability of water in Al Bayda is much lower than that of Yemen's average (70 m^3/c/y) and lower than that in

other cities like Taiz and Sanaa which are considered the most water scariest cities in Yemen.

Table 3: Proposed estimation of groundwater recharge, discharge, and the resulting water balance in the groundwater system of Al Bayda area.

General information	Wadis	Bar rocks & hills	Catchment
Area (km²)	60	270	330
Slope %	< 5	3 -15	< 5
Average annual rainfall (mm/y)	200	200	200
PET (mm/y)	190	-	2000
Runoff Coefficient (% of runoff)	<1	7.4 - 8.6	8
Infiltration Coefficient (% of rainfall)	5	-	-
Infiltration Coefficient (% of runoff)	30	-	-
Total number of wells	300 in 1983, 400 in 2013		
Total abstraction volume (Mm³/y):	5.2 in 1983, 2.2 in 2013		
Total rainfall P (Mm³/y)	0.200 mm x 60 x10⁶ =12	0.200 mm x 270 x10⁶ = 5466	
Total Runoff FR (Mm³/y)	12 x 0.01 = 0.12	54 x 0.08 = 4.42	= 5. 5
Net recharge from Direct rainfall	12 x 0.05 = 0.6		
Indirect runoff (FR)	4.4 x 0.3 = 1.35		
Total recharge (Mm³/y)	1.95		
Net discharge by: Abstraction from 400 wells	2.2		
Groundwater Evaporation	0		
Total discharge (Mm³/y)	2.2		
Groundwater Balance (Mm³/y)	1.95 – 2.2 = - 0.25		

Table 4: Evolution of groundwater demand, consumption, and expected future demand and deficit until 2024 in Al Bayda area, Yemen.

Years	City	Population Villages	Total	Total Demands Mm³	Available GW. Mm³	Deficit Mm³	City Demands Mm³	City Water Supply	Actual per capita share m³/y
1975	7122	7000	14000		6.00			0.012	428
1984	10000	14600	24600	4.80	5.20	+ 0.40	0.90	0.04	216
2004	26600	25400	52000	7.80	3.60	- 4.20	0.97	0.024	69
2014	44000	36000	80000	9.00	1.95	- 7.30	1.6	0.016	24
2024	60000	50000	1100000	11.00	1.40	- 9.60	2.2	0.08	12.7

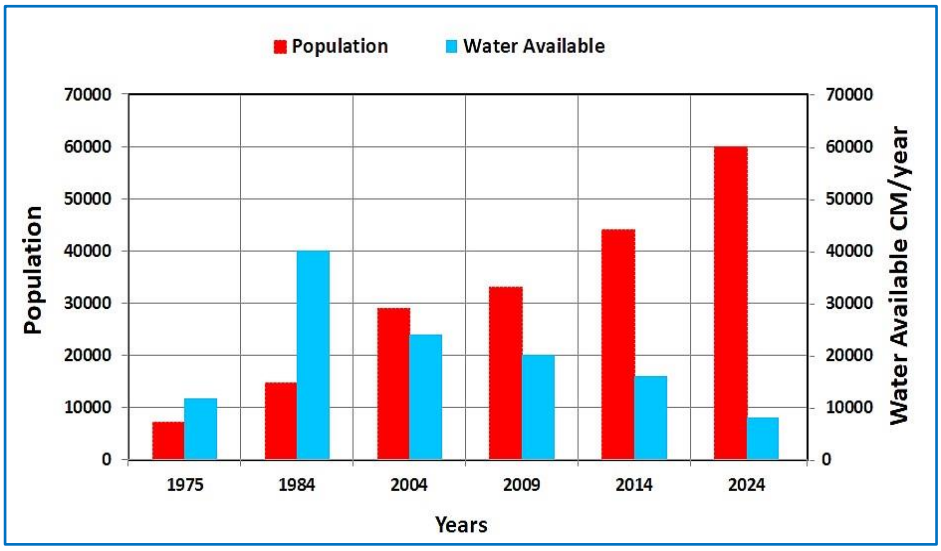

Figure 9: Al Bayda City water supply about its population growth between 1975 and 2014 and expected future demand until 2024.

From the previous discerption, we can conclude that the main causes of water scarcity in the region are low surface run-off and poor infiltration combined with the fundamental problem of limited aquifer storage. Therefore, there is a need to conserve rainwater and increase infiltration to recharge aquifers. An integrated approach to conserve rainwater and recharge aquifers is possible through harvesting of roof water, percolation tanks, ponds, subsurface barriers, minor check dams, injection wells, etc. In this regard, it is suggested that further studies to quantity the of rainwater that could be conserved. Detailed hydrogeological studies should be directed to evaluating the role of runoff water as the source of indirect recharge.

5. Conclusions and Recommendations

Al Bayda City is one of Yemen's urban areas that have witnessed a water supply shortage, mainly due to the continuous decrease in the quantity of groundwater resources. The catchment area of Al Bayda city has been chosen as a case for this study because it represents the source of water for Al Bayda city, in which the well fields that supply the city exist. This research has made a literature review on Al Bayda city groundwater resources. Then the availability of groundwater resources in Al Bayda catchment area has been assessed by an interpolation of the information from DEM, ETM+, and geological maps, well logs as well as field observations and hydrogeological knowledge of the area under study. A general description of the catchment topography, morphology, and geology has been made. These with the aid of well data, allowed the correlation of permeable zones and to identify the nature, extent, and spatial distribution of the aquifer system. The study also made a general review of the groundwater situation within the aquifer system as well as their potential for future water supply.

This research review revealed that the climate is an arid and undulating plateau; narrow Wadis and short tributaries; and small hills and short ridges in the area represent morphology. The area is covered by Precambrian basement rocks for over 85% of the complex. Recent alluvial deposits are covered in the wadis and shallow depressions. Aquifers tend to be developed in local depressions along the valley floors. They consist of topsoil and alluvial deposits and the underlain fracture or fissure zones. Groundwater occurs mainly at the upper weathered/laminated portion of rocks and other pore spaces found in the form of cracks, joints, and fractures. The depth of the groundwater table has declined from the late 1980s by 19 m, with a rate of 0.5 m per year. The lowering of the water table in the aquifers led to the reduction of the well yields. Many wells, which had been productive, became dry. Estimated groundwater recharge indicates only 1.95 Mm^3 while, the total volume of groundwater abstraction is estimated to be 2.2 Mm^3. The share per person of water in the city is estimated to be 23 Mm^3 per year, which represents the lowest in Yemen. The current water shortage is estimated to be 400 % of renewable water resources.

The water shortage in the study area could be mitigated by increasing or decreasing the loss of rainwater in rainy seasons and increasing infiltration to the aquifers. Traditional rainwater harvesting techniques such as storage tanks, and cistern bonds should be encouraged and developed to conserve rainwater. The recharge in Al Bayda catchment must be increased by enhanced by constructing small dams, either surface or subsurface dams. Detailed hydrogeological studies should be directed to evaluating the role of runoff water as the source of indirect recharge. Hopefully, the information provided in this study could be used by the local planners and policymakers to manage the water crises and support sustainable water resources management in Al Bayda City and other cities that are located in the hard basement region of Yemen.

Acknowledgments

This research benefited from the Al Bayda City Water Supply Enhancement Project which was funded by the Al Bayda Governorate Local Council in 2007. The authors are very thankful to the National Water and Sanitation Authority (Al Bayda NWSA), and other departments in Al Bayda and Thamar for their helping and providing us with the data and information used in this research. Thanks a lot, to the engineers who worked with us in the field.

References

[1] Gun A.M. van der. and Ahmed A. A. (1995) The water resource of Yemen. A summary and digest of available information. TNO Institute of Applied Geosciences, 2600 JA. Delft, the Netherlands, pp106.

[2] SOGREAH (1978) Wadi Beihan Irrigation Project. Technical Report no. 4: Water Resources Survey. SOGREAH. Grenoble-France.

[3] ILACO (1984) Study into water resources in Al Bayda province. Main reports, 3V. RlRDP. ILACO, Arnhem. The Netherlands.

[4] GSHEC (2008) A Study on Groundwater resources in uper part of Wadi Bayhan for Enhancing Al Bayda City Water Supply, Technical Report. Prepared by Geo Since Hydro-Environmental Consultant for NWSA, A l Bayda Governorate, Yemen, PP, 110.

[5] Al Selwi, K. (2005) Petrology, geochemistry and mineralization of the basement rocks of Dhi-Na'im-Al-Bayda District, Republic of Yemen. Thesis, Ph D. thesis, Fac. Sci., Zagazig Univ., Banha Branch, pp 175.

[6] AREA (2005) Agricultural climate in Yemen (1981-2004), Agricultural Research& Extension Authority (AREA), Dhamar, pp.165.

[7] World Population (2016) University of Southampton web-site https://www.worldpop.org/doi/10.5 258/SOTON/WP00004.

[8] Topographic series (1981) Scale 1:50,000, Government of Yemen by Directorate of Overseas Surveys DOS, U.K., 1981, Al Bayda sheets 1343 D1 and D2.

[9] Kruck W. and Schäffer U. (1991) Geological map of Republic of Yemen (ROY), Scale 1:250,000, Ministry of Oil and Mineral Resources, Sanaa, Yemen, Fedral Institute of Geosciences and Natural Resources, Hanover (FRG).

[10] Robertson Group pic. (1992) Geological Map of Yemen. Al Bayda sheet 1:250,000. The Natural Resources Project, Republic of Yemen, Contract 2. AFESD and UNDP.

[11] GLCF Global Landcover facility, NASA Landsat Program, U.S. Geological Survey (USGS), Sioux Falls, USA. (http://glcf.umiacs.umd.edu/index.shtml).

[12] NWRA (2011) An annual report, National Water Resources Authority, Sanas, Yemen.

[13] CGM/CGMME (2010) Commission for the Geological Map of the World/Commission for the Geological Maps of the Middle East Yemen (ttp://www.cgmme.com/ Article.aspx?CId=Yemen&Txt=1).

[14] Sakran SH. (1993) The Basement Rocks of As-Swadiyah Area, Al-Bayda District, Yemen Republic. Ph.D. thesis, Cairo Univ., Egypt, pp, 248.

[15] Abdel Wahed M. (2000) Deformational history, metamorphism and tectonic evolution of Archaean gneisses and ophiolitic rocks, As-Swadiyah area, southeastern Yemen, *Egypt. Journal of Geology* **44**:1-18.

[16] Windley B.F., Whitehouse M.J. and Ba-Battat M.A. (1996) Early Precambrian Gneiss Terrains and Pan- African Island Arcs in Yemen, Crustal Accretion of the eastern Arabian Shield, *Journal of Geology* **24**:131-134.

[17] ILACO (1986) Reconnaissance survey on the use of surface water in Al-Bayda province (V)a, and Geophysical survey in the Dhamar and Al-Bayda province (V)b. Final report, Volume 1 and 2. ILACO, Arnhem, The Netherlands.

[18] Greenbaum D. (1992) Remote sensing techniques for hydrogeological mapping in semi-arid basement terrains, British Geological Survey Technical Report. WC/92/28 NERC copyright 1992, British Geological Survey, Keyworth, Nottingham.

[19] Chilton, P.J., Foster, S. (1995) Hydrogeological characterization and water-supply potential of basement aquifers in tropical Africa, *Hydrogeology Journal* **3**: 36-49.

[20] Taylor R., Howard K. (2000) A tectonic-geomorphic model of the hydrogeology of deeply weathered crystalline rock: evidence from Uganda, *Hydrogeology Journal* **8**: 279-294.

[21] Lloyd J.W. (1999) Water resources of hard rock aquifers in arid and semiarid zones. Studies and reports in Hydrology, No. 58, UNESCO, Paris, pp 284. [Guide to hydrogeological methodology in hard rocks].

[22] Darko P.K., Duah, A.A., Dapaah-Siakwan, S. (2003) Groundwater Assessment: An Element of Integrated Water Resources Management – The Case of Densu River Basin. CSIR-Water Research Institute, WRI/CAR No. **54**.

[23] Yidana S.M., Bawoyobie P., Sakyi P. and Fynn O.F. (2018) Evolutionary analysis of groundwater flow:

application of multivariate statistical analysis to hydrochemical data in the Densu Basin, Ghana, *Journal African Earth Science* **138**:167–176.

[24] Ng, G.H.C., McLaughlin, D., Entekhabi, D., Scanlon, B. (2009) Using data assimilation to identify diffuse recharge mechanisms from

chemical and physical data in the unsaturated zone, *Water Resources Research* **45**: W09409.

[25] Akurugu, B.A., Chegbeleh, L.P., Yidana, S.M. (2020) Characterisation of groundwater flow and recharge in crystalline basement rocks in the Talensi district, Northern Ghana, *Journal of African Earth Sciences* **161**: 103665.

[26] Lerner D.N., Issar A. and Simmers I. (1990) A guide to understanding and estimating natural recharge. International Association of Hydrogeology Pub. 9. Hannover Heise. [Compendium of recharge assessment methodology].

[27] Hendricks J. and Walker G. (1997) Recharge from precipitation. In Recharge of Phreatic Aquifers in (Semi) Arid Areas, Simmers I (ed.), A.A. Balkema: Rotterdam, The Netherlands, pp19–98.

[28] Limaye, S.D. (2010) Sustainable groundwater development in hard rock aquifers in low-income countries and the role of UNESCO–IUGS-IGCP Project "GROWNET", *Iranian Journal of Earth Sciences* **2**: 1-91.

[29] Technical Secretariat of the High Water Council (TS-HWC) (1992) Groundwater resources, V (4) of final report UNDP/DESD Project YEM/88/001. UNDP/TS-HWC, Sana'a, Republic of Yemen.

Thamar University Journal of Natural & Applied Sciences **8**(2) (2023) 38 – 46

DOI: https://doi.org/10.59167/tujnas.v8i2.1718

Review Article

A Review on the Green Synthesis of ZnO Nanoparticles Using the Aqueous Extract of *Origanum Majorana* for Antimicrobial Applications

Ammar H. Aldokari[1], Hamid M. Al-Gabr[2], Hussein K. Salam[1,*]

[1]Biology Department, Faculty of Applied Sciences, Thamar University, Dhamar 87246, Yemen
[2]Biology Department, Faculty of Education and Science, Albaydha University, Albaydha, Yemen

*Corresponding author: Hussein K. Salam
Biology Department, Faculty of Applied Sciences, Thamar University, P.O. Box 87246, Dhamar, Yemen
Email: sallam27@gmail.com

Received: 13 November 2023. Revised (in revised form): 6 December 2023. Accepted: 9 December 2023. Published: 31 December 2023

Abstract:

Zinc oxide nanoparticles (ZnO-NPs) have been extensively researched for their potential applications in various fields such as pharmaceuticals, cosmetics, biotechnology, sensing, photocatalysis, and photovoltaics due to their unique nanoscale properties. However, the conventional methods for producing ZnO NPs require the use of hazardous chemicals and high energy consumption, which imposes certain limitations. In contrast, the green synthesis of ZnO-NPs using plant extracts, especially *Origanum majorana*, has gained much attention as a promising alternative approach. Plant extracts contain phytochemicals that are biologically safe and non-toxic, making them a preferred choice. In addition, the ZnO-NPs synthesized with *O. majorana* extracts exhibit higher stability and can be customized in terms of shape and size, unlike the ZnO-NPs obtained by bacterial or fungal methods. The aqueous leaf extract of *O. majorana* contains flavonoids, tannins, and phenolic derivatives, which serve as reducing and capping agents for the biosynthesis of ZnO-NPs. These extracts also contain functional groups such as -OH and -C=O, which further enhance the physicochemical properties of the resulting ZnO-NPs and influence their ability to target specific molecules. The plant-mediated synthesis of ZnO-NPs using *O. majorana* leaf extract is not only fast and straightforward but also offers a wide range of functionalized nanoparticles with specific morphologies and sizes. These ZnO-NPs prepared with *O. majorana* have been shown to have potential applications in various fields, including antimicrobial, antioxidant, and anticancer activities. This review focuses specifically on the antimicrobial applications of ZnO-NPs synthesized using *O. majorana* leaf extract.

Keywords: Zinc Oxide Nanoparticles; Green Synthesis; *Origanum Majorana*; Antimicrobial Activity.

Abbreviations: AFM, Atomic Force Microscopy; EDS, Energy-dispersive X-ray spectroscopy; FTIR, Fourier Transform Infrared Spectroscopy; MIC, Minimum Inhibitory Concentration; NPs, Nanoparticles; ROS, Reactive Oxygen Species; SEM, Scanning Electron Microscopy; TEM, Transmission Electron Microscopy; XRD, X-Ray Diffraction; ZnO-NPs, Zinc oxide nanoparticles.

1. Introduction

The field of nanotechnology is rapidly growing and focuses on the development of materials at the nanoscale, ranging from 1 to 100 nm in diameter. These materials have a wide range of applications in various sectors, including biomedical science, cancer treatment, healthcare, drug delivery, food, cosmetics, electronics, energy science, and chemical industries [1].

The synthesis and characterization of these nanomaterials have garnered significant attention due to their unique properties, such as magnetic, structural, and optical characteristics, which arise from the quantum confinement effect. Furthermore, the ability to control and manipulate the distribution, morphology, size, and interfacial effects of nanoparticles adds to their intriguing nature, resulting in a diverse range of chemical, physical, and biological properties [2].

The ZnO-NPs possess exceptional properties, including high photosensitivity, chemical and physical stability, thermal conductivity, and non-toxicity. These properties make them highly attractive for various applications, such as pharmaceuticals, perfumes, dyes, communication, petroleum, electronic sensors, optics, wastewater treatment, packaged foods, and medicine [3,4]. Additionally, ZnO-NPs find extensive use in biomedical applications, serving as antifungal and antibacterial agents, biological labels, antioxidants, anti-inflammatory agents, coatings for medical implants, facilitators of gene transfer, and promoters of wound healing [3]. Various synthesis methods for ZnO-NPs have been extensively studied and documented in the literature, including chemical, physical, and biological approaches. However, recent research has primarily focused on biosynthesis methods, aiming to eliminate the use of hazardous substances and reduce energy consumption. This shift in focus is a response to the reliance of conventional synthesis methods on hazardous chemicals and significant energy input [5]. Moreover, plants, algae, fungi, and bacteria have been successfully utilized for the synthesis of ZnO-NPs, with plants showing promising results [6,7].

2. Classification of Nanoparticles

Nanoparticles are classified into different categories based on materials used, size, characteristics, fabrication methods and dimensions Figure 1 [8,9].

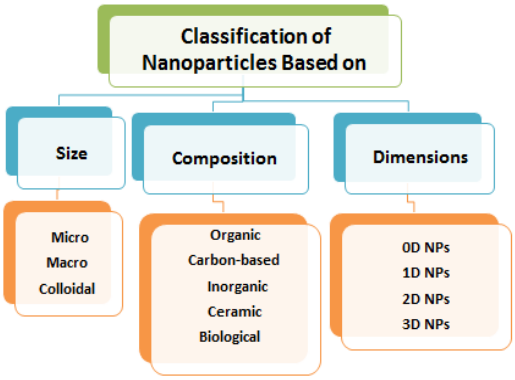

Figure 1: Classification of Nanoparticles.

2.1 Classification of nanoparticles based on their composition

Nanoparticles can be categorized into different classes based on their composition. These classes include carbon-based nanoparticles, organic nanomaterials, nonorganic nanoparticles, ceramic nanoparticles, and biological nanoparticles.

2.1.1 Carbon-based nanoparticles

Carbon-based nanoparticles are composed solely of carbon atoms. These nanoparticles possess unique properties such as electrical conductivity, optical characteristics, electron affinity, high strength, sorption properties, and thermal stability. Due to these properties, carbon-based nanoparticles find applications in a wide range of fields [9].

2.1.2 Organic nanomaterials

Organic nanomaterials are composed of carbohydrates, proteins, polymers, lipids, or other organic compounds. Examples of this class include liposomes, protein complexes, micelles, and dendrimers [10].

2.1.3 Nonorganic nanoparticles

Nonorganic nanoparticles are composed of materials other than organic or carbon, such as nickel, copper, gold, zinc, silver, and iron nanoparticles [11].

2.1.4 Ceramic nanoparticles

Ceramic nanoparticles, also known as nonmetallic solids, are synthesized through cooling or successive heating processes [12].

2.1.5 Biological nanoparticles

Biological nanoparticles are assemblies of atoms or molecules that are prepared within biological systems through methods such as green synthesis or biosynthesis. These methods involve the use of microorganisms such as algae, fungi, yeast, bacteria, and plant extracts as reducing agents [13].

3. Zinc oxide nanoparticles

Zinc oxide nanoparticles possess a range of desirable characteristics that make them an attractive option as a low-cost n-type bandgap semiconductor. One notable feature is their ability to exhibit dielectric and piezoelectric properties while still maintaining transparency.

These nanoparticles have a wide bandgap of 3.37 eV at room temperature, along with high thermal conductivity and a significant exciton binding energy of 60 meV. These unique attributes make them suitable for various applications in fields such as gas sensors, photovoltaics, optoelectronics, light-emitting diodes, aerospace, and photocatalysis [14]. Furthermore, ZnO-NPs exist in the form of white odorless solid powders, which are composed of hexagonal wurtzite crystals.

They can take on different shapes, including spheres for zero-dimensional (0D) structures, nanotubes, nanorods, needles, and dumbbells for one-dimensional (1D) structures, platelets and disks for two-dimensional (2D) structures, and flakes, stars, and flowers for three-dimensional (3D) structures [9]. These physicochemical properties have a significant impact on the ability of ZnO-NPs to effectively target pathogenic bacteria and fungi through their antimicrobial properties. The synthesis techniques used during their preparation also play a crucial role in determining these properties [15]. The superior antibacterial and fungi activity against pathogenic microorganisms is attributed to the porosity, morphology, and particle size of these nanoparticles [16].

4. Synthesis of Zinc oxide nanoparticles

An optimal method for synthesizing zinc oxide nanoparticles should possess environmentally friendly and cost-effective characteristics, while also being capable of producing high-quality ZnO-NPs with the desired morphology and size for their intended applications. The synthesis of nanoparticles has been achieved through biological, physical, and chemical methods, which can be classified into top-down and bottom-up approaches, as illustrated in Figure 2 [17,18]. The top-down approach encompasses both physical and chemical synthesis methods, which typically involve the use of chemicals or force to break down bulk materials into smaller particles.

Examples of top-down methods include laser ablation, ball milling, electrospinning, electron explosion, sputtering, solid state, and mechanochemical techniques [18,19]. On the other hand, various chemical synthesis methods fall under the bottom-up approach, such as microwave synthesis, co-precipitation, spray pyrolysis, sol-gel, hydrothermal, sonochemical, microemulsion, solvochemical, and hydrothermal methods [20].

This approach involves the formation of nanoparticles through the nucleation of molecules, ions, or atoms in a solution, followed by their aggregation. It is a widely reported approach for the preparation of nanoparticles [21]

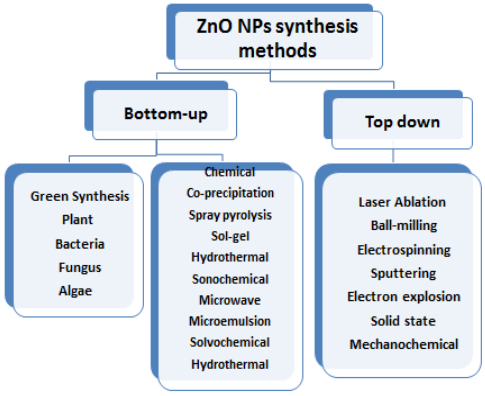

Figure 2: Zinc oxide nanoparticle synthesis methods.

While both physical and chemical conventional synthesis processes have been used for the preparation of ZnO-NPs, some of these methods are limited by high pressure and energy consumption, requiring complex equipment and resulting in high overall costs [20]. Additionally, toxic chemicals used during synthesis, such as hydrazine, polyethylene glycol, sodium borohydride, dimethylformamide, ethylene glycol, pyridine, and cetyltrimethylammonium bromide, can be harmful to the environment and the person handling the chemicals [22]. Therefore, safer and more cost-effective synthesis methods are needed for the preparation of NPs. Green synthesis using microorganisms or plant extracts can be a substitute for conventional physical and chemical synthesis methods.

5. Green Synthesis

Green synthesized nanoparticles possess a diverse array of applications owing to their distinct physical, thermal, chemical, and catalytic characteristics, alongside their substantial surface area to volume ratio, stability, biocompatibility, elevated surface energy, and exceptional adsorption phenomenon [23,24]. The technique of green synthesis for nanomaterials is based on twelve basics of green chemistry, which include pollution prevention, atom economy, designing less grave chemical syntheses, using renewable feedstocks, designing safer chemicals and products, increasing energy efficiency, using safer dissolvent and reaction conditions, using catalysts, designing chemicals and products to break down after use, avoiding chemical derivatives, minimizing the potential for accidents, and analyzing in real time to prevent pollution [25,26]. Zinc oxide nanoparticles have been synthesized using plants, algae, bacteria, and fungi, as depicted in Figure 3. Plant extracts are especially advantageous for the output of metallic nanoparticles due to their genetic variability and diverse chemical composition, which is affected by ecological and environmental factors.

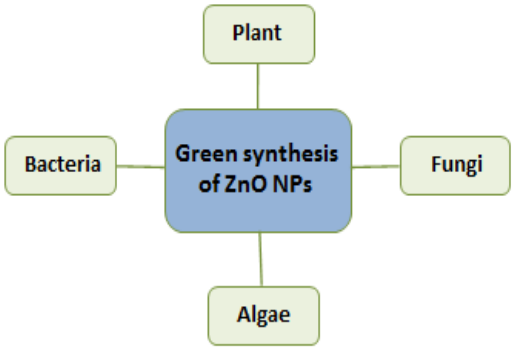

Figure 3: Green synthesis of ZnO NPs.

The presence of diverse components in plant extracts results in varying levels of natural reducing agents, ultimately impacting the properties of nanoparticles [27].

6. *Origanum majorana* L.

Origanum majorana L., a member of the Lamiaceae family, is a herb that holds significant importance in Yemen's traditional medicine and the production of essential oils. It belongs to a vast group of plants within the genus *Origanum*, which consists of 221 genera and 5600 species worldwide, many of which possess medicinal properties. Among the Lamiaceae family, there are 23 endemic species, as documented by [28,29]. Commonly known as 'sweet marjoram' or Majorana hortensis Moench, this herb can reach a height of 30-50 cm. While it is native to the Mediterranean region, *O. majorana* has been cultivated in various countries across Middle Asia, North Africa, Eastern Europe, and America, as reported by [30,31]. In North Yemen, specifically in Sanaa, Taiz, and Ibb, it can be found in the higher mountains [32]. In Islamic Arab traditional medicine, it is referred to as "Bardaqush," while its local Yemeni names are Ozzab or Lizzab [33].

This plant holds great value in Yemen's folk medicine, as it is believed to possess healing properties for a range of ailments, including kidney disease, diabetes, cough, wounds, stomachache, dysentery, and diarrhea [34]. The medicinal uses of *O. marjoram* include treating respiratory, gastrointestinal, and urinary tract disorders, as well as providing relief from spasms, rheumatism, diuretic effects, and asthma[35]. These aromatic plants are widely utilized in the food industry in various countries [36]. In traditional medicine, *O. majorana* L. is used as an antiepileptic and sedative medication [37]. *O. majorana* leaves are rich in phytochemicals such as terpenoids, flavonoid aglycons and glycosides, tannins, and phenolic acids [31,35]. These phytoconstituents, including phenolic compounds, flavonoids, amides, alkenes, and proteins, are responsible for the biofabrication of ZnO-NPs.

They have the ability to reduce or chelate metal ions and act as stabilizing and capping agents for the biogenic ZnO-NPs [38,39]. The polyphenolic ingredients of the plant extract, with their hydroxyl functional groups, also contribute to the reduction and biostabilization of ZnO-NPs [40]. Another study showed that phytochemical components donated their electrons, leading to the biostabilization of Zn^{2+} ions, which were then converted to ZnO-NPs through thermal annealing [41]. *O. majorana* has been found to have a wide range of beneficial effects, including antioxidant, antifungal, analgesic, antitumoral, antispasmodic, antibacterial, and antihyperglycemic properties. It also exhibits insecticide activity against *Anopheles labranchiae* [42,43]. Furthermore, *O. majorana* has potent antibacterial and anti-fungal activity against various pathogenic bacteria, including drug-resistant strains of *S. aureus* and *E. coli*, as reported by [44,45].

In their study, Ghazal *et al.* [46] have provided evidence of the antibacterial properties of terpenoids derived from this plant against both sensitive and drug-resistant strains of *S. aureus* and *E. coli*. Furthermore, *O. majorana* has been found to possess antioxidant and antifungal activity against *Candida albicans* and *Aspergillus niger*, as well as exhibiting antifungal effects against other pathogenic fungi, as reported by [47]. Moreover, have reported that *O. majorana* displays antiparasitic and larvicidal activities, along with anti-inflammatory, antitumor, and antimicrobial properties [48,49]. Considering its potential as a natural antioxidant in the food industry and as a potential anticancer drug, further investigation of *O. majorana* is warranted [50,51].

7. Plant Mediated Synthesis of ZnO-NPs

Plant-mediated synthesis of ZnO-NPs provides a viable and sustainable approach for the mass production of nanoparticles. This method offers several advantages over other synthesis techniques, including its cost-effectiveness, environmental friendliness, and simplicity of operation. Unlike conventional methods, plant-based routes do not necessitate intricate protocols or preparation methodologies. Moreover, the use of plant extracts as a synthetic medium eliminates the requirement for sophisticated equipment, thereby enhancing accessibility for large-scale production. Various plant parts, such as stems, leaves, barks, roots, and flowers, have demonstrated their efficacy in successfully synthesizing ZnO-NPs, as depicted in Figure 4 [7].

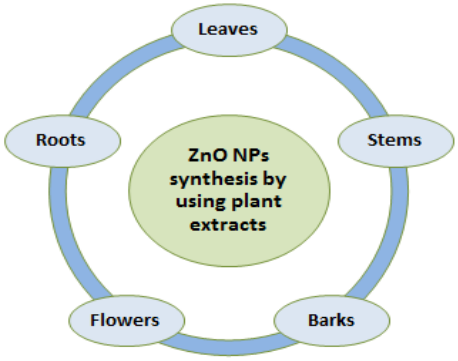

Figure 4: Zinc oxide nanoparticle synthesis by using plant extracts.

The success of synthesizing ZnO-NPs can be attributed to the presence of phytochemicals in plants, which serve as both reducing agents and stabilizing agents during the fabrication process. These phytochemicals encompass a wide range of compounds, including tannins, alkaloids, terpenoids, phenolic compounds, carbohydrates, saponins, and flavonoids. Through their interaction with Zn salt precursors, these compounds effectively reduce them and facilitate the formation of ZnO-NPs throughout the synthesis process [6,7]. Leaves, an integral part of plants, play a vital role in sustaining terrestrial animals through photosynthesis.

Numerous studies have investigated the use of various leaf extracts for the synthesis of ZnO-NPs and their photocatalytic activities, as documented in Table 1. For instance, Khaleghi *et al.* [52] successfully synthesized ZnO-NPs with a hexagonal structure and sizes ranging from 20 to 80 nm using an aqueous leaf extract from *O. majorana*. Similarly, Upadhyay *et al.* [53] conducted a comparative analysis of ZnO-NPs synthesized using leaf extracts of *Ocimum tenuiflorum* and conventional chemical methods, examining their morphological, structural, and visual properties. The results of their study revealed that the biosynthesis approach using plant extracts yielded ZnO-NPs with superior properties compared to those synthesized using chemical methods. Additionally, Yassin *et al.* [54] achieved the successful synthesis of ZnO-NPs using *O. majorana* leaves, employing various analytical techniques to characterize these nanomaterials.

The synthesized ZnO-NPs exhibited exceptional antibacterial properties and possessed a spherical shape with a hexagonal structure. In addition, Karam *et al.* [55] employed the use of thyme leaf extract to generate ZnO-NPs using an environmentally friendly technique. The resulting nanoparticles exhibited a spherical shape and had an average diameter ranging from 39 to 51 nm. Another investigation conducted by researchers utilized *Anacardium occidentale* leaf extract for the synthesis of ZnO nanoparticles. In this process, two zinc salt precursors, namely zinc acetate dihydrate and zinc chloride, were employed [56]. The antibacterial activity of ZnO-NPs, synthesized using *Rumex dentatus* leaf extract and zinc nitrate precursors, was evaluated against *Exiguobacterium aquaticum*, *Staphylococcus aureus*, *Escherichia coli*, and *Acinetobacter baumannii* by the researchers [57]. The study successfully demonstrated the effective antibacterial properties of these nanoparticles. Similarly, Aldalbahi *et al.* [58] utilized zinc nitrate hexahydrate as a precursor to produce ZnO nanoparticles from the Kalanchoe blossfeldiana plant and assessed their anticancer and cytotoxicity properties. The successful application and understanding of nanoparticles heavily rely on their characterization.

Table 1: List of Preparation extract of O.majorana, Zn salt precursors, synthesis conditions, properties, particle sizes and applications of the ZnO-NPs synthesised using *O.majorana*.

Preparation Extract of *O.majorana*	Zn Salt Precursor	Synthesis condition	Properties and Particle Size	Applications	Ref.
50 g, 200 mL Deionised water as a solvent, 80 C for 15 min	(Zn $((NO_3)_2 6H_2O)$	5 mL of extract was combined with 95 mL of zinc nitrate, an hour at70 C	Hexagonal, Particle size (TEM): 12.4 nm, zeta potential be -14.8 mV, hydrodynamic size of 71.93 nm.	Antibacterial activity	[54]
50 g, 200 mL Deionised water as a solvent, 40 °C	$(ZnSO_4.7H_2O)$	3 mL leaves extract of O.majorana and 50 mL (0.2 M) zinc sulfate solution	absorption band has been obtained at 379.75 nm, Particle size (SEM): 90 to 125 nm.	Antibacterial activities	[59]
20 g, 250 mL Deionised water, 50 °C for 30 min	$Zn(CH_3COO)_2.2H_2o$	5 mL extract of O.majorana and 50 mL zinc nitrate, In order to adjust the pH solution to 12,$(NaOH)_2$, for 12 h at 60°C.	Hexagonal, Particle size (TEM): 32 nm,	-	[38]
(10 g) was mixed in distilled water (100 ml) and heated up to 100°C for two hours.	zinc acetate dehydrates (0.5 mM)	added to the filtered solution at a proportion of 1:1 and stirred by magnetic stirrer at 25°C.	spherical, Particle size (TEM): 32 nm,	antioxidant and cytotoxic activities	[52]
20 g, 100 mL Deionised water, 70 °C for 60 min	(Zn(NO3)6H2O) Zinc nitrate hexahydrate	50 mL of O. vulgare extract was added to 2 M zinc nitrate, at 60 C for 2 h	Spherical, crystalline size from 19.67 to 28.78 nm. Particle size (TEM): from 20 to 30nm, zeta potential be -14.7 mV, the hydrodynamic size of 36.15 nm.	Antimicrobial and Biofilm Inhibition Activity	[60]

8. Zinc oxide nanoparticles characterization

The successful application and understanding of nanoparticles heavily rely on their characterization. Numerous studies have demonstrated that the morphology and surface chemistry of nanoparticles significantly impact their safety, biodistribution, and effectiveness in biological systems. However, accurately determining the size of nanoparticles is challenging due to the polydispersity of materials [61].

To characterize nanoparticles, various strategies can be employed, which can be categorized into biological and physicochemical methods. Biological characterization involves assessing genotoxicity, anti-microbial activity, and antibiofilm activity. On the other hand, physicochemical methods encompass a range of techniques such as scanning electron microscopy (SEM), transmission electron microscopy (TEM), atomic force microscopy (AFM), X-Ray Diffraction (XRD), Energy-dispersive X-ray spectroscopy (EDS), Fourier Transform Infrared Spectroscopy (FTIR), and Ultraviolet-visible Spectrophotometry Figure 5 [62].

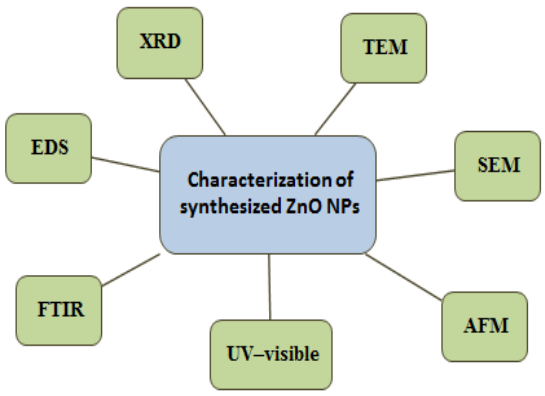

Figure 5: Characterization of synthesized ZnO-NPs.

8.1. Scanning Electron Microscopy

Scanning electron microscopy is a valuable tool for obtaining significant insights into the porosity, size, aggregation, and shape of nanoparticles through imaging[63]. SEM images are particularly effective in evaluating the flatness topography of ZnO-NPs due to their significant field depth and high magnification capabilities [64]. By allowing for the imaging of nanoparticles, SEM provides relevant information on their porosity, size, aggregation, and shape [63]. This technique enables direct visualization, which facilitates the identification of morphological characteristics [61]. When exposed to electron beams, ZnO-NPs generate and detect signals, offering valuable insights into the orientation, morphology, and structure of the crystal particles [65]. The mechanism behind SEM is based on the passage of a finely focused scanned electron beam across the sample surface. These signals are then collected by detectors and displayed as images on a cathode ray tube screen [63].

8.2. Transmission Electron Microscopy

Transmission electron microscopy is a powerful tool that enables precise analysis of nanostructures and compositions. By utilizing a high-energy electron beam to expose ultrathin sections, TEM offers high-resolution imaging. This imaging is achieved by analyzing the imaging and angular distribution of scattered electrons, as well as conducting energy analysis of the emitted X-rays. Through the application of TEM, different phases can be identified and the structure of ZnO-NPs can be characterized. The TEM machine operates by capturing images through transmitted electrons, allowing for the observation of the morphological properties of ZnO-NPs. Furthermore, it is important to note that the size and shape of ZnO-NPs are influenced by the interaction between the sample and the transmitted electron [66].

8.3. Atomic force microscopy

Atomic force microscopy is an advanced technique used to analyze and treat ZnO-NPs at the nanoscale. This powerful tool allows for the characterization of nanomaterials in three dimensions and is particularly valuable for studying the behavior of ZnO-NPs in a biological environment. One of the key advantages of AFM is its ability to acquire high-resolution images in an aqueous medium, providing valuable insights into the structure and properties of ZnO-NPs [67].

8.4. X-Ray Diffraction

X-ray diffraction is a commonly employed method for evaluating the crystallinity of ZnO-NPs. This technique involves subjecting the particles to energetic x-rays emitted by a specialized machine, which then penetrates the particles and gathers important data about their structure [68]. XRD is widely used for non-destructive characterization purposes and offers several advantages. It enables the examination of the crystallographic structure, physical properties, and chemical composition of ZnO-NPs [67]. Additionally, XRD can provide insights into various structural aspects, including defect structure, phase composition, strain, and grain size. Moreover, XRD is utilized for the analysis of atomic arrangements and the limitation of ultrathin sections, as highlighted by [69].

8.5. Energy-dispersive X-ray spectroscopy

Energy-dispersive X-ray spectroscopy is a technique employed to examine the surface of a sample and determine its elemental composition. This method focuses on the analysis of X-rays emitted by the elements of the sample when they are bombarded by an electron beam. It serves as an alternative approach for studying the surface and elemental characteristics of a sample [70]. By investigating the quantity and structure of metal NPs present on the sample's surface, EDS can be utilized to identify the elemental structure of ZnO-NPs and assess their level of purity [71]. Each element's unique atomic structure generates distinct peaks on the X-ray spectrum, enabling accurate analysis of the elemental composition [72].

8.6. Fourier Transform Infrared Spectroscopy

Fourier transform infrared spectroscopy can be employed to identify the functional groups responsible for the reduction process in the interaction between zinc precursors and plant extracts [73]. When biosynthesized ZnO-NPs samples are exposed to infrared radiation, certain wavelengths are absorbed while others remain unabsorbed. These unabsorbed wavelengths serve as a molecular indication that characterizes the ZnO-NPs [74]. Analysis using FTIR has demonstrated that extracts containing biomolecules with functional groups such as C=O, -O-H, C-N, C=C, N-H, and C-H exhibit strong reducing properties for the biosynthesis of ZnO-NPs [68].

8.7. Ultraviolet-visible Spectrophotometry

Ultraviolet-visible spectrophotometry is a technique that allows for the analysis of the ultraviolet-visible spectral region. This method utilizes either reflectance or absorption spectroscopy to measure light in the visible and neighboring ranges, such as near-infrared and near-UV [75]. It is particularly useful in determining the chemical nature, transition metal ions, and highly conjugated chemical structure of molecules. In the context of confirming the formation of ZnO-NPs, UV-visible spectrophotometry proves to be a cost-effective approach [76]. By scanning the synthesized NPs in the UV region of the electromagnetic wave, specifically around 200-700 nm, the presence of ZnO-NPs can be verified. This interaction between light and the mobile surface electrons of ZnO-NPs leads to the phenomenon of surface plasmon resonance [77]. Previous research has demonstrated that the surface plasmon resonance band of ZnO-NPs significantly impacts their morphological properties and can be observed at wavelengths ranging from 289-385 nm [78].

9. Zinc oxide nanoparticles bio-medical applications

The utilization of natural raw materials and living organisms as capping and reducing agents in the biosynthesis of ZnO-NPs has greatly advanced the field of nanomaterials for bio-medical purposes. This novel approach has yielded ZnO-NPs that possess remarkable efficacy in delivering various compounds to diseased tissue, targeting bacterial infections, and quantifying concentrations of specific biomarkers within the body [79]. These nanoparticles demonstrate enhanced biocompatibility and exhibit favorable responses when interacting with biological tissue, resulting in improved performance. Consequently, there is an abundance of literature available that extensively explores the diverse bio-medical applications of ZnO-NPs, as depicted in Figure 6 [3,4,52,59].

9.1. Antifungal action of ZnO-NPs

Numerous studies have been conducted to explore the antifungal properties of ZnO-NPs in the treatment of yeasts and fungi. These nanoparticles are commonly used as antifungal additives in the food industry [80]. ZnO-NPs have shown efficacy against various pathogens, including *Candida albicans*, *Saccharomyces cerevisiae*, *Aspergillus* sp, and *Penicillium* sp [81,82]. In a study by Nasiri *et al.* [83], the antifungal effects of ZnO-NPs synthesized using *Lavandula angustifolia* extract were compared to nystatin. The ZnO-NPs group exhibited significantly better antifungal activity against *C. albicans*. Another study by Shobha *et al.* [84] reported that ZnO-NPs synthesized using *Ricinus communis* extract showed antifungal activity against *Aspergillus* and *Penicillium*, effectively inhibiting their growth. Zhu *et al.* [81] successfully synthesized ZnO-NPs using *Cinnamomum camphora* leaf extract and investigated their antifungal properties. The study revealed that ZnO-NPs treatments at concentrations ranging from 20 to 160 mg/L significantly inhibited the growth of *A. alternata*.

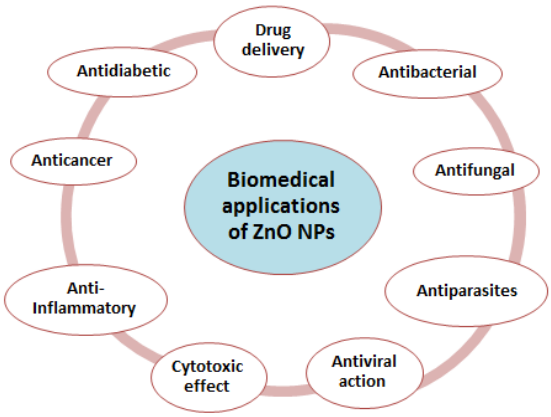

Figure 6: Potential biomedical applications of green synthesized ZnO-NPs.

Zinc oxide nanoparticles synthesized at pH 7 demonstrated the most effective anti-fungal properties, as evidenced by a minimum inhibitory concentration (MIC) value of 20 mg/L. These nanomaterials also exhibited significant inhibition of spore emergence and germ tube protraction of *A. alternata* at a concentration of 20 mg/L. In a study conducted by Krola *et al.* [82], ZnO-NPs were synthesized using *Medicago sativa* L. extract and their antimicrobial potential was evaluated against yeast, specifically Saccharomyces cerevisiae and *Candida albicans*. The MIC values reported for these microorganisms were 9.31 mg/mL and 0.58 mg/mL, respectively [85]. Furthermore, ZnO-NPs synthesized from *Carissa opaca* were found to have the highest zone of inhibition against *Pseudomonas aeruginosa* (a bacterial strain), while exhibiting a greater zone of inhibition against *Candida albican* in the case of fungi [86]. The growth of *Botrytis cinerea* was inhibited by the ZnO-NPs, which caused disfigurement in fungal hyphae and disrupted cellular functions. Similarly, in the case of *P. expansum*, the formation of conidiophores and conidia was prevented, leading to the death of fungal hyphae. This difference in sensitivity between *P. expansum* and *B. cinerea* can be attributed to the microbe-dependent nature of their sensitivity [87]. According to Pasquet *et al.* [88], the antimicrobial activity of ZnO-NPs is influenced by their physicochemical characteristics, such as morphology and size of rods and platelets. The mechanism of action of ZnO-NPs against fungi involves various processes, including protein and DNA binding, disruption of fungal DNA amplification, increased production of reactive oxygen species (ROS), disruption of cell membrane, and alteration of gene expression. Research conducted by [89] observed oxidative damage and changes in mitochondrial function in fungi exposed to ZnO-NPs. These effects may be attributed to modifications in the membrane potential of mitochondria and the expression of antioxidant enzymes, such as superoxide dismutase. Furthermore, Sun *et al.* [90] performed a high-throughput transcriptome sequencing analysis on mycelial cells treated with ZnO-NPs, revealing changes in gene expression levels in *Aspergillus flavus*. These changes involved genes related to oxidative stress, transmembrane transport, zinc ion binding, and oxidative phosphorylation processes [91].

9.2. Antibacterial action of ZnO-NPs

Bacterial diseases pose a significant threat to the global human population. In recent years, individual cells within pathogenic bacterial communities have shown a decrease in susceptibility to antibiotics, leading to a decline in metabolic rates [92]. Consequently, the emergence

of antibiotic resistance has become one of the most pressing health concerns of the 21st century. Therefore, it is crucial to evaluate an antibiotic agent that can effectively eliminate pathogenic bacteria that have developed resistance to medication.

Nanoparticles, due to their small size and large surface area compared to larger molecules, possess potent antibacterial properties. They have the ability to penetrate the bacterial membrane at various levels, disrupting it, inhibiting bacterial protein production, and even infiltrating the cells themselves [93].

Given the growing resistance of traditional antibiotics to microbial growth, numerous experiments have been conducted to enhance antimicrobial activity. In vitro tests on antimicrobial efficacy have consistently shown that metallic nanoparticles effectively inhibit a wide range of bacterial species [94]. Moreover, it is widely acknowledged that ZnO-NPs exhibit antibacterial effects by penetrating the cell membrane and inhibiting the growth of microorganisms. Extensive research has been conducted by various scientists to biosynthesize ZnO-NPs against different bacterial strains, resulting in significant antimicrobial efficacy [54]. Additionally, studies have demonstrated that ZnO-NPs synthesized by *O. majorana* extract display antibacterial and antifungal activity against *E.coli*, *K.pneumoniae*, *Salmonella typhimurium*, *Enterobacter cloacae*, and *P. aeruginosa.* Saini et al. [59] conducted a study to investigate the antibacterial and fungi activity of ZnO-NPs using *O. majorana* leaf aqueous extract. The results showed that these ZnO-NPs exhibited strong bactericidal activity against *S. aureus*, *P. aeruginosa*, *E. coli*, and *S. pneumoniae*. The minimum inhibitory concentration (MIC) for *E. coli* was found to be 100-125 mg/mL, while for P. aeruginosa, it ranged from 150-175 mg/mL. Both *S. aureus* and *S. pneumoniae* showed MIC values of 76-100 mg/mL. Additionally, the biosynthesis of ZnO-NPs using *S. aromaticum* extracts in water and ethanol resulted in the inhibition of *K. pneumonia*, *P. aeruginosa*, and *E. coli* [95]. The study also demonstrated the formation of an inhibition zone against *B. subtills*, *S. aureus*, *K. pneumonia*, and *E. coli* at a concentration of 100 µg/mL of ZnO-NPs synthesized using *Brassica oleracea* var. botrytis leaf extract. Therefore, these findings suggest that the eco-friendly biosynthesized ZnO-NPs can be utilized for various environmental and antipathogenic applications [96]. In another study, ZnO-NPs were fabricated using *P. granatum* peel and coffee ground extracts, showing antibacterial effects against *S. aureus*, *E. aerogenes*, *P. aeruginosa*, and *K. pneumoniae*. Similarly, green synthesized ZnO-NPs using *Bauhinia tomentosa* leaf extract exhibited bactericidal effects against *S. aureus*, *E. coli*, *B. subtilis*, and *P. aeruginosa*, with higher efficiency against gram-negative bacteria [97,98].

9.3. Antiviral action of ZnO-NPs

Zinc oxide nanoparticles have been found to possess notable antiviral properties against various viruses, such as hepatitis C virus, human papillomavirus, human immunodeficiency virus, and herpes simplex virus [99]. The antiviral efficacy of ZnO-NPs is attributed to their ability to activate both the adaptive and innate immune responses through toll-like receptor signaling pathways and downstream proteins. This activation leads to the release of pro-inflammatory cytokines, which impede viral activity [100]. Moreover, ZnO-NPs exhibit antiviral effects by generating ROS, inhibiting the activity of viral RNA-dependent RNA polymerase, and preventing viral infection. They also hinder virus adsorption, block viral coating, and impede replication, assembly, and release throughout the virus's life cycle. Notably, ZnO-NPs synthesized using Plumbago indica extract have shown promising activity against Herpes Simplex Virus Type 1 [101].

9.4. Antiparasites action of ZnO-NPs

Zinc oxide nanoparticles demonstrate a potent anthelminthic effect by inducing the production of ROS and hydroxyl ions, resulting in oxidative stress. This oxidative stress leads to the electrostatic binding and subsequent damage of the helminth membrane [102]. In a study conducted by Kalpana et al. [103], zinc nitrate was utilized as a precursor for the eco-friendly synthesis of ZnO-NPs using an aqueous peel extract of *Lagenaria siceraria*. This approach provides a significant environmentally friendly alternative for combating malaria parasites and vectors.

9.5. Anticancer activity of ZnO-NPs

Cancer is a group of diseases characterized by abnormal tissue growth, leading to the formation of tumors that can metastasize to other tissues and have severe consequences for patients, potentially resulting in fatality [104]. Current treatment modalities for cancer encompass surgical intervention, chemotherapy, and radiotherapy. However, while these treatments are theoretically effective in eradicating cancer cells, they also come with significant adverse effects [105]. In a study conducted by Rafique et al. [106], it was demonstrated that the green synthesis approach for producing ZnO-NPs using *Moringa oleifera*, *Mentha piperita*, and *Citrus lemon* exhibited potent anticancer properties, offering a wide range of potential applications, particularly in the field of biomedicine. Despite their beneficial effects, these non-selective treatment methods have notable drawbacks such as immunosuppression, anemia, nausea, and even mortality. Furthermore, literature suggests that certain cancer cells have developed resistance to these therapies, leading to the emergence of chemotherapy-resistant tumors and rendering these treatments ineffective for specific patients. Consequently, extensive efforts have been dedicated to the development of novel approaches in cancer treatment, with nanotechnology gaining prominence [107]. The remarkable potential of ZnO-NPs lies in their ability to induce apoptosis in leukemic cells without exerting cytotoxic effects on healthy cells. Additionally, ZnO-NPs have been reported to exhibit significant selective toxicity against tumor T cells while sparing normal cells from harm. Moreover, research has elucidated that ZnO-NPs selectively target brain tumor cells without causing damage to normal human astrocytes [7]. The interaction between ZnO-NPs and cells leads to the generation of ROS, resulting in mitochondrial damage and triggering cell death in cancerous tissues. The effectiveness of ZnO-NPs in combating cancer has been confirmed through experiments conducted on various cancer cell lines, utilizing a green synthesis method [108]. A549 lung cancer cells were subjected to a comprehensive investigation in a particular study, which aimed to assess the anticancer characteristics of the NPs that were biosynthesized. The inhibitory concentration of 50 of these ZnO-NPs, which were synthesized using the leaves of *Artocarpus heterophyllus*, was found to be 15.6 mg/ml. The primary objective of this study was to ensure the safety and stability of the biosynthesized NPs [109].

9.6. Anti-Inflammatory activity of ZnO-NPs

Inflammation refers to an exaggerated response of living tissue to injury, which is characterized by pain, redness, swelling, and heat. It plays a vital role in the complex reaction of body tissues to harmful stimuli such as irritants, damaged cells, or pathogens [92]. When a specific area of the body is injured, the arterioles in the surrounding tissue widen, leading to increased blood flow and resulting in redness [110]. The resulting ZnO-NPs biosynthesis have been utilized for their potential antioxidant, antimicrobial, antidiabetic, cytotoxic, anti-inflammatory, and anti-aging properties. Additionally, ZnO-NPs have demonstrated a dose-dependent antidiabetic and cytotoxic effect. Similarly, ZnO-NPs have also shown significant anti-aging properties [111]. ZnO-NPs have been found to possess anti-inflammatory properties by inhibiting the release of pro-inflammatory cytokines, mast cell degranulation, myeloperoxidase, and inducible nitric oxide synthase expression. The mRNA expression of pro-inflammatory cytokines was effectively suppressed in a dose-dependent manner by the ZnO-NPs synthesized using Polygala tenuifolia [112]. A comparison between ZnO-NPs and the standard form of ZnO revealed that ZnO-NPs reduced carrageenan-induced paw edema and enhanced the anti-inflammatory activity of the nonsteroidal anti-inflammatory drug, ketoprofen [113].

10. Conclusion

Zinc oxide nanoparticles have demonstrated great potential in the field of medicine due to their biocompatibility and their ability to combat fungal and bacterial infections, treat cancer, deliver drugs, reduce inflammation, and fight viruses. The use of plant extracts for the biosynthesis of these nanoparticles offers several advantages, such as cost-effectiveness, energy efficiency, and the ability to protect human health and the environment by reducing waste and producing safer products. This approach also encompasses the significant aspects of nanotechnology in various applications. Therefore, the utilization of plant extracts for synthesis has the potential to significantly impact the future diagnosis and treatment of various diseases. However, there is still a need to explore commercially viable and eco-friendly methods to determine the effectiveness of natural reducing agents in forming ZnO-NPs, which requires further investigation.

Conflict of interest

The authors declare that they have no conflict of interest.

Reference

[1] Bayda, S., Adeel, M., Tuccinardi, T., Cordani, M., Rizzolio, F. (2019) The history of nanoscience and nanotechnology: from chemical–physical applications to nanomedicine, *Molecules* **25**: 112.

[2] Nasrollahzadeh, M., Sajadi, S.M., Sajjadi, M., Issaabadi, Z., An introduction to nanotechnology, in Book (2019) An introduction to nanotechnology, Elsevier, Amsterdam, Netherlands, pp. 1-27.

[3] Qin, X., Zhang, J., Wang, B., Xu, G., Yang, X., Zou, Z., Yu, C. (2021) Ferritinophagy is involved in the zinc oxide nanoparticles-induced ferroptosis of vascular endothelial cells, *Autophagy* **17**: 4266-4285.

[4] Taşdemir, A., Aydin, R., Akkaya, A., Akman, N., Altınay, Y., Çetin, H., Şahin, B., Uzun, A., Ayyıldız, E. (2021) A green approach for the preparation of nanostructured zinc oxide: characterization and promising antibacterial behaviour, *Ceramics International* **47**: 19362-19373.

[5] Lučić, A., Stambolić, A., Omanović-Mikličanin, E., Hamidović, S. (2020) Biosynthesis of ZnO Nanoparticles from Basil Extract and Their Antimicrobial Activity, Central European Congress on Food, Springer, pp. 52-58

[6] Drummer, S., Madzimbamuto, T., Chowdhury, M. (2021) Green synthesis of transition-metal nanoparticles and their oxides: a review, *Materials* **14**: 2700.

[7] Akintelu, S. A., Folorunso, A. S. (2020) A review on green synthesis of zinc oxide nanoparticles using plant extracts and its biomedical applications, *BioNanoScience* **10**: 848-863.

[8] Joudeh, N., Linke, D. (2022) Nanoparticle classification, physicochemical properties, characterization, and applications: a comprehensive review for biologists, *Journal of Nanobiotechnology* **20**: 262.

[9] Ahlawat, J., Asil, S. M., Barroso, G. G., Nurunnabi, M., Narayan, M. (2021) Application of carbon nano onions in the biomedical field: Recent advances and challenges, *Biomaterials Science* **9**: 626-644.

[10] Ealia, S.A.M., Saravanakumar, M.P. (2017) A review on the classification, characterisation, synthesis of nanoparticles and their application, IOP conference series: materials science and engineering, IOP Publishing, pp. 032019.

[11] Khan, I., Saeed, K., Khan, I. (2019) Nanoparticles: Properties, applications and toxicities, *Arabian Journal of Chemistry* **12**: 908-931.

[12] Ijaz, I., Gilani, E., Nazir, A., Bukhari, A. (2020) Detail review on chemical, physical and green synthesis, classification, characterizations and applications of nanoparticles, *Green Chemistry Letters and Reviews* **13**: 223-245.

[13] Yuvakkumar, R., Suresh, J., Nathanael, A. J., Sundrarajan, M., Hong, S. I. (2014) Novel green synthetic strategy to prepare ZnO nanocrystals using rambutan (*Nephelium lappaceum* L.) peel extract and its antibacterial applications. *Materials Science and Engineering* C **41**: 17-27.

[14] Chan, Y. Y., Pang, Y. L., Lim, S., Chong, W. C. (2021) Facile green synthesis of ZnO nanoparticles using natural-based materials: Properties, mechanism, surface modification and application, *Journal of Environmental Chemical Engineering* **9**: 105417.

[15] Canta, M., Cauda, V. (2020) The investigation of the parameters affecting the ZnO nanoparticle cytotoxicity behavior: a tutorial review, *Biomaterials Science* **8**: 6157-6174.

[16] Lallo da Silva, B., Abuçafy, M. P., Berbel Manaia, E., Oshiro Junior, J. A., Chiari-Andréo, B. G., Pietro, R. C. R., Chiavacci, L. A. (2019) Relationship between structure and antimicrobial activity of zinc oxide nanoparticles: An overview, *International Journal of Nanomedicine*, 9395-9410.

[17] Weldegebrieal, G. K. (2020) Synthesis method, antibacterial and photocatalytic activity of ZnO nanoparticles for azo dyes in wastewater treatment: A review, *Inorganic Chemistry Communications* **120**: 108140.

[18] Agarwal, H., Kumar, S. V., Rajeshkumar, S. (2017) A review on green synthesis of zinc oxide nanoparticles–An eco-friendly approach, *Resource-Efficient Technologies* **3**: 406-413.

[19] Basnet, P., Chanu, T. I., Samanta, D., Chatterjee, S. (2018) A review on bio-synthesized zinc oxide nanoparticles using plant extracts as reductants and stabilizing agents, *Journal of Photochemistry and Photobiology B: Biology* **183**: 201-221.

[20] Abid, N., Khan, A. M., Shujait, S., Chaudhary, K., Ikram, M., Imran, M., Maqbool, M. (2022) Synthesis of nanomaterials using various top-down and bottom-up approaches, influencing factors, advantages, and disadvantages: A review, *Advances in Colloid and Interface Science* **300**: 102597.

[21] Sharmila, G., Thirumarimurugan, M., Muthukumaran, C. (2019) Green synthesis of ZnO nanoparticles using *Tecoma castanifolia* leaf extract: Characterization and evaluation of its antioxidant, bactericidal and anticancer activities, *Microchemical Journal* **145**: 578-587.

[22] Ishak, N. M., Kamarudin, S. K., Timmiati, S. N. (2019) Green synthesis of metal and metal oxide nanoparticles via plant extracts: an overview, *Materials Research Express* **6**: 112004.

[23] Izadiyan, Z., Shameli, K., Miyake, M., Hara, H., Mohamad, S.E.B., Kalantari, K., Taib, S.H.M., Rasouli, E. (2020) Cytotoxicity assay of plant-mediated synthesized iron oxide nanoparticles using Juglans regia green husk extract, *Arabian Journal of Chemistry* **13**: 2011-2023.

[24] Yew, Y. P., Shameli, K., Miyake, M., Kuwano, N., Bt Ahmad Khairudin, N. B., Bt Mohamad, S. E., Lee, K. X. (2016) Green synthesis of magnetite (Fe_3O_4) nanoparticles using seaweed (*Kappaphycus alvarezii*) extract, *Nanoscale Research Letters* **11**: 1-7.

[25] Rubab, L., Anum, A., Al-Hussain, S. A., Irfan, A., Ahmad, S., Ullah, S., Zaki, M. E. (2022) Green chemistry in organic synthesis: Recent update on green catalytic approaches in synthesis of 1, 2, 4-Thiadiazoles, *Catalysts* **12**: 1329.

[26] Varghese, R.J., Zikalala, N., Oluwafemi, O.S., Green synthesis protocol on metal oxide nanoparticles using plant extracts, in: Book (2020) Green synthesis protocol on metal oxide nanoparticles using plant extracts, Elsevier, Amsterdam, Netherlands, pp. 67-82.

[27] Shaik, M.R., Ali, Z.J.Q., Khan, M., Kuniyil, M., Assal, M.E., Alkhathlan, H.Z., Al-Warthan, A., Siddiqui, M.R.H., Khan, M., Adil, S.F. (2017) Green synthesis and characterization of palladium nanoparticles using Origanum vulgare L. extract and their catalytic activity, *Molecules* **22**: 165.

[28] Al-Khulaidi, A. (2013) Flora of Yemen, The sustainable natural resource management project (SNRMP II).EPA and UNDP, Republic of Yemen: 1-136.

[29] Miller, A.G., Morris, M. (2004) Ethnoflora of the Soqotra Archipelago, ed., Royal Botanic Garden Edinburgh, Edinburgh, UK, pp. 759.

[30] Wang, S., Zhou, L., Attia, F.A.-Z.K., Tang, Q., Wang, M., Liu, Z., Waterhouse, G.I., Liu, L., Kang, W. (2021) Origanum majorana L.: a nutritional supplement with immunomodulatory effects, *Frontiers in Nutrition* **8**: 748031.

[31] Tripathy, B., Satyanarayana, S., Khan, K. A., Raja, K. (2017) An updated review on traditional uses, taxonomy, phytochemistry, pharmacology and toxicology of *Origanum majorana*, *International Journal of Pharma Research and Health Sciences* **5**: 1717-23.

[32] Aqlan, E., Al-dubaie, A., Al-Hammadi A. (2012) Flora of Ibb: Studies on the Flora of Ibb Governorate, Republic of Yemen, ed., Lap Lambert Academic Publishing, Saarbrücken, Germany, pp. 372

[33] Al-Fatimi, M. (2018) Volatile constituents, antimicrobial and antioxidant activities of the aerial parts of *Origanum majorana* L. from Yemen, *Journal of Pharmaceutical Research International* **23**: 1-10.

[34] Al-Hakimi, A., Ya'ni, A., Pelat, F., Health Issues in the Mountains of Yemen: Healing Practices as Part of Farmers' Traditional Knowledge, in: Regourd, A., Ed., Book (2012) Health Issues in the Mountains of Yemen: Healing Practices as Part of Farmers' Traditional Knowledge, Brill, Leiden, Netherlands, pp. 203-217.

[35] Bina, F., Rahimi, R. (2017) Sweet marjoram: a review of ethnopharmacology, phytochemistry, and biological activities, *Journal of Evidence-based Complementary & Aternative Medicine* **22**: 175-185.

[36] Quiroga, P. R., Grosso, N. R., Lante, A., Lomolino, G., Zygadlo, J. A., Nepote, V. (2013) Chemical composition, antioxidant activity and anti-lipase activity of *Origanum vulgare* and *Lippia turbinata* essential oils, *International Journal of Food Science & Technology* **48**: 642-649.

[37] Abdollahi Fard, M., Shojaii, A. (2013) Efficacy of Iranian Traditional Medicine in the Treatment of Epilepsy, *BioMed Research International* **2013**: 692751

[38] Mohammadian, M., Es'haghi, Z., Hooshmand, S. (2018) Green and chemical synthesis of zinc oxide nanoparticles and size evaluation by UV–vis spectroscopy, *Journal of Nanomedicine Research* **7**: 52-58.

[39] Ahmed, S., Chaudhry, S. A., Ikram, S. (2017) A review on biogenic synthesis of ZnO nanoparticles using plant extracts and microbes: a prospect towards green chemistry, *Journal of Photochemistry and Photobiology B: Biology* **166**: 272-284.

[40] Babu, K. S., Reddy, A. R., Sujatha, C., Reddy, K. V. (2013) Optimization of UV emission intensity of ZnO nanoparticles by changing the excitation wavelength, *Materials Letters* **99**: 97-100.

[41] Gharagozlou, M., Naghibi, S. (2016) Sensitization of ZnO nanoparticle by vitamin B12: Investigation of microstructure, FTIR and optical properties, *Materials Research Bulletin* **84**: 71-78.

[42] Duletić-Laušević, S., Aradski, A.A., Kolarević, S., Vuković-Gačić, B., Oalđe, M., Živković, J., Šavikin, K., Marin, P.D. (2018) Antineurodegenerative, antioxidant and antibacterial activities and phenolic components of Origanum majorana L.(Lamiaceae) extracts, *Journal of Applied Botany and Food Quality* **91**: 126-134.

[43] El-Akhal, F. O. U. A. D., Guemmouh, R. A. J. A., Maniar, S., Taghzouti, K., El Ouali Lalami, A. (2016) Larvicidal activity of essential oils of *Thymus vulgaris* and *Origanum majorana* (Lamiaceae) against of the malaria vector Anopheles labranchiae (Diptera: Culicidae), *International Journal of Pharmacy and Pharmaceutical Sciences* **8**: 372-6.

[44] Amor, G., Caputo, L., La Storia, A., De Feo, V., Mauriello, G., Fechtali, T. (2019). Chemical composition and antimicrobial activity of *Artemisia herba-alba* and *Origanum majorana* essential oils from Morocco, *Molecules* **24**: 4021.

[45] Abduljalil, J. M., AL-Rakhami, A. A., AL-Haj, T. M., AL-Rrimy, A. M., Al-Wheabi, A. S. (2018) Preliminary phytochemical analysis and antibacterial activity of methanol extracts from *Origanum majorana*, *Rumex nervosus*, and *Withania somnifera*, *International Journal of Pharma Research and Health Sciences* **6**: 2844-50.

[46] Ghazal, T. S. A., Schelz, Z., Vidács, L., Szemerédi, N., Veres, K., Spengler, G., Hohmann, J. (2022) Antimicrobial, multidrug resistance reversal and biofilm formation inhibitory effect of *Origanum majorana* extracts, essential oil and monoterpenes, *Plants* **11**: 1432.

[47] Paudel, P. N., Satyal, P., Satyal, R., Setzer, W. N., Gyawali, R. (2022) Chemical Composition, enantiomeric distribution, antimicrobial and antioxidant activities of *Origanum majorana* L. essential oil from Nepal, *Molecules* **27**: 6136.

[48] Della Pepa, T., Elshafie, H.S., Capasso, R., De Feo, V., Camele, I., Nazzaro, F., Scognamiglio, M.R., Caputo, L. (2019) Antimicrobial and phytotoxic activity of Origanum heracleoticum and O. majorana essential oils growing in Cilento (Southern Italy), *Molecules* **24**: 2576.

[49] Thanh, V. M., Bui, L. M., Bach, L. G., Nguyen, N. T., Thi, H. L., Hoang Thi, T. T. (2019) *Origanum majorana* L. essential oil-associated polymeric nano dendrimer for antifungal activity against Phytophthora infestans, *Materials* **12**: 1446.

[50] Ozturk, H., Cetinkaya, A., Duzcu, S. E., Tekce, B. K., Ozturk, H. (2018) Carvacrol attenuates histopathogic and functional impairments induced by bilateral renal ischemia/reperfusion in rats, *Biomedicine & Pharmacotherapy* **98**: 656-661.

[51] Erenler, R., Sen, O., Aksit, H., Demirtas, I., Yaglioglu, A. S., Elmastas, M., Telci, I. (2016) Isolation and identification of chemical constituents from *Origanum majorana* and investigation of antiproliferative and antioxidant activities, *Journal of the Science of Food and Agriculture* **96**: 822-836.

[52] Khaleghi, S., Khayatzadeh, J., Neamati, A. (2022) Biosynthesis of zinc oxide nanoparticles using *Origanum majorana* L. leaf extract, its antioxidant and cytotoxic activities, *Materials Technology* **37**: 2522-2531.

[53] Upadhyay, P., Jain, V.K., Sharma, S., Shrivastav, A., Sharma, R. (2020) Green and chemically synthesized ZnO nanoparticles: A comparative study, IOP Conference Series: Materials Science and Engineering, IOP Publishing, pp. 012025.

[54] Yassin, M. T., Al-Askar, A. A., Maniah, K., Al-Otibi, F. O. (2022) Green synthesis of zinc oxide nanocrystals utilizing *Origanum majorana* leaf extract and their synergistic patterns with colistin against multidrug-resistant bacterial strains, *Crystals* **12**: 1513.

[55] Karam, S.T., Abdulrahman, A.F. (2022) Green synthesis and characterization of ZnO nanoparticles by using thyme plant leaf extract, Photonics, MDPI, pp. 594.

[56] Droepenu, E. K., Asare, E. A., Wee, B. S., Wahi, R. B., Ayertey, F., Kyene, M. O. (2021) Biosynthesis, characterization, and antibacterial activity of ZnO nanoaggregates using aqueous extract from *Anacardium occidentale* leaf: comparative study of different precursors, *Beni-Suef University Journal of Basic and Applied Sciences* **10**: 1-10.

[57] Nazir, A., Raza, M., Abbas, M., Abbas, S., Ali, A., Ali, Z., Younas, U., Al-Mijalli, S.H., Iqbal, M. (2022) Microwave assisted green synthesis of ZnO nanoparticles using Rumex dentatus leaf extract: photocatalytic and antibacterial potential evaluation, *Zeitschrift für Physikalische Chemie* **236**: 1203-1217.

[58] Aldalbahi, A., Alterary, S., Ali Abdullrahman Almoghim, R., Awad, M.A., Aldosari, N.S., Fahad Alghannam, S., Nasser Alabdan, A., Alharbi, S., Ali Mohammed Alateeq, B., Abdulrahman Al Mohsen, A. (2020) Greener synthesis of zinc oxide nanoparticles: Characterization and multifaceted applications, *Molecules* **25**: 4198.

[59] Saini, M., Mushtaq, A., Yadav, S., Rawat, S., Rani, N., Gupta, K., Saini, K. (2022) Green Synthesis of Rod Shaped ZnO Using Extract of Origanum Majorana Leaf and Investigation for Antibacterial Applications, IOP Conference Series: Materials Science and Engineering, IOP Publishing, pp. 012048.

[60] Kamli, M. R., Malik, M. A., Srivastava, V., Sabir, J. S., Mattar, E. H., Ahmad, A. (2021) Biogenic ZnO nanoparticles synthesized from *Origanum vulgare* abrogates quorum sensing and biofilm formation in opportunistic pathogen Chromobacterium violaceum, *Pharmaceutics* **13**: 1743.

[61] Velsankar, K., Sudhahar, S., Parvathy, G., Kaliammal, R. (2020) Effect of cytotoxicity and aAntibacterial activity of biosynthesis of ZnO hexagonal shaped nanoparticles by Echinochloa frumentacea grains extract as a reducing agent, *Materials Chemistry and Physics* **239**: 121976..

[62] Karthik, S., Suriyaprabha, R., Vinoth, M., Srither, S. R., Manivasakan, P., Rajendran, V., Valiyaveettil, S. (2017) Larvicidal, super hydrophobic and antibacterial properties of herbal nanoparticles from *Acalypha indica* for biomedical applications, *RSC Advances* **7**: 41763-41770.

[63] Palmqvist, S., Schöll, M., Strandberg, O., Mattsson, N., Stomrud, E., Zetterberg, H., Blennow, K., Landau, S., Jagust, W., Hansson, O. (2017) Earliest accumulation of β-amyloid occurs within the default-mode network and concurrently affects brain connectivity, *Nature Communications* **8**: 1214.

[64] Hamelian, M., Hemmati, S., Varmira, K., Veisi, H. (2018) Green synthesis, antibacterial, antioxidant and cytotoxic effect of gold nanoparticles using *Pistacia atlantica* extract, *Journal of the Taiwan Institute of Chemical Engineers* **93**: 21-30.

[65] Vijayakumar, S., Vaseeharan, B., Malaikozhundan, B., Shobiya, M. (2016) *Laurus nobilis* leaf extract mediated green synthesis of ZnO nanoparticles: Characterization and biomedical applications, *Biomedicine & Pharmacotherapy*, **84**: 1213-1222.

[66] Aljabali, A.A., Akkam, Y., Al Zoubi, M.S., Al-Batayneh, K.M., Al-Trad, B., Abo Alrob, O., Alkilany, A.M., Benamara, M., Evans, D.J. (2018) Synthesis of gold nanoparticles using leaf extract of Ziziphus zizyphus and their antimicrobial activity, *Nanomaterials* **8**: 174.

[67] Rathod, T., Padalia, H., Chanda, S. (2017) Green synthesized zinc oxide nanoparticles as a therapeutic tool to combat candidiasis, AIP Conference Proceedings, AIP Publishing.

[68] Agarwal, H., Nakara, A., Menon, S., Shanmugam, V. (2019) Eco-friendly synthesis of zinc oxide nanoparticles using *Cinnamomum tamala* leaf extract and its promising effect towards the antibacterial activity, *Journal of Drug Delivery Science and Technology* **53**: 101212.

[69] Castillo-Michel, H. A., Larue, C., Del Real, A. E. P., Cotte, M., Sarret, G. (2017) Practical review on the use of synchrotron based micro-and nano-X-ray fluorescence mapping and X-ray absorption spectroscopy to investigate the interactions between plants and engineered nanomaterials, *Plant Physiology and Biochemistry* **110**: 13-32.

[70] Rades, S., Hodoroaba, V.-D., Salge, T., Wirth, T., Lobera, M.P., Labrador, R.H., Natte, K., Behnke, T., Gross, T., Unger, W.E. (2014) High-resolution imaging with SEM/T-SEM, EDX and SAM as a combined methodical approach for morphological and elemental analyses of single engineered nanoparticles, *RSC Advances* **4**: 49577-49587.

[71] Taziwa, R., Meyer, E., Katwire, D., Ntozakhe, L. (2017) Influence of Carbon Modification on the Morphological, Structural, and Optical Properties of Zinc Oxide Nanoparticles Synthesized by Pneumatic Spray Pyrolysis Technique, *Journal of Nanomaterials* **2017**: 9095301.

[72] Bala, N., Saha, S., Chakraborty, M., Maiti, M., Das, S., Basu, R., Nandy, P. (2015) Green synthesis of zinc oxide nanoparticles using *Hibiscus subdariffa* leaf extract: effect of temperature on synthesis, anti-bacterial activity and anti-diabetic activity, *RSC Advances* **5**: 4993-5003.

[73] Rupa, E. J., Anandapadmanaban, G., Mathiyalagan, R., Yang, D. C. (2018) Synthesis of zinc oxide nanoparticles from immature fruits of *Rubus coreanus* and its catalytic activity for degradation of industrial dye, *Optik* **172**: 1179-1186

[74] Dhanemozhi, A. C., Rajeswari, V., Sathyajothi, S. (2017) Green synthesis of zinc oxide nanoparticle using green tea leaf extract for supercapacitor application, *Materials Today: Proceedings* **4**: 660-667.

[75] Korkmaz, N. (2020) Bioreduction: the biological activity, characterization, and synthesis of silver nanoparticle, *Turkish Journal of Chemistry* **44**: 325-334.

[76] Jamdagni, P., Khatri, P., Rana, J. S. (2018) Green synthesis of zinc oxide nanoparticles using flower extract of *Nyctanthes arbor-tristis* and their antifungal activity, *Journal of King Saud University-Science* **30**: 168-175.

[77] Al-Dhabi, N. A., Valan Arasu, M. (2018) Environmentally-friendly green approach for the production of zinc oxide nanoparticles and their anti-fungal, ovicidal, and larvicidal properties, *Nanomaterials* **8**: 500.

[78] Rajakumar, G., Thiruvengadam, M., Mydhili, G., Gomathi, T., Chung, I. M. (2018) Green approach for synthesis of zinc oxide nanoparticles from *Andrographis paniculata* leaf extract and evaluation of their antioxidant, anti-diabetic, and anti-inflammatory activities, *Bioprocess and Biosystems Engineering* **41**: 21-30.

[79] Hamrayev, H., Shameli, K., Korpayev, S. (2021) Green synthesis of zinc oxide nanoparticles and its biomedical applications: A

review, *Journal of Research in Nanoscience and Nanotechnology* **1**: 62-74.

[80] Rahimi Kalateh Shah Mohammad, G., Homayouni Tabrizi, M., Ardalan, T., Yadamani, S., Safavi, E. (2019) Green synthesis of zinc oxide nanoparticles and evaluation of anti-angiogenesis, anti-inflammatory and cytotoxicity properties, *Journal of Biosciences* **44**: 1-9.

[81] Zhu, W., Hu, C., Ren, Y., Lu, Y., Song, Y., Ji, Y., Han, C., He, J. (2021) Green synthesis of zinc oxide nanoparticles using Cinnamomum camphora (L.) Presl leaf extracts and its antifungal activity, *Journal of Environmental Chemical Engineering* **9**: 106659.

[82] Król, A., Railean-Plugaru, V., Pomastowski, P., Buszewski, B. (2019) Phytochemical investigation of *Medicago sativa* L. extract and its potential as a safe source for the synthesis of ZnO nanoparticles: The proposed mechanism of formation and antimicrobial activity, *Phytochemistry Letters* **31**: 170-180.

[83] Nasiri, S., Mahmoudvand, H., Shakibaei, M., Mousavi, S. A. H., Sepahvand, A. (2022) Antifungal effects of zinc nanoparticles green synthesized by *Lavandula angustifolia* extract, alone and combined with nystatin against Candida albicans, a major cause of oral candidiasis, *Journal of Herbmed Pharmacology* **11**: 540-545.

[84] Shobha, N., Nanda, N., Giresha, A. S., Manjappa, P., Sophiya, P., Dharmappa, K. K., Nagabhushana, B. M. (2019) Synthesis and characterization of Zinc oxide nanoparticles utilizing seed source of *Ricinus communis* and study of its antioxidant, antifungal and anticancer activity, *Materials Science and Engineering C* **97**: 842-850.

[85] Abomuti, M. A., Danish, E. Y., Firoz, A., Hasan, N., Malik, M. A. (2021) Green synthesis of zinc oxide nanoparticles using salvia officinalis leaf extract and their photocatalytic and antifungal activities, *Biology* **10**: 1075.

[86] Mehta, M., Chopra, C., Sistla, S., Bhushan, I. (2023) Potential of biosynthesized silver and zinc oxide nanoparticles from *Carissa opaca* extracts for antimicrobial activity and wastewater treatment, *Sustainability* **15**: 8911.

[87] Motazedi, R., Rahaiee, S., Zare, M. (2020) Efficient biogenesis of ZnO nanoparticles using extracellular extract of *Saccharomyces cerevisiae*: Evaluation of photocatalytic, cytotoxic and other biological activities, *Bioorganic Chemistry* **101**: 103998.

[88] Pasquet, J., Chevalier, Y., Couval, E., Bouvier, D., Noizet, G., Morlière, C., Bolzinger, M. A. (2014) Antimicrobial activity of zinc oxide particles on five micro-organisms of the Challenge Tests related to their physicochemical properties, *International Journal of Pharmaceutics* **460**: 92-100.

[89] Wang, J., Deng, X., Zhang, F., Chen, D., Ding, W. (2014) ZnO nanoparticle-induced oxidative stress triggers apoptosis by activating JNK signaling pathway in cultured primary astrocytes, *Nanoscale Research Letters* **9**: 1-12.

[90] Sun, Q., Li, J., Le, T. (2018) Zinc oxide nanoparticle as a novel class of antifungal agents: current advances and future perspectives, *Journal of Agricultural and Food Chemistry* **66**: 11209-11220.

[91] Sharma, D., Rajput, J., Kaith, B. S., Kaur, M., Sharma, S. (2010) Synthesis of ZnO nanoparticles and study of their antibacterial and antifungal properties, *Thin Solid Films* **519**: 1224-1229.

[92] Miri, A., Mahdinejad, N., Ebrahimy, O., Khatami, M., Sarani, M. (2019) Zinc oxide nanoparticles: Biosynthesis, characterization, antifungal and cytotoxic activity, *Materials Science and Engineering C* **104**: 109981.

[93] Singh, J., Dutta, T., Kim, K. H., Rawat, M., Samddar, P., Kumar, P. (2018) Green synthesis of metals and their oxide nanoparticles: applications for environmental remediation, *Journal of Nanobiotechnology* **16**: 1-24.

[94] Sharma, V., Anderson, D., Dhawan, A. (2012) Zinc oxide nanoparticles induce oxidative DNA damage and ROS-triggered mitochondria mediated apoptosis in human liver cells (HepG2), *Apoptosis* **17**: 852-870.

[95] Javad, S., Akhter, I., Aslam, K., Tariq, A., Ghaffar, N., Iqbal, S., Naseer, I. (2017) Antibacterial activity of plant extract and zinc nanoparticles obtained from *Syzigium aromaticum* L, *Pure and Applied Biology* **6**: 1079-1087.

[96] Manojkumar, U., Kaliannan, D., Srinivasan, V., Balasubramanian, B., Kamyab, H., Mussa, Z.H., Palaniyappan, J., Mesbah, M., Chelliapan, S., Palaninaicker, S. (2023) Green synthesis of zinc oxide nanoparticles using Brassica oleracea var. botrytis leaf extract: Photocatalytic, antimicrobial and larvicidal activity, *Chemosphere* **323**: 138263.

[97] Abdelmigid, H. M., Hussien, N. A., Alyamani, A. A., Morsi, M. M., AlSufyani, N. M., Kadi, H. A. (2022) Green synthesis of zinc oxide nanoparticles using pomegranate fruit peel and solid coffee grounds vs. chemical method of synthesis, with their biocompatibility and antibacterial properties investigation, *Molecules* **27**: 1236.

[98] Sukri, S. N. A. M., Shameli, K., Wong, M. M. T., Teow, S. Y., Chew, J., Ismail, N. A. (2019) Cytotoxicity and antibacterial activities of plant-mediated synthesized zinc oxide (ZnO) nanoparticles using *Punica granatum* (pomegranate) fruit peels extract, *Journal of Molecular Structure* **1189**: 57-65.

[99] Gupta, J., Irfan, M., Ramgir, N., Muthe, K. P., Debnath, A. K., Ansari, S., Surjit, M. (2022) Antiviral activity of zinc oxide nanoparticles and tetrapods against the Hepatitis E and Hepatitis C viruses, *Frontiers in Microbiology* **13**: 881595.

[100] Byk, L. A., Iglesias, N. G., De Maio, F. A., Gebhard, L. G., Rossi, M., Gamarnik, A. V. (2016) Dengue virus genome uncoating requires ubiquitination, *MBio* **7**: 10-1128.

[101] Melk, M. M., El-Hawary, S. S., Melek, F. R., Saleh, D. O., Ali, O. M., El Raey, M. A., Selim, N. M. (2021) Antiviral activity of zinc oxide nanoparticles mediated by *Plumbago indica* L. extract against Herpes Simplex Virus Type 1 (HSV-1), *International Journal of Nanomedicine* 8221-8233.

[102] Li, X., Xing, Y., Jiang, Y., Ding, Y., Li, W. (2009) Antimicrobial activities of ZnO powder-coated PVC film to inactivate food pathogens, *International Journal of Food Science & Technology* **44**: 2161-2168.

[103] Kalpana, V. N., Alarjani, K. M., Rajeswari, V. D. (2020) Enhancing malaria control using *Lagenaria siceraria* and its mediated zinc oxide nanoparticles against the vector *Anopheles stephensi* and its parasite Plasmodium falciparum, *Scientific Reports* **10**: 21568.

[104] Noor, H. M. (2018) Potential of carrageenans in foods and medical applications, *Global Health Management Journal* **2**: 32-36.

[105] Tang, Q., Xia, H., Liang, W., Huo, X., Wei, X. (2020) Synthesis and characterization of zinc oxide nanoparticles from *Morus nigra* and its anticancer activity of AGS gastric cancer cells, *Journal of Photochemistry and Photobiology B: Biology* **202**: 111698.

[106] Rafique, S., Bashir, S., Akram, R., Jawaid, S., Bashir, M., Aftab, A., Awan, S. U. (2023) In vitro anticancer activity and comparative green synthesis of ZnO/Ag nanoparticles by *Moringa oleifera*, *Mentha piperita*, and *Citrus lemon*, *Ceramics International* **49**: 5613-5620.

[107] Thi, T. U. D., Nguyen, T. T., Thi, Y. D., Thi, K. H. T., Phan, B. T., Pham, K. N. (2020) Green synthesis of ZnO nanoparticles using orange fruit peel extract for antibacterial activities, *RSC Advances* **10**: 23899-23907.

[108] Mishra, P. K., Mishra, H., Ekielski, A., Talegaonkar, S., Vaidya, B. (2017) Zinc oxide nanoparticles: a promising nanomaterial for biomedical applications, *Drug Discovery Today* **22**: 1825-1834.

[109] Majeed, S., Danish, M., Ismail, M. H. B., Ansari, M. T., Ibrahim, M. N. M. (2019) Anticancer and apoptotic activity of biologically synthesized zinc oxide nanoparticles against human colon cancer HCT-116 cell line-in vitro study, *Sustainable Chemistry and Pharmacy* **14**: 100179.

[110] Sadhasivam, S., Shanmugam, M., Umamaheswaran, P. D., Venkattappan, A., Shanmugam, A. (2021) Zinc oxide nanoparticles: green synthesis and biomedical applications. *Journal of Cluster Science* **32**: 1441-1455.

[111] Rehman, H., Ali, W., Khan, N. Z., Aasim, M., Khan, T., Khan, A. A. (2023) Delphinium uncinatum mediated biosynthesis of zinc oxide nanoparticles and in-vitro evaluation of their antioxidant, cytotoxic, antimicrobial, anti-diabetic, anti-inflammatory, and anti-aging activities, *Saudi Journal of Biological Sciences* **30**: 103485.

[112] Nagajyothi, P. C., Cha, S. J., Yang, I. J., Sreekanth, T. V. M., Kim, K. J., Shin, H. M. (2015) Antioxidant and anti-inflammatory activities of zinc oxide nanoparticles synthesized using *Polygala tenuifolia* root extract, *Journal of Photochemistry and Photobiology B: Biology* **146**: 10-17.

[113] Olbert, M., Gdula-Argasińska, J., Nowak, G., Librowski, T. (2017) Beneficial effect of nanoparticles over standard form of zinc oxide in enhancing the anti-inflammatory activity of ketoprofen in rats, *Pharmacological Reports* **69**: 679-682.

Thamar University Journal of Natural & Applied Sciences ***8****(2) (2023) 47 – 53*

DOI: https://doi.org/10.59167/tujnas.v8i2.1719

TUJNAS

Original Article

Two-dimensional Materials AlSI, AlSeBr, AlSeI, ScSI, ScSeBr, ScSeCl, ScSeI and InSI for Photocatalytic Water Splitting under Visible Light

Abdulrahman Alhaidar[1,2]

[1] Centre for Materials Science, Queensland University of Technology, Brisbane, QLD 4000, Australia
[2] School of Chemistry and Physics, Science and Engineering Faculty, Queensland University of Technology, Gardens Point Campus, Brisbane, QLD 4000, Australia

Corresponding author: Abdulrahman Alhaidar
Email: e.alhaidar@gmail.com

Received: 16 November 2023. Revised (in revised form): 8 December 2023. Accepted: 9 December 2023. Published: 31 December 2023

Abstract:

This article aims to investigate possible 2D photocatalysts for water splitting and to provide a comprehensive overview of some selected candidate materials from the Computational 2D Materials Database (C2DB). In this article, several 2D materials that have not yet been synthesized or investigated are reviewed. The structure, electronic and optical properties were investigated for many materials, taking into account some criteria for the selection of candidates, such as ABC materials from groups 6 and 7, a band gap of 1.6 to 2.8 eV by HSE calculation, and that these monolayers should be non-magnetic. In this article, it was found that AlSI, AlSeBr, AlSeI, ScSI, ScSeBr, ScSeCl, ScSeI, and InSI (the space groups of these materials are Pmmn (No. 59)) can be used for photocatalytic water splitting. These materials were dynamically stable and possessed excellent visible light absorption. The calculated band gaps were between 2.2 and 2.8 eV and their edge positions of CBM and VBM perfectly matched the oxidation and reduction potentials of water.

Keywords: 2D Materials; Photocatalysis; Water Splitting; Electronic Properties; Optical Properties

1. Introduction

Due to the growing demand for clean and renewable energy, photocatalytic water splitting has attracted intense research interest [1,2]. Photoactive semiconductive photocatalysts play a key role in sunlight-driven water splitting by generating photoexcited electron-hole pairs with redox properties upon light irradiation [3–5]. Traditional three-dimensional (3D) photocatalysts have a low specific surface area, which results in a limited number of reactive sites involved in the water redox reaction. For the interior photoexcited carriers to recombine, they must migrate to the surface. The photocatalytic efficiency of 3D photocatalysts can be limited by such intrinsic flaws [6,7]. Due to their inherent high specific surface areas and low carrier migration distances, 2D photocatalysts have been receiving a great deal of attention in the past decade [8–13].

Utilizing sunlight exposure and photocatalysts, water splitting into (H_2) and (O_2) stands out as a viable technique for converting solar energy into chemical energy. The effectiveness of these photocatalysts is intricately linked to the width of the semiconductor bandgap. Given the inherent advantages of 2D materials, there has been an increasing interest in the potential applications of such materials in the context of photocatalytic water splitting [8,14]. By analyzing the light absorption coefficient and energy band of 2D materials, it becomes possible to explore promising candidates for photocatalysts in water splitting.

Despite the wealth of theoretical and computational studies conducted on various photocatalytic materials, along with proposed strategies to enhance hydrogen evolution efficiency, there remains a critical need for researching novel 2D materials in the realm of photocatalytic water splitting for efficient H_2 fuel production. Furthermore, there has been a recent surge in interest surrounding multi-component metal-oxyhalides in many applications such as photocatalysis and electrocatalysis. Although research into 2D metal oxyhalides is still relatively new compared to other 2D materials like graphene or transition metal dichalcogenides. However, their potential for diverse applications, including photocatalysis, is driving significant attention and investigation in the scientific community.

Several 2D MXY (M= metal; X= O, S, Se, Te; Y= Br, Cl, F, and I) have been recently studied for their unique properties. Others proved the efficacy of lithium oxyhalides, and bismuth oxyhalides in electrocatalysis [15], and photocatalysis [16]. BiOX monolayers (X= Br, Cl and I) have been proven to be potential photocatalysts for water splitting [17]. GaOI and InOI are predicted to have suitable band gaps and band edge for photocatalytic water splitting [18].

A photocatalyst must satisfy several criteria to split water effectively. To split water under sunlight, photoexcited electron-hole pairs must be generated with redox capabilities irradiation [3–5, 9]. Photocatalysts must have band edge positions above and below water's

redox potentials to efficiently utilize solar energy. It is necessary to have a band gap greater than 1.238 eV but less than 3.0 eV to harvest solar energy efficiently [10,19–27]. Photogenerated carriers must also be separated as efficiently as possible to prevent the recombination of surface charges. Additionally, the band edge alignment of the photocatalyst must be suitable. Therefore, the conduction band minimum (CBM) should exceed the reduction potential of H+ / H_2, and the valence band maximum (VBM) should be lower than the oxidation potential of O_2/H_2O (−5.67 eV) [21,22, 24, 28–35]. There are a limited number of qualified photocatalysts that can produce hydrogen because of such stringent requirements.

This article focuses on providing a comprehensive study of materials selected from the Computational 2D Materials Database (C2DB). This database is well-curated and stands out as an exceptional resource for material researchers seeking to explore and select suitable materials for certain applications. It provides detailed computational and structural information, allowing researchers to efficiently screen and evaluate potential candidates for various applications. C2DB contains a large number of materials that might be suitable for water splitting. Since it might be infeasible and time-consuming to study all these materials, are limited for this study to a small subset of photocatalysts by considering some criteria for candidate selection. First, inspired by previous studies on metal-oxyhalides, ABC materials from groups 6 and 7 were selected. The band gaps are from 1.6 to 3.0 eV via HSE calculation, and these monolayers should not be magnetic. Then, conducted a computational study to confirm the reliability of the selected materials for water splitting. Therefore, this study aims to offer an early guideline for further experimental studies on the investigated materials. This article shows that AlSI, AlSeBr, AlSeI, ScSI, ScSeBr, ScSeCl, ScSeI and InSI monolayers possess band gaps from 2.2 and 2.8 eV. In addition, these monolayers have pronounced absorption in the visible light region of the solar spectrum. Their suitable band edge positions and light absorption make them promising photocatalysts.

2. Computational Details

All the calculations were based on Density Functional Theory [36–38] as implemented in the Vienna Ab initio Simulation Package [39–41]. Generalized Gradient Approximation (GGA) of the Perdew-Burke-Ernzerhof (PBE) function was utilized to describe the exchange-correlation function [42,43]. Long-range van der Waals (vdW) interaction was considered based on Grimme scheme s[44]. The gamma-centered k-points grids of 6×8×1 was used for AlSI, AlSeBr, AlSeI, ScSI, ScSeBr, ScSeCl, ScSeI and InSI, and the plane-wave energy cut-off was set to be 500 eV [45]. Atomic positions and cell shapes were fully relaxed until the maximum force acting on atoms and the energy converged to 0.005 eV/Å and 10-6 eV, respectively. A vacuum slab of a minimum of 18 Å was introduced to avoid interaction between neighboring images.

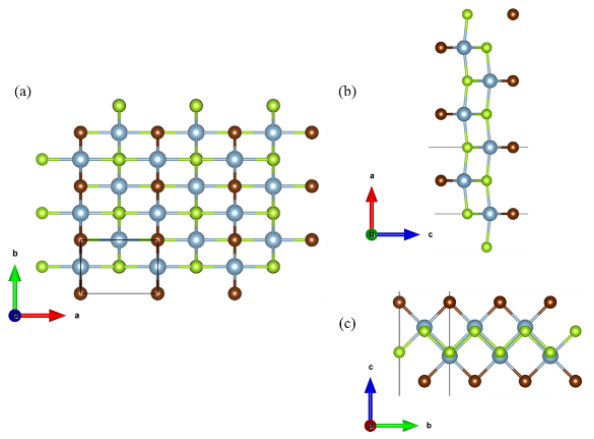

Figure 1: (a) top view and (b and c) sides view of the structure of AlSI, AlSeBr, AlSeI, ScSI, ScSeBr, ScSeCl, ScSeI and InSI monolayers.

The PBE functional method was used to calculate the band gap for these materials to determine if they could be used for water splitting. This calculation was very fast, and the band gap could be seen as a result. To save time, the calculation was stopped if the band gap was higher than 3.0 eV. The PBE functional can underestimate the calculation of band gaps of materials [46], so more accurate results were calculated based on the Heyd-Scuseria-Ernzerhof (HSE06) hybrid functional [47,48]. One important condition to assess the photocatalyst properties of 2D semiconductors is sunlight absorption, and this article used the density functional perturbation (DFPT) method. The spectrum in the visible light region is from 350 to 800 nm. The Phonon calculation was performed by PHONOPY code based on the finite-displacement method [49,50] with the convergence criteria for force and energy at 0.001 eV/Å and 10-8 eV, respectively. Moreover, ab into molecular dynamics simulations was carried out to study the thermal the selected monolayers, performed with a 3×3×1 supercell at 300 K. The simulations lasted for a duration of 10 ps in the NVT ensemble controlled by a Nose–Hoover thermostat [8], [51]. The standard oxidation and reduction potentials, namely, O_2/H_2O = $-5.67\ eV$ and H^+/H_2 = $-4.44\ eV$, were employed.

3. Results and Discussion

3.1 Geometry structure

Optimizing the structure of 2D materials is crucial because their properties are highly sensitive to their atomic arrangement. By tuning the arrangement of atoms, it can enhance specific properties like electronic conductivity, mechanical strength, and optical behavior, making them suitable for various applications in electronics, optics, energy storage, and more. After selecting the materials from the 2D database and the criteria that it has mentioned in the introduction, the zyx file was downloaded and opened via Materials Studio for checking and setup the correct lattice parameter and space group. Then the optimized structure for these monolayers, so can checked if the structures have changed during this calculation. The optimized monolayers for AlSI, AlSeBr, AlSeI, ScSI, ScSeBr, ScSeCl, ScSeI and InSI monolayers crystals are shown in Figure 1. They have trigonal symmetry [52] and Figure 1 (a) shows the top view and (b and c) shows the sides view of these monolayers.

This article has calculated several ABC materials, and it was found that only eight materials could potentially be used for water splitting. However, some of the materials that are not suitable for water splitting might be useful for other applications, such as solar cells. Table 1 shows the eight materials used and the calculated lattice parameters. As shown in Table 1 the calculated lattice parameters of AlSI, AlSeBr, AlSeI, ScSI, ScSeBr, ScSeCl, ScSeI, and InSI monolayers data from previous theoretical studies are well consistent with these findings [53,54]. As the results in Table 1 indicate, lattice constants calculated for the x-axis (a-axis) are larger than for the y-axis (b-axis). It is interesting to note that with increasing atomic mass, the substitution of X atoms has a greater impact on lattice constants and bonds than Y atoms, but the substitution of Y atoms has a greater effect on buckling distances.

To investigate the thermodynamic stability of AlSI, AlSeBr, AlSeI, ScSI, ScSeBr, ScSeCl, ScSeI, and InSI monolayers, their phonon spectra were calculated within the framework of PHONOP. The phonon dispersion spectra of these monolayers were calculated to investigate their dynamic stability. Phonon spectra represent the vibrational modes of a crystalline material as a function of the wave vector in the Brillouin zone. The dispersion diagram generated after this calculation can be used to determine whether the material is dynamically stable, as no imaginary frequencies are present. As can be seen in Figure 2, there are no imaginary frequencies for the phonon modes in the entire Brillouin zone. This shows that these monolayers are dynamically stable. There are six atoms in a primitive cell, resulting in 18 phonon modes, of which three are acoustic and fifteen are optical. According to the calculations, some monolayers were not stable because they did not match the water splitting devices, as shown in Table 2.

Table 1: Calculated structural parameters of AlSI, AlSeBr, AlSeI, ScSI, ScSeBr, ScSeCl, ScSeI and InSI monolayers.

Lattice Parameters	Materials							
	AlSI	**AlSeI**	**AlSeBr**	**ScSeBr**	**ScSeCl**	**InSI**	**ScSI**	**ScSeI**
a (Å)	4.85	5.31	5.23	5.39	5.38	5.32	5.09	5.37
b (Å)	3.71	3.79	3.61	3.83	3.67	3.99	3.92	3.98

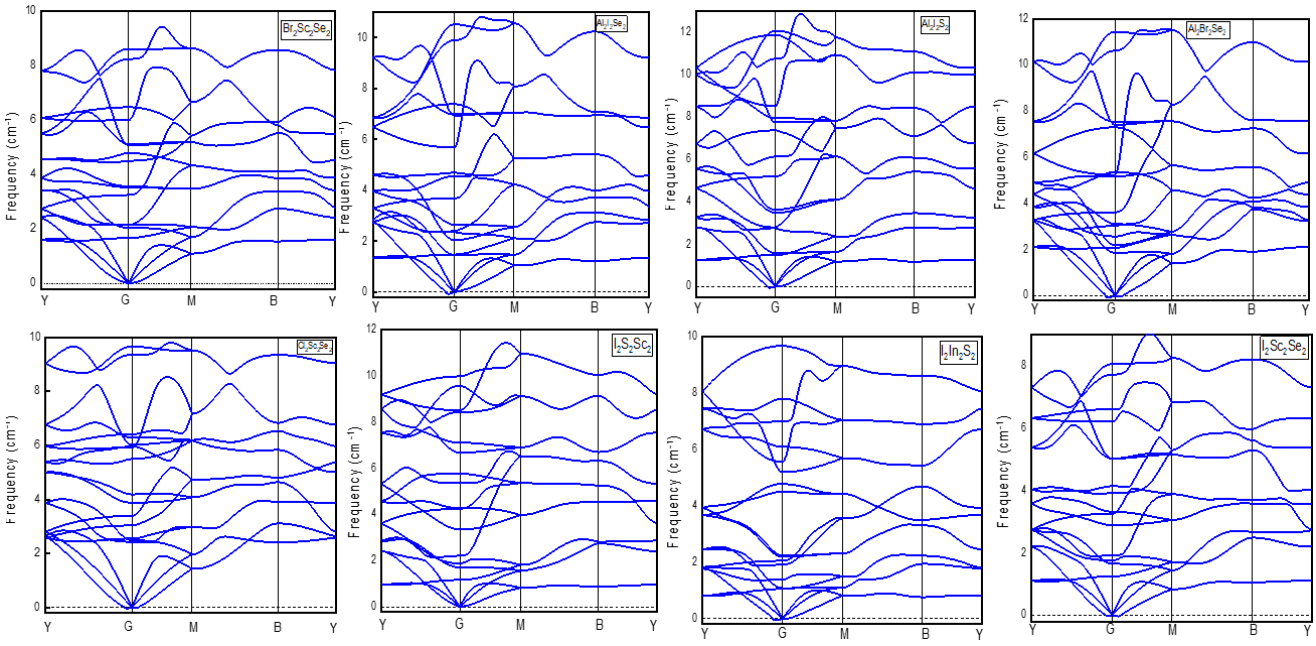

Figure 2: Phonon spectra of AlSI, AlSeBr, AlSeI, ScSI, ScSeBr, ScSeCl, ScSeI, and InSI monolayers with no imaginary frequency in any wave vector.

In addition, AIMD simulations prove thermal stability, for the suitable materials out of the materials that have been selected as the mentioned criteria in the introduction section. Thermal stability typically refers to the ability of a material to maintain its structural and energetic integrity at elevated temperatures. AIMD simulations involve modeling the dynamic behavior of atoms and molecules at finite temperatures and understanding the thermal stability of the system is crucial for various applications including water splitting. The performed colorations for AIMD are set with a 3×3×1 supercell at 300 K and simulation lasting for 10 ps. The time step of 1 fs and NVT ensemble controlled by the Nose-Hoover thermostat [51] was applied in the simulation. As illustrated in Figure 3, the AlSI, AlSeBr, AlSeI, ScSI, ScSeBr, ScSeCl, ScSeI, and InSI monolayers with the energy 300 K and by the time are stable. Moreover, there was no significant structural destruction, and the total energy per atom only fluctuated within a small range (< 0.1 eV) for a period of 10 ps.

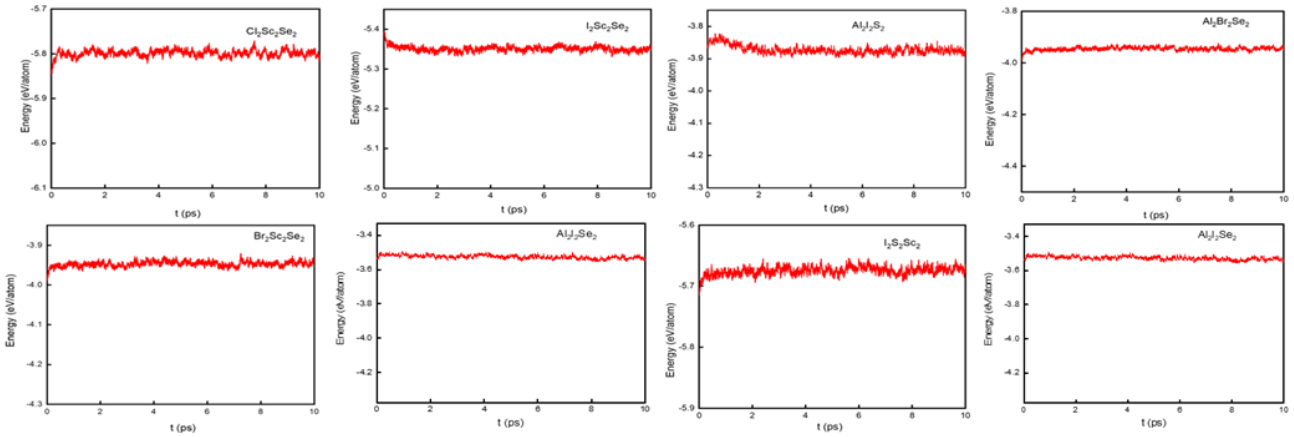

Figure 3: AIMD simulation at 300 K shows the evolution of total energy per atom. The insets are the structures of AlSI, AlSeBr, AlSeI, ScSI, ScSeBr, ScSeCl, ScSeI and InSI monolayers at 0 ps and 10.

3.2 Electronic structures.

The band gap is another important calculation that is composed for water splitting and two methods can get the band gap BPE and HSE06. For accurate results, HSE06 was applied to determine the accurate electronic structure and band gaps of these materials [47,48]. Figure 4 shows the HSE06 functional calculation obtained from indirect band gaps of AlSI, AlSeBr, AlSeI, ScSI, ScSeBr, ScSeCl, ScSeI, and InSI monolayers are 2.56, 2.27, 2.22, 2.8, 2.4, 2.29, 2.38 and 2.49, respectively. By comparing these values with the band gap of Ag2S and NaTAO3 monolayer, which is approximately 2.83 and 2.25 eV, most of the values are quite close to Ag2S and NaTAO3 which have been identified as photocatalysts for water splitting [55], [56]. After that, several materials were investigated (see Table 2), however, some of these materials are not used as photocatalytic water splitters due to large band gaps (over 3 eV).

3.3 Photocatalytic properties.

As described in the introduction, for 2D materials to be used as efficient photocatalysts, they must have suitable band edge positions. That is, the CBM of the photocatalyst should be above the reduction potential of water, -4.44 eV, and the VBM should be lower than the oxidation potential of water, -5.67 eV [21,28,57]. The VBMs are calculated from the difference between the vacuum potential and Fermi level. As shown in Figure 5, the CBMs of the monolayers were above -4.44 eV, which is greater than the hydrogen reduction potential. The VBMs of these monolayers were not below the water oxidation potential, -5.67 eV. The band edge positions are connected to the water redox potentials, which means that these monolayers could work as photocatalysts without an external bias voltage [8,58,59]. The calculated positions of VBM and CBM are shown in a schematic diagram in Figure 5 the red line indicates the CBM level, and the blue line indicates the VBM level. The VBM band edges of these monolayers were located at approximately -7.1 eV, which is significantly lower than the oxidation potential of water, whereas the CBM of the monolayers was slightly higher than the reduction potential of water. Therefore, the AlSI, AlSeBr, AlSeI, ScSI, ScSeBr, ScSeCl, ScSeI, and InSI monolayers are suitable for water splitting after approval via this calculation. There are some monolayers that are laminated after checking the band position because the CBM or VBM does not fit with the requirement mentioned and shown in Table 2.

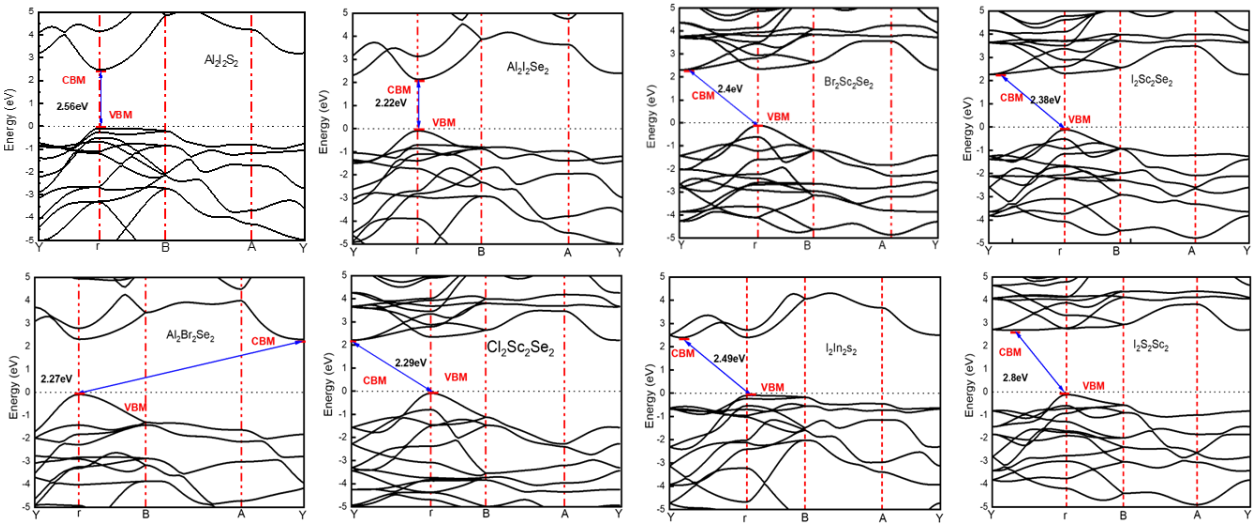

Figure 4: The band structures on the HSE06 level of the AlSI, AlSeBr, AlSeI, ScSI, ScSeBr, ScSeCl, ScSeI, and InSI monolayers and the range are between 2.2 to 2.8 eV.

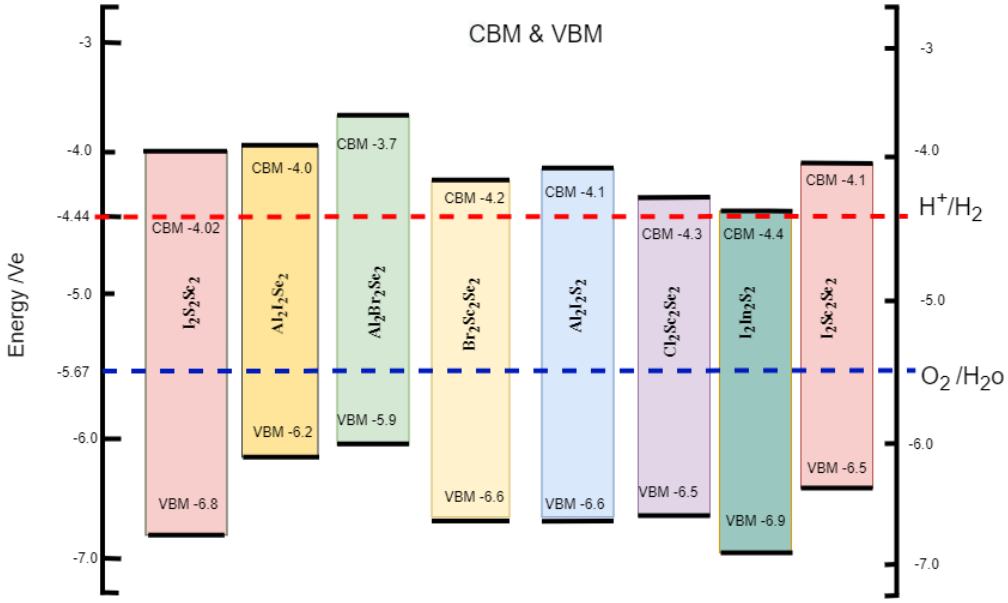

Figure 5: shows the band positions of AlSI, AlSeBr, AlSeI, ScSI, ScSeBr, ScSeCl, ScSeI, and InSI monolayers compared to the redox potential of water splitting.

Table 2: the selected materials from the 2D database (D2CB).

Materials	HSE band gap	eV	CBM	VBM
BrInS	2.8046	3.469	-4.445	-7.249
AsClTe	1.5756	3.097	-4.533	-6.109
BrGaS	2.3418	3.25	-4.677	-7.02
BrSSc	3.2455	3.162	-4.149	-7.394
ClGaS	2.3179	3.276	-4.646	-6.966
ClHfN	3.325	3.295	-3.534	-6.86
ClInO	4.1147	3.789	-4.563	-8.677
ClInS	2.7986	3.531	-4.489	-7.288
ClSSc	3.1288	3.153	-4.204	-7.333
ClScSe	2.2973	2.966	-4.257	-6.554
AsClSe	2.26	3.328	-4.937	-7.197
BrSbSe	1.8102	3.823	-5.139	-6.948
AlBrS	3.1703	3.466	-3.57	-6.74
AlClS	3.2446	3.5	-3.2	-6.45
AlClSe	2.1058	3.231	-3.53	-5.64
AlIS	2.5641	4.05	-4.08	-6.64
AlISe	2.2269	3.731	-3.96	-6.19
BrGaO	4.0447	3.475	-3.5	-7.55
BrHfN	3.279	3.325	-3.572	-6.851
BrInO	3.6043	3.769	-4.385	-7.990
BrNZr	3.7087	4.328	-3.027	-6.728
AlBrSe	2.2725	3.205	-3.682	-5.954
AsClTe	1.5756	3.097	-4.533	-6.109
HfIN	2.7113	4.03	-3.637	-6.168
IInS	2.49	3.93	-4.41	-6.901
ISSc	2.8	3.701	-4.026	-6.827
IScSe	2.381	3.52	-4.106	-6.488
AsClSe	2.26	3.328	-4.937	-7.20
BrSbSe	1.8102	3.823	-5.139	-6.948

3.4 Optical absorption.

Another important property to assess for a photocatalyst is its ability to absorb sunlight. High response to a broad range of solar light is highly desirable for generating more electron-hole pairs for the full utilization of solar energy. Using the dielectric function with the HSE06 hybrid functional, the absorption coefficient was calculated from the complex dielectric constants and Energy conversion can be more efficient when there is a high response to solar light. A spectrum of visible light (approximately 350 - 800 nm). Figure 6 shows that light absorption occurs predominantly in the ultraviolet (UV) range, with a small contribution from the visible range. These monolayers have significant absorption peaks in the ultraviolet range, as well as in the x- and y-directions. Usually, solar blind deep-UV detectors operate under severe conditions, which allows these monolayers to be used in UV optoelectronic devices in solar blinds. Moreover, the light absorption of AlSI, AlSeBr, AlSeI, ScSI, ScSeBr, ScSeCl, ScSeI, and InSI monolayers were 500, 420, 430, 550, 420, 510, 510, and 440 nm, as shown in Figure 6. These materials exhibit highly favorable phonon spectra that closely resemble those of synthesized and experimentally investigated materials such as the CdS nanorod/ZnS nanoparticle composite [60]. It is worth mentioning that there are some of the materials having large band gaps (over 3 eV) which indicate that large band gaps can have poor light absorption, as can be seen in Table 2.

4. Conclusion

In this article, the electronic structure, band edge positions, phonon spectra, and light absorption were calculated for a wide range of unsynthesized materials. After calculating their phonon spectra, it is found that there is no imaginary frequency in the monolayers AlSI, AlSeBr, AlSeI, ScSI, ScSeBr, ScSeCl, ScSeI, and InSI. This finding indicates that some of these monolayers are dynamically stable, while for the remaining monolayers, which have a small imaginary frequency, the problem could be solved by enlarging the supercell. Furthermore, the light absorption was calculated, and these monolayers have good light absorption at around 420 and 680 nm. Moreover, the band gaps of the AlSI, AlSeBr, AlSeI, ScSI, ScSeBr, ScSeCl, ScSeI, and InSI monolayers are between 2.2 and 2.8 eV, which is an excellent position for water splitting. The CBMs and the VBMs have exceptional suitability for the oxidation and reduction potentials of water. According to our findings, these materials have an excellent band gap position, and some of these monolayers are dynamically stable and have good light absorption. These 2D materials are suitable photocatalysts for photoelectrochemical water splitting. Therefore, they could be promising photocatalysts for water splitting. Our work not only enriches the family of 2D materials but also reveals new candidates for the development of highly efficient photocatalysts soon.

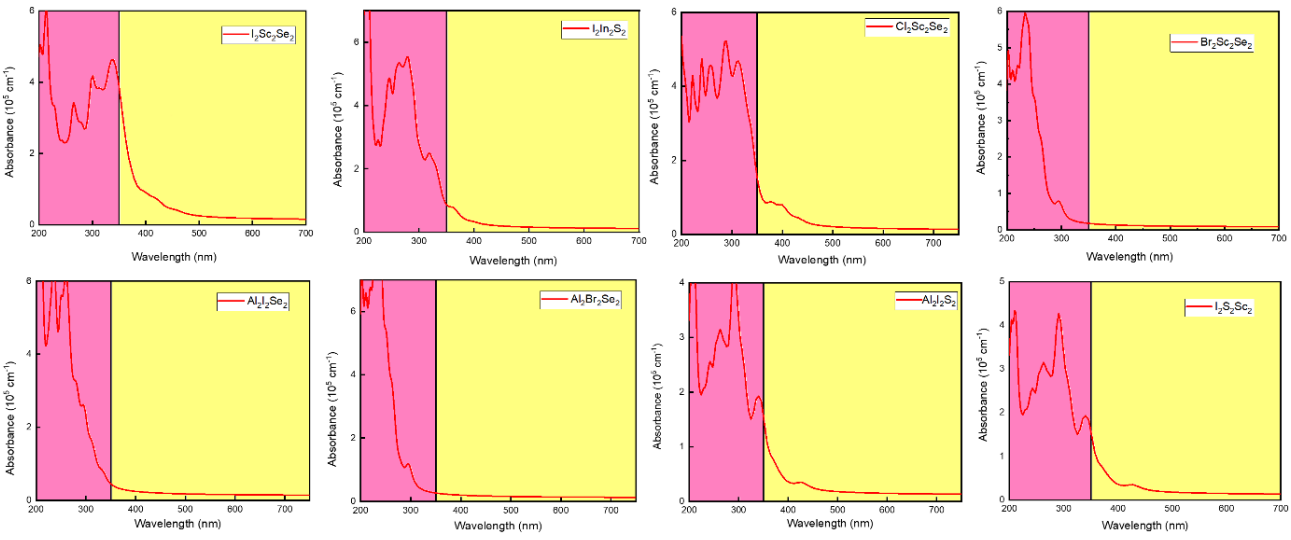

Figure 6: Calculated light absorption of these monolayers in direction. Purple and yellow areas represent the ultraviolet and visible regions of sunlight.

References

[1] Fujishima, A., Honda, K. (1972) Electrochemical photolysis of water at a semiconductor electrode, *Nature* **238**: 37-38.

[2] Grätzel, M. (2001) Photoelectrochemical cells, *Nature* **414**: 338-344.

[3] McCrory, C.C., Jung, S., Ferrer, I.M., Chatman, S.M., Peters, J.C., Jaramillo, T.F. (2015) Benchmarking hydrogen evolving reaction and oxygen evolving reaction electrocatalysts for solar water splitting devices, *Journal of the American Chemical Society* **137**: 4347-4357.

[4] Chen, X., Shen, S., Guo, L., Mao, S.S. (2010) Semiconductor-based photocatalytic hydrogen generation, *Chemical Reviews* **110**: 6503-6570.

[5] Walter, M.G., Warren, E.L., McKone, J.R., Boettcher, S.W., Mi, Q., Santori, E.A., Lewis, N.S. (2010) Solar water splitting cells, *Chemical Reviews* **110**: 6446-6473.

[6] Kudo, A., Miseki, Y. (2009) Heterogeneous photocatalyst materials for water splitting, *Chemical Society Reviews* **38**: 253-278.

[7] Takanabe, K. (2017) Photocatalytic water splitting: quantitative approaches toward photocatalyst by design, *ACS Catalysis* **7**: 8006-8022.

[8] Qiao, M., Liu, J., Wang, Y., Li, Y., Chen, Z. (2018) $PdSeO_3$ monolayer: promising inorganic 2D photocatalyst for direct overall water splitting without using sacrificial reagents and cocatalysts, *Journal of the American Chemical Society* **140**: 12256-12262.

[9] Li, Y., Li, Y.-L., Sa, B., Ahuja, R. (2017) Review of two-dimensional materials for photocatalytic water splitting from a theoretical perspective, *Catalysis Science & Technology* **7**: 545-559.

[10] Zhang, X., Zhao, X., Wu, D., Jing, Y., Zhou, Z. (2016) $MnPSe_3$ monolayer: A promising 2D visible-light photohydrolytic catalyst with high carrier mobility, *Advanced Science* **3**: 1600062.

[11] Zhao, P., Ma, Y., Lv, X., Li, M., Huang, B., Dai, Y. (2018) Two-dimensional III2-VI3 materials: Promising photocatalysts for overall water splitting under infrared light spectrum, *Nano Energy* **51**: 533-538.

[12] Fu, C.-F., Sun, J., Luo, Q., Li, X., Hu, W., Yang, J. (2018) Intrinsic electric fields in two-dimensional materials boost the solar-to-hydrogen efficiency for photocatalytic water splitting, *Nano Letters* **18**: 6312-6317.

[13] Alhaidar, A., Du, A., Zhang, L. (2022) Two-dimensional $MgAl_2S_4$ as potential photocatalyst for water splitting and strategies to boost its performance, *Applied Surface Science* **605**: 154826.

[14] Yao, S., Zhang, X., Zhang, Z., Chen, A., Zhou, Z. (2019) 2D Triphosphides: SbP_3 and GaP_3 monolayer as promising photocatalysts for water splitting, *International Journal of Hydrogen Energy* **44**: 5948-5954.

[15] García de Arquer, F.P., Bushuyev, O.S., De Luna, P., Dinh, C.T., Seifitokaldani, A., Saidaminov, M.I., Tan, C.S., Quan, L.N., Proppe, A., Kibria, M.G. (2018) 2D metal oxyhalide-derived catalysts for efficient CO_2 electroreduction, *Advanced Materials* **30**: 1802858.

[16] Di, J., Xia, J., Li, H., Guo, S., Dai, S. (2017) Bismuth oxyhalide layered materials for energy and environmental applications, *Nano Energy* **41**: 172-192.

[17] Cheng, H., Huang, B., Dai, Y. (2014) Engineering BiOX (X= Cl, Br, I) nanostructures for highly efficient photocatalytic applications, *Nanoscale* **6**: 2009-2026.

[18] He, J., Lyu, P., Nachtigall, P. (2020) Two-dimensional tetragonal GaOI and InOI sheets: In-plane anisotropic optical properties and application to photocatalytic water splitting, *Catalysis Today* **340**: 178-182.

[19] Ji, Y., Yang, M., Dong, H., Hou, T., Wang, L., Li, Y. (2017) Two-dimensional germanium monochalcogenide photocatalyst for water splitting under ultraviolet, visible to near-infrared light, *Nanoscale* **9**: 8608-8615.

[20] Wang, Q., Nakabayashi, M., Hisatomi, T., Sun, S., Akiyama, S., Wang, Z., Pan, Z., Xiao, X., Watanabe, T., Yamada, T. (2019) Oxysulfide photocatalyst for visible-light-driven overall water splitting, *Nature Materials* **18**: 827-832.

[21] Ni, M., Leung, M.K., Leung, D.Y., Sumathy, K. (2007) A review and recent developments in photocatalytic water-splitting using TiO_2 for hydrogen production, *Renewable and Sustainable Energy Reviews* **11**: 401-425.

[22] Cook, T.R., Dogutan, D.K., Reece, S.Y., Surendranath, Y., Teets, T.S., Nocera, D.G. (2010) Solar energy supply and storage for the legacy and nonlegacy worlds, *Chemical Reviews* **110**: 6474-6502.

[23] Zhang, X., Zhang, Z., Wu, D., Zhang, X., Zhao, X., Zhou, Z. (2018) Computational screening of 2D materials and rational design of heterojunctions for water splitting photocatalysts, *Small Methods* **2**: 1700359.

[24] Zhuang, H.L., Hennig, R.G. (2013) Single-layer group-III monochalcogenide photocatalysts for water splitting, *Chemistry of Materials* **25**: 3232-3238.

[25] Chowdhury, C., Karmakar, S., Datta, A. (2017) Monolayer group IV–VI monochalcogenides: low-dimensional materials for photocatalytic water splitting, *The Journal of Physical Chemistry C* **121**: 7615-7624.

[26] Jiang, X., Wang, P., Zhao, J. (2015) 2D covalent triazine framework: a new class of organic photocatalyst for water splitting, *Journal of Materials Chemistry A* **3**: 7750-7758.

[27] Peng, Q., Xiong, R., Sa, B., Zhou, J., Wen, C., Wu, B., Anpo, M., Sun, Z. (2017) Computational mining of photocatalysts for water splitting hydrogen production: two-dimensional InSe-family monolayers, *Catalysis Science & Technology* **7**: 2744-2752.

[28] Khaselev, O., Turner, J.A. (1998) A monolithic photovoltaic-photoelectrochemical device for hydrogen production via water splitting, *Science* **280**: 425-427.

[29] Lin, Y., Yuan, G., Liu, R., Zhou, S., Sheehan, S.W., Wang, D. (2011) Semiconductor nanostructure-based photoelectrochemical water splitting: a brief review, *Chemical Physics Letters* **507**: 209-215.

[30] Su, J., Guo, L., Bao, N., Grimes, C.A. (2011) Nanostructured WO_3/$BiVO_4$ heterojunction films for efficient photoelectrochemical water splitting, *Nano Letters* **11**: 1928-1933.

[31] Singh, A.K., Mathew, K., Zhuang, H.L., Hennig, R.G. (2015) Computational screening of 2D materials for photocatalysis, *The Journal of Physical Chemistry Letters* **6**: 1087-1098.

[32] Hisatomi, T., Kubota, J., Domen, K. (2014) Recent advances in semiconductors for photocatalytic and photoelectrochemical water splitting, *Chemical Society Reviews* **43**: 7520-7535.

[33] Luo, B., Liu, G., Wang, L. (2016) Recent advances in 2D materials for photocatalysis, *Nanoscale* **8**: 6904-6920.

[34] Rahman, M.Z., Kwong, C.W., Davey, K., Qiao, S.Z. (2016) 2D phosphorene as a water splitting photocatalyst: fundamentals to applications, *Energy & Environmental Science* **9**: 709-728.

[35] Yang, L., Li, X., Zhang, G., Cui, P., Wang, X., Jiang, X., Zhao, J., Luo, Y., Jiang, J. (2017) Combining photocatalytic hydrogen generation and capsule storage in graphene based sandwich structures, *Nature Communications* **8**: 16049.

[36] Sham, L.J., Schlüter, M. (1983) Density-functional theory of the energy gap, *Physical Review Letters* **51**: 1888.

[37] Gross, E., Kohn, W. (1985) Local density-functional theory of frequency-dependent linear response, *Physical Review Letters* **55**: 2850.

[38] Kresse, G., Furthmüller, J., Hafner, J. (1995) Ab initio force constant approach to phonon dispersion relations of diamond and graphite, *Europhysics Letters* **32**: 729.

[39] Kresse, G., Hafner, J. (1994) Ab initio molecular-dynamics simulation of the liquid-metal–amorphous-semiconductor transition in germanium, *Physical Review B* **49**: 14251.

[40] Kresse, G., Furthmüller, J. (1996) Efficiency of ab-initio total energy calculations for metals and semiconductors using a plane-wave basis set, *Computational Materials Science* **6**: 15-50.

[41] Kresse, G., Furthmüller, J. (1996) Efficient iterative schemes for ab initio total-energy calculations using a plane-wave basis set, *Physical Review B* **54**: 11169.

[42] Perdew, J.P., Burke, K., Ernzerhof, M. (1996) Generalized gradient approximation made simple, *Physical Review Letters* **77**: 3865.

[43] Grimme, S. (2006) Semiempirical GGA-type density functional constructed with a long-range dispersion correction, *Journal of Computational Chemistry* **27**: 1787-1799.

[44] Perdew, J.P., Ernzerhof, M., Burke, K. (1996) Rationale for mixing exact exchange with density functional approximations, *The Journal of Chemical Physics* **105**: 9982-9985.

[45] Monkhorst, H.J., Pack, J.D. (1976) Special points for Brillouin-zone integrations, *Physical Review B* **13**: 5188.

[46] Krukau, A.V., Vydrov, O.A., Izmaylov, A.F., Scuseria, G.E. (2006) Influence of the exchange screening parameter on the performance of screened hybrid functionals, *The Journal of Chemical Physics* **125**.

[47] Heyd, J., Peralta, J.E., Scuseria, G.E., Martin, R.L. (2005) Energy band gaps and lattice parameters evaluated with the Heyd-Scuseria-Ernzerhof screened hybrid functional, *The Journal of Chemical Physics* **123**.

[48] Heyd, J., Scuseria, G.E., Ernzerhof, M. (2003) Hybrid functionals based on a screened Coulomb potential, *The Journal of Chemical Physics* **118**: 8207-8215.

[49] Togo, A., Tanaka, I. (2015) First principles phonon calculations in materials science, *Scripta Materialia* **108**: 1-5.
[50] Baroni, S., De Gironcoli, S., Dal Corso, A., Giannozzi, P. (2001) Phonons and related crystal properties from density-functional perturbation theory, *Reviews of Modern Physics* **73**: 515.
[51] Martyna, G.J., Klein, M.L., Tuckerman, M. (1992) Nosé–Hoover chains: The canonical ensemble via continuous dynamics, *The Journal of Chemical Physics* **97**: 2635-2643.
[52] Ma, F., Zhou, M., Jiao, Y., Gao, G., Gu, Y., Bilic, A., Chen, Z., Du, A. (2015) Single layer bismuth iodide: computational exploration of structural, electrical, mechanical and optical properties, *Scientific Reports* **5**: 17558.
[53] Qi, H., Sun, Z., Wang, N., Qin, G., Zhang, H., Shen, C. (2021) Two-dimensional $Al_2I_2Se_2$: a promising anisotropic thermoelectric material, *Journal of Alloys and Compounds* **876**: 160191.
[54] Haastrup, S., Strange, M., Pandey, M., Deilmann, T., Schmidt, P.S., Hinsche, N.F., Gjerding, M.N., Torelli, D., Larsen, P.M., Riis-Jensen, A.C. (2018) The Computational 2D Materials Database: high-throughput modeling and discovery of atomically thin crystals, *2D Materials* **5**: 042002.
[55] Peng, R., Ma, Y., He, Z., Huang, B., Kou, L., Dai, Y. (2019) Single-layer Ag_2S: a two-dimensional bidirectional auxetic semiconductor, *Nano Letters* **19**: 1227-1233.
[56] Liu, Y.-L., Yang, C.-L., Wang, M.-S., Ma, X.-G., Yi, Y.-G. (2018) Te-doped perovskite $NaTaO_3$ as a promising photocatalytic material for hydrogen production from water splitting driven by visible light, *Materials Research Bulletin* **107**: 125-131.
[57] Bai, Y., Zhang, Q., Luo, G., Bu, Y., Zhu, L., Fan, L., Wang, B. (2017) $GaS_{0.5}Te_{0.5}$ monolayer as an efficient water splitting photocatalyst, *Physical Chemistry Chemical Physics* **19**: 15394-15402.
[58] Matta, S.K., Zhang, C., Jiao, Y., O'Mullane, A., Du, A. (2018) Versatile two-dimensional silicon diphosphide (SiP_2) for photocatalytic water splitting, *Nanoscale* **10**: 6369-6374.
[59] Ashwin Kishore, M., Ravindran, P. (2017) Tailoring the electronic band gap and band edge positions in the C_2N monolayer by P and as substitution for photocatalytic water splitting, *The Journal of Physical Chemistry C* **121**: 22216-22224.
[60] Jiang, D., Sun, Z., Jia, H., Lu, D., Du, P. (2016) A cocatalyst-free CdS nanorod/ZnS nanoparticle composite for high-performance visible-light-driven hydrogen production from water, *Journal of Materials Chemistry A* **4**: 675-683.

Thamar University Journal of
Natural & Applied Sciences

ISSN-Print: 203-0764
ISSN-Online: 2959-4340

Volume 8, Issue 2, 2023

CONTENTS

Articles

Thamar University Publications